Title
Circadian and cardiovascular dysfunction in the Huntington's disease mouse models

Author
Park, Saemi

Publication Date
2020

Peer reviewed|Thesis/dissertation

UNIVERSITY OF CALIFORNIA

Los Angeles

Circadian and cardiovascular dysfunction in the Huntington's disease mouse models

A dissertation submitted in partial satisfaction of

the requirements for the degree Doctor of Philosophy in

Molecular, Cellular and Integrative Physiology

by

Saemi Park

2020

ABSTRACT OF THE DISSERTATION

Circadian and cardiovascular dysfunction in the Huntington's disease mouse models

by

Saemi Park

Doctor of Philosophy in Molecular, Cellular and Integrative Physiology

University of California, Los Angeles, 2020

Professor Christopher S. Colwell, Chair

Circadian and sleep disruptions have been shown to lead to an increased risk for cardiovascular (CV) events. Huntington's disease (HD) patients are reported to have various symptoms including circadian and motor deficits. In addition, CV symptoms are implicated as the cause of death in over 30% of the HD patient population. However, very little is understood about the intersection between circadian disruption, CV disease, and HD. Here we utilized two mouse models, BACHD and Q175, to investigate CV pathology in HD. Reduced diurnal and circadian resting heart rate rhythms, heart rate variability, and baroreceptor reflex support that the autonomic regulation of the CV system is compromised in both HD mouse lines. In addition, age-dependent reduction in the heart function and cardiac fibrosis were observed. These results led us to test the hypothesis that reducing the mutant huntingtin (mHtt) expression in the cardiomyocytes is sufficient to rescue CV symptoms seen in BACHD mice by crossing with the cardiomyocyte-specific Cre, Myh6-Cre. Our results show that reduced mHtt expression in the

cardiomyocytes help improve left ventricular ejection fraction, several heart disease markers, and grip strength, a behavioral marker of cardiovascular health in the BACHD mice. Together this data indicates that heart disease in HD patients is likely to be driven both by cardiomyocyte specific pathology as well as dysfunction in the ANS.

The dissertation of Saemi Park is approved.

Gene D. Block

Holly R. Middlekauff

Kenneth P. Roos

Yibin Wang

Christopher S. Colwell, Committee Chair

University of California, Los Angeles

2020

Dedication

I would like to thank my parents for their sacrifice, love and constant support. They never stopped showing me the big world and letting me have so many opportunities to learn and explore growing up. I never imagined myself getting a doctoral degree. They always encouraged me and never lost faith in me. Thanks to them, I could accomplish this! I also want to thank my husband Hak Jo for love and encouragement. He has been always there beside me for better or worse. I cannot thank enough my little sister and best friend Sumin for her constant support, love, and prayer.

I thank my advisor and mentor Dr. Chris Colwell. He has been always there to support and guide me through graduate school during both good and bad times. I appreciate invaluable input and support from my committee members Drs. Gene Block, Holly Middlekauff, Ken Roos, and Yibin Wang.

I would like to thank the past and present lab members of the Colwell Lab for all their help, support and friendship. They have been the best colleagues and friends that everyone wishes for. Especially, Huei-Bin, Yu, Chris L, Olivia, Aly, and Dawn, I cherish all the memories inside and outside the lab. I also want to thank my friends from MCIP, Shuin, Michael, Iris and Albert for making the graduate school life more enjoyable.

Table of Contents

List of Figures

List of Tables

Acknowledgements

All of the chapters represent the collaborative efforts of multiple individuals as directed by PI Christopher S. Colwell. These chapters include materials from manuscripts that have been published or currently in preparation for publication.

Chapter 1 is a version of a published review entitled "Do Disruptions in the Circadian Timing System Contribute to Autonomic Dysfunction in Huntington's Disease?" by Park and Colwell.

Park, S., & Colwell, C. (2019). Do Disruptions in the Circadian Timing System Contribute to Autonomic Dysfunction in Huntington's Disease? *The Yale journal of biology and medicine*, 92(2), 291-303.

Author Contributions: SP wrote the first draft; CSC finalized text and generated figures.

We would like to acknowledge the prior intellectual contributions of Dr. Analyne Schroeder and Ms. Tamara Cutler

Chapter 2 is a version of two published papers entitled "Neurocardiovascular deficits in the Q175 mouse model of Huntington's disease" by Cutler et al. 2017 and "Cardiac Dysfunction in the BACHD Mouse Model of Huntington's Disease" by Schroeder at el. 2016.

Cutler TS, Park S, Loh DH, Jordan MC, Yokota T, Roos KP, Ghiani CA, and Colwell CS. (2017) Neurocardiovascular deficits in the Q175 mouse model of Huntington's disease. Physiol Rep. (11). pii: e13289.

Schroeder AM, Wang HB, Park S, Jordan MC, Gao F, Coppola G, Fishbein MC, Roos KP, Ghiani CA, and Colwell CS. (2016) Cardiac Dysfunction in the BACHD Mouse Model of Huntington's Disease. PLoS ONE 11(1): e0147269.

Author Contributions: SP contributed to the editing of these ms as well as data collection and analysis.

Chapter 3 is in preparation for publication. I would like to acknowledge Drs. Maria Jordan and Kenneth P. Roos at the mouse physiology core for their contributions on echocardiography and Ms. Iris Wang (Yibin Lab) for her help on RT-qPCR assays.

Biographical Sketch

Education

Ph.D. Doctoral Candidate, Molecular, Cellular and Integrative Physiology

University of California, Los Angeles
Los Angeles, California
2014-current

Master of Science, Physiological Sciences

University of California, Los Angeles
Los Angeles, California
2012-2014
Bachelor of Arts, Major: Biology and Chemistry; Minor: Mathematics and Global Studies

Drury University
Springfield, Missouri
2006-2010

Publications

Park, S., & Colwell, C. (2019). Do Disruptions in the Circadian Timing System Contribute to Autonomic Dysfunction in Huntington's Disease? *The Yale journal of biology and medicine*, 92(2), 291-303.

Cutler TS, **Park S**, Loh DH, Jordan MC, Yokota T, Roos KP, Ghiani CA, and Colwell CS. (2017) Neurocardiovascular deficits in the Q175 mouse model of Huntington's disease. Physiol Rep. (11). pii: e13289.

Schroeder AM, Wang HB, **Park S**, Jordan MC, Gao F, Coppola G, Fishbein MC, Roos KP, Ghiani CA, and Colwell CS. (2016) Cardiac Dysfunction in the BACHD Mouse Model of Huntington's Disease. PLoS ONE 11(1): e0147269.

Chapter 1: Do disruptions in the circadian timing system contribute to autonomic neuropathy in Huntington's disease?

Abstract:

Huntington's disease (HD) patients suffer from a progressive neurodegenerative process that inflicts both motor and non-motor dysfunction. HD is caused by a CAG repeat expansion within the first exon of the *huntingtin* (*Htt*) gene that produces a polyglutamine repeat that leads to protein misfolding, soluble aggregates, and inclusion bodies detected throughout the body including the heart. Both the clinical and preclinical research indicate that cardiovascular dysfunction should be considered a core symptom of at least a subset of HD patients. There is some evidence for cardiomyopathy, but these is even stronger evidence for dysautonomia (dysfunctional autonomic nervous system, ANS) in HD patients that can be detected early in the disease progression. The temporal patterning of ANS function is controlled by the circadian timing system based in the anterior hypothalamus. At the molecular level, circadian rhythms are generated by a transcriptional/translational feedback system that regulates transcription and has a major impact on cellular functions. Patients with neurodegenerative diseases including HD exhibit disrupted sleep/wake cycle and, in preclinical models, there is compelling evidence that the circadian timing system is compromised early in the disease process. We have been using preclinical models of HD to test the hypothesis that dysfunction in the circadian system contributes to the CV disease in neurodegenerative diseases. If correct, this work would lead to new therapeutic strategies and standards of care for HD and other neurodegenerative diseases.

Introduction:

HD is a genetic determined neurodegenerative disease.

Huntington's disease (HD) patients suffer from a progressive neurodegenerative process that inflicts cognitive, psychiatric and motor dysfunction [1,2]. HD is caused by a CAG repeat expansion within the first exon of the huntingtin (Htt) gene which produces a polyglutamine repeat that leads to protein misfolding, soluble aggregates, and inclusion bodies detected throughout the body [3,4]. The normal function of the protein (HTT) is unknown; however, the mutated form leads to dysfunction of a broad range of cellular processes including cytoskeletal organization, protein folding, metabolism, and transcriptional activities. Based on the broad distribution of the HTT, the mutation would be expected to produce symptoms throughout the body. Indeed, recent work suggests HD alters function in the heart, testes, liver, muscle, as well as in the brain. HD is a genetic disease, and a large number of animal models have been developed, each with strengthens and weaknesses (see [5]). The work covered in this review was mostly conducted on the Q175, BACHD, R6/2, and R6/1 mouse lines.

Cardiovascular dysfunction may be common in HD.

Cardiovascular events are a major cause of early death in the HD population and occur at a higher rate compared to the rest of the population [6,7]. Possible cardiomyopathies have not been well explored in HD patients. One recent study examined the electrocardiograms of over 500 early symptomatic HD patients and found evidence for low heart rate (bradycardia) and conduction abnormalities in a significant fraction of the patients [8]. Preclinical models of HD

have found clear evidence for reduced contractility and cardiac output [9–14]. For example, a recent study of the cardiomyocytes of BACHD mice found evidence for increased calcium/calmodulin-dependent protein kinase II activity as well as structural abnormalities in the mitochondria [15]. The cardiac-specific expression of polyQ repeats leads to cardiovascular dysfunction, suggesting that cardiovascular disease may be the result of local abnormalities [16,17]. There is even stronger evidence for dysautonomia (dysfunctional autonomic nervous system, ANS) in HD patients that can be detected early in the disease progression. The sympathetic nervous system appears to be most impacted during the very early stages of HD [18–20]. As the disease advances, the parasympathetic activity progressively decreases as well [20–22]. Therefore, both the clinical and preclinical research indicate that cardiovascular dysfunction should be considered a core symptom of at least a subset of HD patients.

Sleep and circadian dysfunction are an integral component of HD pathophysiology.

Sleep disorders are prevalent in HD patients and have detrimental effects on the daily functioning and quality of life of patients and their caregivers [23,24]. The most common symptoms found in these studies include a delay in sleep onset, fragmented sleep during the night, and daytime sleepiness. Importantly, these disruptions in the sleep/wake cycle occur early in the disease progression and so could serve as a biomarker for HD as well as a target for interventions. The sleep/wake cycle is conceptualized as being driven by two, anatomically-distinct processes: a homeostatic sleep mechanism (process S) as well as by the circadian timing system (process C). To date, there is little evidence that HD impacts sleep homeostasis but there is growing evidence for HD-driven disruption in circadian timing. Still, it is difficult to

determine whether the disease alters the circadian timing system in humans and animal models provide critical insights. Mouse models of HD also exhibit a progressive and rapid breakdown of the circadian rest/activity cycle that closely mimics the condition observed in human patients, typified by loss of consolidated sleep, increased activity during the rest phase, and more sleep during the active phase [10,25–27]. Importantly, the disruptions are seen under both light/dark (LD) cycle as well as the mice are held in constant darkness (DD). This latter step is critical to establish that the circadian system is compromised. Disorganized circadian timing leads to undesirable effects throughout the body [28], altering the function of key organ systems including heart, pancreas, liver, lungs as well as the brain. Collectively this prior research supports the hypothesis that circadian dysfunction is an integral component of HD pathophysiology. We have been testing the hypothesis that dysfunction in the circadian system contributes to the CV disease in HD (Fig 1.1) and, in this review, we will summarize our progress.

Topics:

Baroreceptor reflex is blunted in HD

One of the classic physiological tests of the ANS function is the measurement of the baroreceptor reflex in which changes in blood pressure (BP) evoke alterations in the heart rate (HR). Baroreceptors are mechanoreceptors located in the carotid sinus and aortic arch which sense the pressure changes. Although they are sensitive to both increases and decreases in arterial pressure, their primary role is to respond to a sudden fall in arterial pressure. This sudden

decrease is detected by baroreceptors and signals are sent to the medulla to elevate the sympathetic activity and reduce the parasympathetic activity. These changes lead to vasoconstriction and increased HR to bring back arterial pressure into the normal range. Recordings from the BACHD [29] as well as the Q175 [14] lines of HD mice indicate that the baroreceptor reflex is dramatically altered (Fig 1.2). The administration of Angiotensin II (ATII) or Nitroprusside (NP) leads to episodes of hypertension or hypotension, respectively. Changes in BP as a result of drug administration should elicit a compensatory response of HR via the baroreceptor reflex in order to normalize BP levels. The Q175 mutants showed a dramatically blunted response in HR to the transient hypotension induced by NP suggesting that the sympathetic branch has impaired. The BACHD mutants showed a blunted response to both ATII and NP indicating both sympathetic and parasympathetic arms were impacted. In both cases, we confirmed that there were no genotypic differences in the change in BP evoked by the injected drug as well as performed pharmacological controls to showing that appropriate receptor blockers prevented the change in HR.

HD patients complain of dizziness and light-headedness upon standing, all symptoms of baroreceptor dysregulation resulting in orthostatic hypotension [18,30]. While not well documented in HD patients, orthostatic hypotension has been extensively examined in Parkinson's Disease (PD) [31]. In this neurodegenerative disease, the neurogenic hypotension impacts about 30% of the patients with dizziness or lightheadedness, fatigue when standing, and difficulty walking to be the most common symptoms [32,33]. In a significant number of patients, the hypotension is responsible for the falls which one of the main complications of PD that has a

major impact on the quality of life. Patients with neurogenic orthostatic hypotension exhibit in enhanced reduction in systolic BP (~40 vs. 20 mmHg) in response to a stressor and thus are vulnerable for falls due to failure to maintain BP [34]. Like the PD patients, we expect that a subset of HD patients will be vulnerable to neurogenic orthostatic hypotension.

Heart rate variability is reduced in HD

HRV is a measure of variation in the beat-to-beat (R-R) interval that reflects the dynamic balance of sympathetic and parasympathetic control of heart function. Traditionally, HRV is generally considered an indication of cardiovascular health and low HRV proposed as a predictor for cardiovascular disease and mortality [35,36]. More recently, HRV has become a popular index of cardiac autonomic control in the biobehavioral sciences due to its relationship with stress disorders and other illnesses [37]. In humans, it is typically measured for short intervals and is increasingly available in health records as a non-invasive measure of cardiovascular function. One of the most commonly used methods for HRV evaluation is power spectral density analysis in which high-frequency (HF) and low-frequency (LF) bands are extracted from the HRV signal, and the spectral power is calculated (e.g., [38]). Traditionally, the LF power is viewed as a measure of regulation by the sympathetic branch of the ANS, although it is more likely a general index of ANS function [39,40].

In our work, we measured HRV in WT and HD mutant mice over several days in both LD and DD conditions. In WT mice, HRV displayed a robust diurnal and circadian rhythm consistent with circadian regulation of the ANS (Fig 1.3). Both the LF and HF domains of the HRV

exhibited robust daily rhythms. In the Q175 line [14], the HRV was low in young mutants, and this reduction was largest during the rest phase. The power in the LF domain was significantly reduced in the young mutants with the most prominent effects during the night. A similar reduction in HRV was previously observed in the BACHD line [10,13] as well as in the R6/1 model [41].

In HD patients, a similar decrease in HRV has also been reported during the presymptomatic and early stages of HD progression [18,19,21]. Prior studies reported HRV deficits during the Valsalva maneuver, hand-grip test, and the head up tilt test in HD patients [20,22,42,43]. As far as we know, the spectral power analysis has not been carried out on data from patients. In human subjects, HRV changes with daily cycle and with sleep state (e.g., [44]) but we do not have this data from the HD patients. Thus, both the preclinical and clinical work is consistent with a disruption in the sympathetic branch early in the disease progression that is reflected as a decrease in HRV.

Abnormal diurnal and circadian rhythms in HR observed in HD

In humans and other animals, HR varies dramatically with acute physical demands, i.e. higher HR when we are physically active while low HR when sedentary. In addition to these acute changes, there are also robust 24-hr circadian rhythms in the heart and vasculature to prepare the cardiovascular system for higher output during the day in humans. Interestingly, these natural rhythms may increase the risk for vulnerable individuals and daily rhythms in the symptoms of cardiovascular disease peak in the morning hours (e.g., [45]).

In nocturnal mice, diurnal and circadian of cardiovascular output peak in the night. While influenced by activity levels, the rhythms occur even when measured in windows of time when the mice were inactive. As measured by telemetry, diurnal and circadian rhythms in HR are disrupted in the BACHD, Q175, R6/1 lines of mice [10,13,14,41]. For example, the Q175 exhibited highly pronounced tachycardia during their normal sleep time, with high HR and reduced amplitude in the HR rhythm (Fig 1.4). Besides, the normal strong correlation between activity and HR, which is mediated by the ANS, was dramatically reduced in the mutants. These changes suggest that ANS disruption occurs early in disease progression in the Q175 line. In agreement, we also saw evidence in the BACHD of the circadian system failing to lower BP during sleep [29]. The HR rhythm in R6/1 mice are disrupted with the mutants showing a higher HR than WT littermates as young adults but ultimately exhibiting low HR [41]. In two other models (R6/2 and HdhQ150 lines), the HR was significantly reduced in symptomatic mice [46]. Therefore, overlapping data from several studies using different mouse models all found evidence for disrupted diurnal or circadian rhythms of HR.

As far as we know, the question of whether the rhythms in HR and BP are disrupted have not been examined in HD patients. The preclinical data suggest that the disruptions are most likely to occur at the beginning of the sleep and can be difficult to diagnosis. Office visits are unlikely to coincide with the expression of the hypertension. This type of "masked" or nocturnal hypertension is associated with poor clinical outcomes as the symptoms are likely to be untreated and patients frequently develop organ damage prior to transitioning to sustained hypertension which can be detected [47,48]. Based on the preclinical data, HD patients should be strong

candidates for 24-hr BP monitoring which is the best method for uncovering this type of hypertension.

Possible mechanisms underlying the dysautonomia

The circuits involved in the generation of rhythms in HR and autonomic function are relatively well defined. The central circadian clock in the suprachiasmatic nucleus (SCN) orchestrates the peripheral clocks via ANS [49–53]. Complete separation between pre-sympathetic and pre-parasympathetic neurons starts from the SCN (Fig 1.5) [53,54]. These separate pre-sympathetic and pre-parasympathetic neurons project to the paraventricular nucleus (PVN) and its separated pre-autonomic neurons have projections to either the preganglionic sympathetic neurons in the intermediolateral (IML) column of the spinal cord or the preganglionic neurons of the dorsal motor nucleus of the vagus (DMV). There are axon collaterals of the pre-sympathetic PVN neurons in the nucleus tractus solitarius (NTS). Particularly, the SCN utilizes completely separated sympathetic and parasympathetic neurons to convey the circadian information to the periphery including the heart, liver and adrenal gland. Various neuroendocrine and autonomic neurons are located in the PVN. Appropriate hormonal and autonomic responses are coordinated by the PVN [53,54].

HD is a neurodegenerative disease so the most obvious cause of dysautonomia is the loss of cell populations in the hypothalamus or brain stem. We examined possible anatomical changes within the SCN of the BACHD mouse at 3 months of age just as the motor symptoms can first be measured. We found that the male, but not the female, SCN was smaller than WT controls. There

were no differences in peptide expression (arginine vasopressin, AVP; vasoactive intestinal peptide, VIP) within the SCN with genotype or sex. In the more severely impacted R6/2 mice, the SCN shows decreased expression of VIP and its receptor, VPAC2 [55]. The SCN sends projections out to regulate the temporal patterns of activity in several major arousal centers including the orexin expressing cell population in the lateral hypothalamus. The expression levels of orexin and AVP are reduced in HD models (e.g., [56,57]). Changes in the expression of brain-derived neurotrophic factor (BDNF) have also been observed. Expression of BDNF is normally high in the brainstem where this neuromodulator plays a crucial for regulating HR [58–60]. The levels of BDNF are known to be reduced in the brainstem of mutant mice and resorting BDNF level can ameliorate HD pathology and prolong the lifespan in HD mice [61]. Importantly, restoring BDNF levels also returned the HR of the HD mice to the control levels [62]. So in the mouse models, HD alters the expression of peptides and neuromodulators in the brain regions involved in the neural regulation of cardiovascular function without necessarily causing a significant loss of hypothalamic neurons.

In HD patients, there is evidence that the disease causes similar changes in expression as well as degeneration in the brain regions involved in the CNS regulation of cardiovascular function. In the hypothalamus, there is evidence for the reduction in the expression of orexin and AVP in the brains of the HD patients [63,64]. In addition, the levels of BDNF and its receptors (TrkB) are reduced in HD patients [65], and the HD aggregates directly interfere with the transcription of BDNF [66]. Finally, there is evidence for degeneration in the brainstem nuclei in HD patients including loss of neurons in the substantia nigra, pontine nuclei, reticulotegmental nucleus of the

pons, superior and inferior olives [67]. This study also reported the strong expression of p62 immunopositive protein aggregates in axons of brainstem fiber tracts including the vagal nerve and the nucleus of the solitary tract. These structures are centrally involved in the CNS regulation of the CV system. Thus, by the end of life, HD certainly impacts the brain regions responsible for the CNS regulation of CV function and establishes a possible structural cause for this dysfunction.

Altered SCN-driven physiology output in HD

The circadian system is composed of cell-autonomous clock gene expression rhythms that are synchronized and adaptively phase aligned in tissues throughout the body by a rhythmic output from the SCN [68]. Individual SCN neurons express rhythms in spontaneous firing rate, with high firing rates observed during the day and low rates at night [69,70]. The BACHD and Q175 mouse models of HD exhibit decreased electrical activity in the SCN during the day [10,71]. This decrease in daytime firing in the SCN was not seen in the R6/2 model [72] although firing rate deficits were seen in an SCN-driven output in the orexin neurons [57]. Using electrophysiological techniques, we found that SCN neural activity rhythms were lost early in the disease progression and were accompanied by loss of the normal daily variation in resting membrane potential in the mutant SCN neurons [71]. The low neural activity could be transiently reversed by direct current injection thus demonstrating that the neurons have the capacity to discharge at WT levels. Exploring the potassium currents known to regulate the electrical activity of SCN neurons, our most striking finding was that these cells in the mutants exhibited an enhancement in the large-conductance calcium- and voltage-activated potassium (BK)

currents. The expression of the pore-forming subunit (*Kcnma1*) of the BK channel was higher in the mutant SCN. These findings demonstrate that SCN neurons of both BACHD and Q175 HD models exhibit early pathophysiology and that dysregulation of BK current may be responsible.

Circadian molecular feedback loop may be impacted by HD.

The rhythms in neural activity in the SCN are driven by cell autonomous molecular feedback loops. At a molecular level, circadian rhythms are generated by the intracellular transcriptional/translational feedback loop, driving daily oscillations with a period of approximately 24-hrs in the expression of core clock proteins. CLOCK (Circadian Locomotor Output Cycles Kaput) and BMAL1 (Brain and muscle aryl-hydrocarbon receptor nuclear translocator-like 1) the positive components of the clock bind to E-box sequences and drive the expression of the negative elements period (*Per*) and cryptochrome (*Cry*) which can inhibit their own transcription by repressing the CLOCK/BMAL1 heterodimer. Once the levels of PER and CRY are decreased, the new cycle of transcription/translation is started by CLOCK-BMAL1. This feedback loop constitutes a 24-hr period of the internal circadian rhythms. The circadian nuclear receptor, Rev-erba and a retinoic acid-related orphan receptor (ROR) regulate the *Bmal1* expression via activation and repression, respectively. Post-translational modifications are crucial for regulating the clock. Casein kinase 1 (CK1) phosphorylate PER and CRY which is vital for the circadian cycle length. The expression of other clock-controlled genes and output genes is modulated by the CLOCK/BMAL1 heterodimer, which involving many physiological functions [73]. We found that the circadian rhythms in PER2-driven bioluminescence were not altered in the SCN in the BACHD [74]; however, deficits in gene expression rhythms were found

in the SCN of the more severely impacted R6/2 model [25]. Thus the evidence that the molecular circadian clockwork is disrupted is so far mixed, and more work is required to identify at what age in the disease progression these disruptions occur.

These molecular rhythms are not just expressed in the SCN and work done in the R6/2 model clearly demonstrates that circadian rhythms of clock-driven genes that are critical metabolic outputs in the liver are abolished *in vivo* [75]. This deficiency is accompanied by arrhythmic expression of the clock genes *Cry1* and *Dbp*, and a phase-advanced *Per2* cycle. There is overwhelming evidence that circadian clock genes including *Bmal1*, *Clock*, *Rev-erba*, *Per 1*, *Per 2*, *Cry1*, and *Cry2* are rhythmically expressed in cardiomyocytes [76,77]. Functionally this timing system has a major impact on the expression of the genes involved in cardiac metabolism and electrical activity display circadian expression. For example, the metabolic genes, pyruvate dehydrogenase kinase 4 (*pdk4*) and uncoupling protein 3 (*ucp3*), are known to be regulated by peroxisome proliferator activated receptor alpha (PPARα). PPARα displays a robust rhythmic expression in the heart and is also shown to modulate *Bmal1* by directly binding to the *Bmal1* promoter [78]. Daily oscillations of the expression in *Pdk4* and *ucp3* are associated with oscillations in the clock gene expression with the peak during the active phase. Glucose levels are shown to exhibit diurnal rhythms. Glucose transporters 1 and 4 (Glut1,4) have a peak in the expression level at the same time, suggesting increased glucose transport and utilization at the same time with diurnal variations. Potassium channels, Kv1.5 and Kv4.2, as well as calcium transients show rhythmicity in the protein expression levels [79].

There is still much work to do to understand how the molecular clock controlling transcription interacts with the physiology of CV function. The general assumption is that the temporal pattern of transcription favors ATP production and energy utilization during the active phase while allowing remodeling and repair to dominate during rest. One particularly interesting case study involves the rhythmically expressed kruppel-like factor 15 (KLF15). Depletion of KLF15 in cardiomyocytes leads to a disorganized circadian behavior despite an intact core clock [80]. KLF15 transcriptionally controls the rhythmic expression of Kv channel-interacting protein 2, a critical subunit required for generating a transient potassium current. Deficiency or excess of KLF15 causes loss of rhythmic QT variation, abnormal repolarization and enhanced susceptibility to ventricular arrhythmias [81]. We do not know whether the HD mutation impacts KLF15 or other critical rhythmic outputs. We consider this lack of knowledge a major hole in the literature as HD-driven alterations in circadian output could be an important clinical symptom of the disease.

Genetic or environmental disruption of the circadian timing system leads to CV symptoms

Regardless of the specific cause, prior work has shown that the genetic or environmental disruption in circadian rhythms can result in CV symptoms. For example, mice held in a 20-hr (LD10:10) cycle are exhibited worse cardiac damage in response to high BP compared to controls held on a normal 24-hr cycle (LD 12:12) [82]. These lighting conditions alter rhythms in clock gene expression in both the heart and brain. Furthermore, "tau" mutant hamsters have a mutation in CK1 which results in a short endogenous cycle length of approximately 22-hrs [83] and, when they are held under a 24-hr LD cycle, these mutant hamsters die early with

cardiomyopathy including fibrosis[83]. However, when the mutant hamsters are housed in a 22-hr LD cycle or are made arrhythmic by destruction of their circadian clock (SCN), the hamsters are protected from developing cardiac dysfunction [83]. These results suggest that discord between the internal circadian clock (22 hrs) and external environment (24 hrs) can trigger cardiac disease. To provide a final example, *Bmal1*-knock out (KO) mice exhibit arrhythmic circadian behavior, age-related dilated cardiomyopathy, and shorten life span [84–87]. These symptoms are also seen in the cardiomyocyte-specific *Bmal1* KO mice [88]. To understand the role of circadian clock within the cardiomyocyte on myocardial biology, a cardiomyocyte-specific Clock mutant (CCM) mouse model was assessed [89,90]. CCM mice show decreased diurnal rhythms in HR, reduced cardiac efficiency, and bradycardia [89]. The cardiac hypertrophic markers are elevated in CCM mice [90]. These data suggest an essential role of cardiomyocyte circadian clock in CV function and highlight the possibility that at least some of the CV symptoms seen in HD could be the consequence of the well-established circadian dysfunction.

Finally, sleep disruption and work schedules that disrupt the circadian system are also risk factors for CV disease in humans [45]. Epidemiological studies show that approximately 40% of the population in North America do not get the recommended amount of sleep, and the reduced sleep duration is associated with a high risk of cardiac disease [91]. In the laboratory, placing healthy adults in an inverted sleep/wake and meal cycle for three days is sufficient to increase their BP and levels of the inflammatory markers [92]. A short 2 hr disruption of the sleep/wake can increase resting HR and cortisol levels in healthy subjects [93]. The sleep and rhythms

disruption due to work schedule is associated with the adverse endocrine and CV profiles in subjects, putting them at increased CV risk [93]. In a study performed on healthy male shift workers, 24-hr electrocardiogram recordings are used to investigate the effect of the work schedule on the cardiac autonomic control [94]. Results show a reduction in the cardiac sympathetic modulation based on the HRV analysis, suggesting an increased risk for CV events [94]. Therefore, the data from humans is consistent with our assertion that the sleep and circadian dysfunction seen in HD could contribute to the CV symptoms seen in the patients.

Conclusions and outlook:

The body of evidence presented in this review is consistent with the hypothesis that the disruption of the SCN circuit contributes to the autonomic dysfunction seen in HD. If correct, this hypothesis has a number of predictions. First, the normal diurnal and circadian rhythms in HR and BP driven by the ANS will be disrupted in HD. To date, the disrupted rhythms in HR, BP and baroreceptor reflex from data in HD animal models and patients support this hypothesis. Second, removing the mutant *Htt* from the heart will not be sufficient to rescue cardiac function. In contrast, reducing *Htt* in the brain will be sufficient, and specifically the CNS circuit controlling autonomic function will be a critical target. This prediction is clinically important as a number of clinical trials with *mHtt* lowering agents are ongoing. Third, treatment with drugs focusing on dysautonomia should be targeted to specific times of the daily cycle. For example, beta-adrenergic receptor blockers may produce the most substantial benefits when taken before bed. Fourth, cardiac function shows a robust diurnal variation including rhythms in HR and BP.

This body of preclinical data described in this review suggests that monitoring of the cardiovascular system in HD patients should start at an early age so therapeutic interventions can be employed to slow the progression of these pathological processes and prevent early death. Most importantly, our data suggest that this early screening must include observations during the usual sleep hours of the day, as early anomalies may go undetected at the times of day that patients would usually interact with clinicians. Finally, we predict that treatments or lifestyle changes that improve the circadian timing system will reduce the autonomic dysfunction in HD.

Chapter 2: Cardiovascular dysfunction in the Huntington's Disease models, Q175 and BACHD

Introduction:

Over the course of a lifetime, Huntington's disease (HD) patients are subject to a progressive neurodegenerative process that inflicts cognitive, psychiatric and motor dysfunction [1,95]. HD is caused by a CAG repeat expansion within the first exon of the *huntingtin* (*Htt*) gene and when translated, produces a polyglutamine (polyQ) repeat that leads to protein misfolding, soluble aggregates, and inclusion bodies detected throughout the body [3,4]. The normal function of the protein (HTT) is unknown; however, the mutated form leads to dysfunction of a large range of cellular processes including cytoskeletal organization, protein folding, metabolism and transcriptional activities. Cardiovascular events are a major cause of early death in the HD population and these events occur at higher rates compared to the rest of the population [6,96,97]. The limited cardiovascular studies in HD patients attribute the increased cardiovascular susceptibility in part to a dysfunctional autonomic nervous system (ANS) that can be detected early in the disease progression [18–22,30]. Additional studies are needed to better understand the time-course and cause of cardiovascular pathology in HD that could potentially help improve symptoms and prevent early death.

While there is no perfect animal model of HD [5], several models recapitulate aspects of the cardiovascular dysfunction seen in human disease. For example, dysfunction of the ANS has been reported in the several mouse models of HD as measured by heart rate variability and baroreceptor reflex experiments [10,29,41,46]. Reduced contractility and cardiac output is also a

common feature in mouse models [9–12,29]. The cardiac-specific expression of polyQ repeats leads to dysfunction, suggesting that cardiovascular disease is a result of both local dysfunction as well as improper input [16,17]. Advances in these preclinical models are critical if we are to develop a mechanistic understanding of the cardiovascular pathology in HD but establish models to evaluate therapeutic interventions.

In this chapter, we focus on examining possible cardiovascular dysfunction in the Q175 model of HD. The heterozygote (Het) Q175 offers advantages including: a single copy of the mutation, genetic precision of the insertion and control of mutation copy number [98,99]. These features make the Het Q175 line perhaps the most clinically relevant among the animal models; however, possible autonomic dysfunction has not been examined. We sought to test the dual hypotheses that cardiovascular dysautonomia can be detected early in disease progression in the Q175 model and that this dysfunction varies with the daily cycle. We used radiotelemetry to assess diurnal and circadian rhythms in activity, core body temperature (CBT), and heart rate (HR) in young (3–4 months of age) and middle aged (9–10 months of age) Q175 and wild-type (WT) mice. To further explore possible autonomic dysfunction, we measured HRV throughout the 24-h cycle as well as the baroreceptor reflex during the normal rest cycle. In addition, we evaluated the age-dependent progression in heart dysfunction in a separate cohort of mice using echocardiograms starting at 3 months of age and progressing to 12 months of age when the motor symptoms are pronounced and brain atrophy can be detected. Tissue was then collected to examine histoanatomical features of the Q175 hearts.

In addition, we sought to confirm some of our findings with the Q175 using the better studied BACHD line. Specifically, using this disease model, we evaluated the age-dependent progression in heart dysfunction using echocardiograms starting at the beginning of motor symptoms at 3 mo of age and progressing to an age (15 mo) when the motor symptoms are pronounced and brain atrophy can be detected. In addition, we examined gene expression profiles in the heart early (3 mo) and late (15 mo) in the disease progression in the BACHD model.

Methods:

Experimental Animals and Ethics Statement

BACHD mice on the C57BL6/J background along with littermate wild-type (WT) controls were acquired from the mouse mutant resource at The Jackson Laboratory, (JAX, Bar Harbor, Maine) in a colony maintained by the CHDI Foundation. The mice start showing symptoms at 2–3 mo of age and by 12 mo manifest full symptoms. In our colony, the BACHD mice commonly live to 18 mo of age but their health declines precipitously after 16 mo. Therefore, we stopped the present study when mice reached 15 mo of age. Five separate cohorts of mice of each genotype were used for this study: 1) longitudinal measurement of cardiac function using echocardiograms; 2) chronic treatment with isoproterenol (ISO) to boost cardiac output from 3 to 6 mo of age; 3) transcriptional comparison between the hearts of genotypes at 3 and 15 mo

of age; 4) measurement of serum cytokines in 3 mo old animals using a multiplex assay; 5) measurement of an apoptotic marker in 12–15 mo hearts by western blot.

Homozygous (Hom) and Het Q175 mice on the C57BL6/J background along with littermate WT controls were acquired from the mouse-mutant resource at The Jackson Laboratory, (JAX, Bar Harbor, Maine; stock No: 370476). The mice are full backcrossed into the C57 line (>12 crosses) and are monitored for the number of CAG repeats (approximately 190). Het Q175 mice commonly live to 24 months of age but the health of the Hom Q175 declines precipitously after 16 months. Therefore, we stopped this study well before this age point. Three separate cohorts of mice of each genotype were used for this study: (1) Telemetry studies measuring activity, CBT and electrocardiograms (ECG). Recordings (6–8 weeks in duration) were made from mice in a light-dark (LD) cycle as well as in constant darkness (DD) starting when the mice were 3 months and then again at 9 months of age; (2) Baroreceptor reflex measurements at 9 months of age; (3) longitudinal measurement of cardiac function using echocardiograms with measurements made at 3, 6, 9 and 12 months. The hearts of this third cohort of mice were then used for histological analysis. The LD cycle consisted of 12 h of light and 12 h of dark. By convention, the time of lights-on being defined as zeitgeber time zero (ZT 0). By convention, when the mice were held in DD, the beginning of activity onset is defined at circadian time zero (CT 0).

All procedures followed guidelines of the National Institutes of Health and were approved by the UCLA Animal Research Committee. To provide some details, the health of the mice was monitored daily. We looked for a set of symptoms including restlessness, impaired mobility, licking or guarding wound, failure to groom, open sores, loss of appetite or weight loss. At any

sign of ill health, a member of the veterinary staff was consulted for the course of treatment. If the animal did not improve, then it would be humanely sacrificed with an overdose of isoflurane and followed by decapitation. For pain management, the mice were given carprofen at 5 mg/kg every 24 hrs for 48 hr minimum. The first dose was given before surgery, and the remaining post-operatively.

Telemetry measurements

Methods employed were similar to those previously described [10,13]. WT, Hom Q175, and Het Q175 mice (n = 10 per genotype) were surgically implanted with a wireless radio-frequency transmitter (ETA-F20, Data Sciences International, St. Paul, MN). Three of the WT mice and one of the Hom Q175 did not exhibit measurable signals and had to be excluded from the final analysis. Mice were housed in individual cages in the absence of a running wheel. Cages were placed atop telemetry receivers (Data Sciences International) in a light and temperature-controlled chamber. Standard rodent chow was provided ad libitum. Data collection began 2-weeks postsurgery, to allow mice to recover in the 12:12 LD cycle. HR is extrapolated from ECG waveforms using the RR interval. All measurements were made in both LD and DD conditions at 3 months (young) and 9 months (middle age). At each age, the recordings took 6–8 weeks to complete. Cage activity in DD was also examined by periodogram analysis (ClockLab program, Actimetrics, Wilmette, IL) to estimate the free-running period.

Echocardiograms

WT (n = 10) and BACHD mice (n = 10) were group housed and kept in a 12:12 light/dark (LD) cycle with rodent chow provided ad libitum. Mice were examined with echocardiograms at 3, 6, 9, 12 and 15 mo of age. After the last echocardiogram measure, the mice were perfused and morphologic and histological measurements were taken. During the course of the study, 1 BACHD and 2WT mice died and the data from these mice were excluded from the analysis.

WT (*n* = 12), Q175 Het (*n* = 10) and Q175 Hom mice (*n* = 10) were group housed and kept in a 12:12 LD cycle with rodent chow provided ad libitum. Mice were examined with echocardiograms at 3, 6, 9, 12 months of age. After the final measurement, the mice were perfused and morphological and histological measurements of the heart were taken.

WT (n = 8), BACHD (n = 8), and BMYO mice (n = 8) were group housed and kept in a 12:12 light/dark (LD) cycle with rodent chow provided ad libitum. Mice were examined with echocardiograms at 3 and 6 mo of age. After the last echocardiogram measure, the heart and brain tissues of the mice were collected and morphologic and histological measurements were taken.

Echocardiograms were measured using a Siemens Acuson Sequoia C256 instrument equipped with a 15L8 15MHz probe (Siemens Medical Solutions, Mountain View, CA) as previously described. Briefly, two-dimensional, M-mode echocardiography and spectral Doppler images enabled measurement of heart dimension and function (Left Ventricle (Lv) Mass), end-diastolic dimension (EDD), end-systolic dimension (ESD), posterior wall thickness (PWT), ventricular

septal thickness (VST), Lv Ejection Fraction (Lv EF). The mice were sedated with 1% isoflurane vaporized in oxygen (Summit Anesthesia Solutions, Bend, OR) and HR was monitored using electrocardiogram to maintain physiological levels (between 450 and 650).

Isoproterenol (ISO) Treatment

BACHD and WT mice (2–3 mo) were subjected to echocardiograms before subcutaneous implantation of an osmotic pump (Alzet model 2001, Durect Corp, Cupertino, CA) containing either saline (WT: n = 4; BACHD: n = 4) or ISO (WT: n = 10; BACHD: n = 8). To determine an effective dose of isoproterenol, each treated mouse received sequentially increased doses of ISO, beginning with 0.24 mg/day, then 0.48 mg/day, and finally 0.97mg/day. It was this final concentration that proved effective at significantly increasing HR and was used in this study. At the end of the treatments (3 months duration), the cardiovascular function was assessed using electrocardiogram recording and echocardiography. After the last echocardiogram measure, the mice were perfused and morphologic and histological measurements were taken.

Electrocardiogram (ECG) Measurements

ECG traces were obtained under isoflurane anesthesia by inserting two platinum needle electrodes (Grass Technologies, West Warwick, RI) under the skin in the lead II configuration. The ECG signal was amplified (Grass Technologies), acquired and analyzed with HEM V4.2 software (Notocord Systems, Croissy sur Seine, France). The ECG data were recorded for 5 to 10 mins from each mouse monthly for the duration of the study. Heart rate (HR) was calculated using the RR-interval for all animals.

Heart Rate Variability

Data were extracted in 20-sec intervals then filtered to remove extreme noise. Remaining valid data segments were averaged into 1 h bins across the 24-h cycle. The following parameters for time domain analysis were calculated: mean normal-to-normal intervals (NN, in msec) and, standard deviation of all NN intervals (SDNN, in msec). For frequency domain analysis, spectra were calculated with a FFT (fast Fourier transform) with 20,000 data points per bin and a periodogram resolution of 8192, three overlapping subseries and a Hamming window (HRV Module, Data Sciences International). Frequency bins were defined as high-frequency (HF 1.5–5.0 Hz), low-frequency (LF: 0.2–1.5 Hz) and very low frequency (VLF: 0.01–0.2 Hz), and the power in these bands was calculated [100,101]. While it is common for LF and HF to be expressed in normalized units, this normalization minimizes the circadian regulation that we are interested in examining [102]. Therefore, we reported the raw LF and HF values (mV/Hz).

Baroreceptor reflex

Methods employed were similar to those described previously [29]. The administration of angiotensin II (ATII) or nitroprusside (NP) triggers acute hypertension or hypotension, respectively. Changes in blood pressure (BP) as a result of administering these drugs should elicit a compensatory response of HR. Differences in the ratio of change in HR to BP (ΔHR/ΔBP) are suggestive of aberrant signaling to the heart by the ANS. Baroreceptor function was examined during the day (ZT4-9) in middle age (9 months) mice of each genotype: WT (n = 8), Hom Q175 (n = 10) and Het Q175 (n = 8). These measurements took 4 weeks to

complete. The procedure was unsuccessful in some of the mice (WT, $n = 1$; Het Q175, $n = 2$; Hom Q175, $n = 1$) and data could not be used. During the experiment, HR was determined from the R-R interval of the ECG. Mice were anesthetized and both femoral arteries were catheterized, whereby BP measurements were collected from one artery and drugs were administered through the other artery. Following catheterization, isoflurane levels were decreased to between 1 and 1.5% and the mice were allowed to rest for at least 10 min. Baseline BP and HR were then recorded. AT II (4.0 μg/kg) and NP (40 μg/kg) were administered in sequence to probe the HR response to the changes in BP. Each treatment was followed by a flush of saline (+heparin 3 U/mL) to ensure full delivery of the drugs. As a control, muscarinic (75 μg/kg glycopyrrolate) and β-adrenergic (750 μg/kg propranolol) receptors were blocked before administering another dose of ATII or NP. The absolute value of the maximum change in BP as well as the subsequent directional change in HR was determined. Ratios of these two values (ΔHR/ΔBP) reflected the magnitude HR change relative to the change in BP that characterizes the sensitivity of the baroreceptor response.

Morphometry and Histology

Following the longitudinal echocardiogram measurements as well as the ISO treatments (described above), animals were deeply anaesthetized using isoflurane and perfused with phosphate-buffered saline (PBS, pH 7.4) with heparin (2 units/ml, Henry Schein, Melville, NY) followed by 4% (w/v) paraformaldehyde (Sigma-Aldrich) in PBS (pH 7.4). A motorized pump was used to deliver the solutions in order to control and maintain similar pressure between animals. Hearts were dissected, weighed and post-fixed at 4°C. Tibia length (TL) was also

measured. Heart weight (HW)/TL and HW/body weight (BW) ratios were calculated to determine any differences in morphometry that would indicate cardiac hypertrophy. Following a series of dehydration steps using ethanol and xylene, hearts were embedded in paraffin. Paraffin-embedded hearts were sectioned and stained with H&E or Masson's Trichrome. Heart dimensions were measured using two mid-ventricular cross sections from each H&E and/or Masson's Trichrome-stained heart with the aid of Image J software. The presence or absence of fibrotic staining was visually scored by two researchers masked to the experimental conditions. In order to quantitate the degree of fibrosis, images were acquired from each heart. Areas of fibrosis were captured, and in sections lacking positive fibrotic staining, an area of the left ventricle (Lv) wall was imaged. Pictures were processed using Corel Draw, to remove pixels of background and pink cardiomyocyte tissue, leaving areas of positive blue stain in the image. Integrated density of these processed images was measured using Image J, where pixel areas less than 3 were excluded from the measurements in order to minimize noise. The resulting density numbers were divided by the area of the heart tissue in the image.

Trichrome stained sections were used to estimate the cardiomyocyte cross-sectional area in aged (15 mo) WT and BACHD mice (n = 4 per group). Measurements were performed by three observers masked to the genotype of the mice. Images from multiple fields (3–5) at the level of the papillary muscles were acquired on a Zeiss Axioskop with an Axiocam using the AxioVision software (Zeiss, Pleas- anton, CA, USA), and measurements (in μm) obtained using the AxioVision software. Only cells with a well-defined round shape were considered. The cross-sectional areas of 7–12 cells/animal were averaged and analyzed for the statistical difference.

Two mid-ventricular-stained cross sections were used to obtain morphometric measurements and to estimate the number of fibrotic areas in WT (n = 5), Hom and Het Q175 mice (both n = 6 per genotype). Images of the mid-ventricular cross sections from each heart were acquired on a Zeiss Stereomicroscope (Stemi SV 11 Apo) equipped with an Axiocam using the AxioVision software (Carl Zeiss). Measurements were performed by two observers masked to the genotype of the mice using the Zeiss Axiovision software. The thickness of the left ventricular wall was measured in three different nonseptal parts to obtain an average thickness. Values from the two sections were averaged. Fibrotic areas, suggestive of necrotic areas, that is, infarcts, were visually identified and counted by three observers masked to the genotype on a Zeiss Axioskop (Carl Zeiss, Pleasanton, CA). To determine which chamber or part of the interventricular septum was more affected, the locations of the infarctions in the heart were also annotated.

For wheat germ agglutinin (WGA) staining, deparaffinized sections were rehydrated through an alcohol gradient starting at 95% ethanol to 50%. Heat-induced antigen retrieval was performed using 10 mmol/L Citrate buffer (pH 6.0), followed by blocking in 10% BSA/PBS for 1 h. Slides were incubated with Alexa Fluor 594-WGA (50 μg/mL, 10 min, Invitrogen) in PBS and mounted using ProLong Gold (Invitrogen, Carlsbad, CA). Confocal images of stained sections at the levels of the papillary muscles were captured, using a confocal scanning microscope (Nikon, Melville, NY) and the cross-sectional area of the cardiomyocytes was measured using the NIS Elements (Nikon) software (50-100 cells from 6 to 8 areas per mouse heart, n = 6 per genotype).

RNA Extraction

A separate cohort of young (3 mo) and older (15 mo) WT and BACHD mice (n = 4 per group) were used for gene expression analysis. Total RNA from the ventricles were extracted using Trizol RNA isolation protocol (LifeTechnologies, Carlsbad, CA), then DNAse treated (TURBO DNA-free kit, Life Technologies) and column purified (Pureline RNA Mini-kit, Life Technologies). RNA was used for microarray and Quantitative Real-Time PCR experiments described below.

Microarray Hybridization

Microarray processing was performed by the Southern California Genotyping Consortium at UCLA. Briefly, whole genome gene expression profiling protocols began with 100 ng of total RNA isolated as described above. Samples were quantitated using Ribogreen fluorescent assay and normalized to10 ng/ul prior to amplification. Amplified and labeled cRNA was produced using the Illumina-specific Ambion TotalPrep kit. 1st and 2nd strand cDNA was produced using the Ambion kit (Life Technology) and purified using a robotic-assisted magnetic capture step. Biotinylated cRNA was produced from the cDNA template in a reverse transcription reaction. After a second Ribogreen quant and normalization step, amplified and labeled cRNA was hybridized overnight at 58°C to Illumina MouseRef-8 v2.0 expression arrays. Hybridization was followed by washing, blocking, staining and drying on a Little Dipper processor. Array chips were scanned using an iScan reader, and expression data were extracted and compiled using BeadStudio software (Illumina, San Diego, CA).

Quantitative Real-Time PCR

One μg of total RNA was reverse transcribed using High Capacity cDNA Reverse Transcription Kit (Applied Biosystems, Foster City, CA). Quantitative real-time RT-PCR was performed using SYBR Green Mix (Applied Biosystems, Foster City, CA). Using Primer3 [103] following primers were designed to flank intron-exon broundaries: *Hspa1a* (sense: 5'-GGT CTC AAG GGC AAG CTC AG-3' and anti-sense: 5'-CTT GTG CAC GAA CTC CTC CT-3') *Nppb* (sense: 5'-TCC TCT GGG AAG TCC TAG CC-3' and anti-sense: 5'-AGC TGT CTC TGG GCC ATT TC-3') *Kcnip2* (sense: 5'-AAT CCC GAG ATT TGG ACG GC-3' and antisense: 5'-GCT TGA GGA AAC GCT GCT TC-3') *Acot1* (sense: 5'-AGA AGC CGT GAA CTA CCT GC-3' and antisense: 5'-GGA AGG AGG CCA TAG CAA GG-3') *Tbp* (sense: 5' CAC GGA CAA CTG CGT TGA TT-3' and antisense: 5'-AGC CCA ACT TCT GCA CAA CT-3') *B2M* (sense: 5'-GGT GAC CCT GGT CTT TCT GG-3' and antisense: 5'-TGT TCG GCT TCC CAT TCT CC-3'). Specificity and efficiency of the reactions were verified using melting curves and dilution series, respectively. Expression levels of *Hspa1a*, *Nppb*, *Kcnip2*, and *Acot1* were calculated using the $2^{-\Delta\Delta Ct}$ method where *Tbp* and *B2m* were used as normalizing genes. *Tbp* and *B2m* did not vary between genotypes and we report gene expression normalized to *Tbp*.

Multiplex Assay

Blood sample was collected from a separate cohort of young (3-4mo) WT (n = 8) and BACHD (n = 8) mice using the facial vein technique. Blood was allowed to clot for at least 30 mins at room temperature, and serum was collected following centrifugation at 3000rpm for 15 mins and frozen at -80^{C} until analyzed. A volume of 25μL serum was used to assess cytokine levels of IFNγ, IL-10, IL-12, IL-1A, IL-1B, IL-2, MIP1A, RANTES, IL-6, MCP-1, and TNF-α using the

Millipore cytokine milliplex kit (EMD Millipore Corporation, Billerica, MA, USA) and the Biorad Bio-plex 200 systems machine (Hercules, CA, USA).

Western Blot

Hearts from aged WT (n = 4) and BACHD (n = 4) mice were rapidly dissected and homogenized in lysis buffer containing 50 mM Tris/HCl, 0.25% (w/v) DOC (sodium deoxycholate), 150 mM NaCl, 1 mM EDTA, 1nM EGTA, 1% (w/v) Nonidet P40, 1 mM Na3VO4 (sodium orthovanadate), 1 mM AEBSF [4-(2-aminoethyl)benzenesulfonyl fluoride], 10 μg/ml aprotinin, 10 μg/ml leupeptin, 10 μg/ml pepstatin and 4 μM sodium fluoride. Total protein concentration in cleared extracts was estimated using the Thermo Scientific™ Pierce™ BCA Protein Assay Kit (Thermo Fisher Scientific, Waltham, MA USA). Fifty μg of total proteins were loaded on to a 4–20% Tris-glycine gel (Invitrogen, Carlsbad, CA). Western blots were performed as previously described [104]. Equal protein loading was verified by Ponceau S solution (Sigma, Saint Louis, MO) reversible staining of the blots. Each extract was analyzed for the relative protein levels of Heat-Shock protein (Hsp)-70, by using a mouse monoclonal antibody (Sigma, Saint Loius, Mo), and Cleaved Caspase-3, by using rabbit polyclonal antibodies (EMD Millipore Corporation, Billerica, MA & Cell Signaling, Danvers, MA). Each extract was also analyzed for relative protein levels of GAPDH (Genetex, Irvine, CA) by stripping and re-probing. Protein bands were detected by chemiluminescence using the Thermo Scientific™ Pierce™ ECL 2 Western Blotting Substrate or the Amersham ECL kit (GE Healthcare; Piscataway, NJ) with HRP (horseradish peroxidase)-conjugated secondary antibodies (Cell Signaling, Danvers, MA). Relative intensities of the protein bands were quantified by scanning densitometry using the NIH Image Software

(Image J, http://rsb.info.nih.gov/ij/). For the comparison of relative protein levels in the heart from WT and BACHD animals, each background-corrected value was normalized according to the relative GAPDH levels of the sample, and then referred to the average of the WT values calculated from the same immunoblot image.

Statistical Analysis

A two-way repeated measures ANOVA was used to analyze the long-term changes in echocardiographic measurements between WT and BACHD animals using genotype and age as factors. Other comparisons between the two genotypes were made using a Student's t-test. If the data set failed to pass a test for equal variance, a Rank-Sum Test was used. These statistical analyses were performed using the SigmaStat (San Jose, CA) or Prism 5 (GraphPad Software, San Diego, CA) statistical software. Data are shown as the mean ± SEM. Raw microarray data were analyzed by using Bioconductor packages as previously described [105]. Briefly, quality assessment was performed by examining the inter-array Pearson correlation and clustering based on the top variant genes. Contrast analysis of differential expression was performed by using the LIMMA (Linear Models for Microarray and RNA-Seq Data) package [106]. After linear model fitting, a Bayesian estimate of differential expression was calculated, and the P -value threshold was set at 0.005. The fold change of gene expressions is calculated by comparing the signal intensity of young hearts and old hearts. Differentially expressed genes were then classified according to gene ontology and pathways using Ingenuity Pathway Analysis (IPA, Ingenuity Systems, Redwood City, CA). After applying threshold at P = 0.005, the top 10 genes up-regulated and down-regulated in BACHD compared to WT at the same age are selected

according to their P-value. In other words, they are the most significantly changed genes in the comparison.

For most of our experiments, two-way analysis of variance (ANOVA) was used to determine statistical significance with genotype (WT, Het Q175, Hom Q175) and time (either ZT or CT) as the two factors. If the data did not exhibit a normal distribution, a two-way ANOVA on ranks was used. Post hoc *t*-test with Bonferroni's corrections was applied to determine significant differences between genotypes at each of the hourly bins (ZT or CT). In the cases in which we only obtained the measurements at one age (baroreceptor, histological measurements), we used a one-way ANOVA followed by Bonferroni's multiple comparison test or a one-way ANOVA on ranks. Correlations between activity and heart rate were examined by applying the Spearman correlation analysis to 21,700 contiguous, 20 sec, time-matched, heart rate and activity bins per mouse at two ages (3 months, 9 months). *R*-values were then compared between groups using a two-way ANOVA. For a comparison of the number of infarcts, we used a Kruskal–Wallis ANOVA followed by Dunn's multiple comparison test. These statistical analyses were performed using the SigmaStat (San Jose, CA) or Prism 5 (GraphPad Software, San Diego, CA) statistical software. Values are reported as the mean ± Standard Error of the Mean (SEM).

Results:

Altered diurnal and circadian resting HR rhythms in the Q175 line.

We examined the HR when the Q175 animals were physically inactive, that is, the resting HR. The young Q175 exhibit abnormally high resting HR under both LD and DD, mostly during the late day and early night (Fig 2.1A and B). By middle age in DD, this tachycardia reversed and we actually saw low resting HR in the Hom Q175. The low HR in the Hom Q175 occurred primarily during the early subjective day (Fig 2.1C and D). The simultaneous recording of HR and activity allows the analysis of HR evoked by movement; hence, we measured HR when the animals were physically active, that is, the active HR. Again, a significant effect of genotype in young animals was found under both LD and DD conditions. The Hom Q175 exhibited a significantly increased active HR during the early day and subjective day. Similar results were obtained in middle aged mutants, with a significant effect of genotype under both LD and DD conditions.

A significantly increased activity-evoked HR was observed in the Hom Q175 during the early day and subjective day as well as a reduced correlation between activity and HR (Fig 2.2). For example, in WT mice, the Spearman correlation between activity and HR was 0.56 ± 0.03 while in the Hom Q175 the correlation was reduced to 0.42 ± 0.02 (genotype, $F = 10.4$; $P < 0.001$). Finally, we compared a number of parameters of the ECG waveform (RR, PR, QRS, QT, QAT, MxdV) in WT and the Q175 mutants under LD conditions (Table 1). Significant differences between the genotypes were seen with RR, QRS, and QAT intervals. In summary, the Hom Q175 exhibited tachycardia during rest and activity with the high HR being most pronounced during the day when HR was normally low. Even in young animals, the ANS-driven rhythms in HR were disrupted in the Q175 line.

Reduced HRV in the Q175 line.

To further explore autonomic dysfunction in the Q175 line, we measured HRV throughout the 24-hr cycle. HRV measures the variability in the time between individual heartbeats and reflects the balance of the sympathetic and vagal inputs regulating heart rate. High HRV is associated with cardiovascular health, while low HRV is a sign of poor cardiovascular function. We observed high HRV during the day and lower at night (Fig 2.3A) in WT mice. Conversely, the HRV was abnormally low in the HD mutants (Hom, Het) and this damping was largest during the sleep phases. HRV measures were separated into low-frequency (LF: 0.2–1.5 Hz) and high-frequency (HF, 1.5–5.0 Hz) bands, which are commonly used to quantify parasympathetic and sympathetic regulation, respectively. In WT mice, the power of both the LF and HF bands exhibited a daily rhythm which peaked during the night (Fig 2.3B and C). The power of the HF band was minimally impacted with the young Hom Q175 exhibiting significant differences only in the late night (Fig 2.3B). In contrast, the power of the LF band was greatly impacted throughout the night in the mutants (Fig 2.3C). These results demonstrate that the temporal patterning as well as the overall level of autonomic regulation of the cardiovascular system is compromised in the Q175 mice.

Baroreceptor reflex is compromised in the Q175 line.

The baroreceptor reflex is a rapid homeostatic mechanism by which perturbations in blood pressure are countered by change in HR mediated by the ANS. In previous work, we have shown that the BACHD mice show an abnormally weak baroreceptors response to decreases in blood

pressure, consistent with a weak sympathetic regulation of heart rate [29]. We performed baroreceptor evaluations to determine the autonomic responsivity to drug-induced changes in BP (Fig 2.4A and B). As expected, the middle-aged WT mice had normal reflex responses, that is, when the BP was transiently increased with angiotensin II (ATII, 4 μg/kg), the heart rate dropped in compensation, and when the BP was transiently lowered with nitroprusside (NP, 40 μg/kg), the heart rate was elevated. The effects of ATII and NP were completely blocked by pretreatment with sympathetic and parasympathetic receptor antagonists (750 μg/kg propranolol, 75 μg/kg glycopyrrolate) (Fig 2.4). Interestingly, the Hom Q175 mice had very blunted HR responses to NP (one-way ANOVA on ranks: $H = 11.3$, $P = 0.004$). While some of the Het Q175 (2/6) showed a greatly reduced response to the NP injection, the overall NP-response was not significantly different from the WT (Fig 2.4A). There were no significant changes in response to ATII injection although we did observe an abnormal instability in the Hom Q175 HR (Fig 2.4B). Systolic BP did not significantly vary with genotype (WT: 83 ± 4 mm Hg; Het Q175: 76 ± 4; Hom Q175: 71 ± 3; $F = 2.8$; $P = 0.08$). These data provide further evidence of diminished autonomic function, especially of the sympathetic branch.

Echocardiograms characterize age-related decline in the Q175 and BACHD lines.

The age-dependent progression in heart dysfunction of the Q175 mice was evaluated in a separate cohort of mice using echocardiograms beginning at 3 months of age and progressing to 12 months (Fig 2.5D and E; Table 2). Both the cardiac structure [Lv mass, EDD, ESD] and function (FS%, E/A ratio, Lv EF) were significantly influenced by age and genotype (Table 3).

For example, the Lv mass of the Hom Q175 was significantly smaller compared to WT and Het Q175 by 6 months of age (Fig 2.5D). Cardiac function, measured by Lv EF, was significantly diminished in the Hom Q175 beginning at 9 months. Both the Hom and Het Q175 exhibited a reduction in this parameter compared to WT at 12 months (Fig 2.5E). By 9 months of age, the hearts of Hom Q175 mice were smaller and functionally depressed compared to WTs.

We assessed cardiac structure and function in a group of BACHD and WT mice throughout most of their adult life in order to follow changes in cardiovascular parameters and establish a time course for pathology. We use echocardiography to follow the same BACHD and WT littermate control mice longitudinally from 3 to 15 mo (Fig 2.5A-C; Table 4). The hearts of WT mice slowly increased in dimension as they aged, with significance in EDD and PWT starting at 12 mo while Lv Mass and ESD were significantly larger at 15mo (Fig 2.5A and B; Table 4). Cardiac function as measured by Lv EF showed an increase between 3 and 6 mo as is typical with development of WT mice and then declined with age (Fig 2.5C). The hearts of BACHD mice also increased in size as they aged, with a significant increase in Lv Mass and PWT measures starting at 9 mo of age (Fig 2.5A; Table 4). Cardiac function of BACHD mice did not significantly change with age (Fig 2.5C; Table 4). The hearts of BACHD mice were larger (ESD and EDD) and thicker (PWT) than WT mice starting at 3 mo of age (Fig 2.5B; Table 4). Lv Mass was significantly higher in BACHD compared to WT with significant differences starting at 9 mo (Fig 2.5A). Functional measurements (Lv EF) were depressed in BACHD mice compared to WTs starting at 3 mo of age, and remained lower at all ages (Fig 2.5C). Throughout adult life, the hearts of BACHD mice were larger and functionally depressed compared to WTs.

Cardiac Fibrosis observed in both the Q175 and BACHD lines.

We observed a significant reduction in both the body (−25%) and heart (−18%) weight in the Hom Q175 as compared to WT (Table 5). Therefore, at the end of the echocardiogram measurements, histological analysis of the hearts was performed to further characterize these abnormalities. The total area of coronal heart sections at the mid-ventricular level in the Hom Q175 was 33% and 23% smaller than that of WT and Het Q175, respectively (Table 5, Fig 2.6A). In agreement with the echocardiogram data, the Lv lumen cross sectional area (CSA) (54%) and circumference (23%) were greatly reduced in the Hom Q175 (Table 5). No differences were found in the thickness of the Lv wall or the interventricular septum. The dimensions of the Het Q175 hearts were not significantly different from WT (Table 5). Next, we measured the CSA of individual cardiomyocytes stained with WGA (Fig 2.6B). While the WT cardiomyocytes exhibited a medium CSA of 204 ± 11 μm^2, the CSA was 151 ± 4 μm^2 and 95 ± 8 μm^2 in the Het and Hom Q175, respectively (ANOVA on ranks, $H = 15.15$, $P < 0.0001$). This dramatic reduction in size (53%) of the CSA of the cardiomyocyte in the Hom hearts was accompanied by an apparent disorganized cytoarchitecture of the myocardium (Fig 2.6B). Finally, histopathological analysis of the heart with Masson's trichrome stain revealed local pockets of fibrosis where the cardiomyocytes appeared to be replaced by scar tissue (Fig 2.6C). These areas, an indication of small necrotic lesions or infarcts, were present in the heart of all three genotypes with an average of 9.6 infarcts/section in the Hom Q175 vs 2–3 infarcts/section in the WT and Het Q175 (Fig 2.6D). Small fibrotic areas were occasionally seen in all the WT mice examined, frequently on the edge of the papillary formations in the Lv (Fig 2.6C). In the

mutants, the fibrotic pockets were seen in the ventricular wall of both the left and right ventricles, some of which were extensive. Interestingly, in the Hom Q175, these lesions were most commonly seen in the anterior part of the interventricular septum near the anterior groove, suggesting disruption of the blood supply to the heart (Fig 2.6C and D).

To further assess the cardiac structure of WT and BACHD hearts, we sacrificed the mice at about 15 mo of age and processed their hearts Masson's Trichrome to visualize fibrotic tissue or H&E staining. We did not detect any fibrotic staining in the WT hearts, while positive staining was present in 6 of the 9 BACHD mice (Fig 2.7A). Optical density measurements of fibrotic staining were significantly higher in BACHD mice compared to WTs (Fig 2.7B; Table 6). BACHD hearts displayed enlarged Lv (Fig 2.7C). Although these values did not reach significance, an increase in Lv diameter (19%) and septal thickness (20%) were observed in BACHD compared to WT, whilst no difference in right ventricle dimensions were found between genotypes (data not shown). Furthermore, no changes were found in the cross-sectional area of the BACHD cardiomyocytes (103 ± 15 μm^2; n = 4) as compared to WT (121 ± 13 μm^2, n = 4).

Discussion:

In this study, we sought to test the dual hypotheses that cardiovascular dysautonomia can be detected early in disease progression in the Q175 model and that this dysfunction varies with the daily cycle. We found overwhelming evidence for autonomic dysfunction including blunted daily rhythms in HR, reduced HRV, and almost a complete failure of the sympathetic arm of the

ANS during the baroreceptor challenge. Importantly, several aspects of the Q175 phenotype were found to vary with a diurnal and circadian phase dependence. For example, HRV deficits were more prominent during the day but it would have been difficult to detect during the night. Hence, the time of measurement and the circadian cycle has to be considered as a critical factor in the expression of HD symptoms. The Q175 mouse model of HD exhibits cardiovascular symptoms comparable to those seen in HD patients with a prominent sympathetic dysfunction during the resting phase.

Q175 (Hom, Het) mice showed deficits in both diurnal and circadian activity rhythms in HR (Fig. 2.1) with the deficits in HR occurring in young adults while the deficits in CBT were not observed until middle age. The circadian rhythms in HR are independent of locomotor activity but dependent on an intact SCN [107–112]. The SCN projects to the dorsal subparaventricular zone [113,114], which is necessary for driving circadian rhythms of body temperature [115]. Young Hom Q175 exhibited highly pronounced tachycardia during their normal sleep time, with high HR and a reduced amplitude in the HR rhythm (Fig. 2.1). In addition, the normal strong correlation between activity and HR, which is mediated by the ANS, was dramatically reduced in the mutants (Fig. 2.2). These changes suggest that ANS disruption occurs early in disease progression in the Q175 line. In agreement, we also saw evidence in the BACHD of the circadian system failing to lower blood pressure during sleep [29]. Similarly, R6/1 mice have a higher HR than WT littermates in young but not older mutant mice [41]. However, in two other models (R6/2 and HdhQ150 lines), the HR was significantly reduced in symptomatic mice [46].

HRV is a measure of variation in the beat-to-beat (R-R) interval that reflects the dynamic balance of sympathetic and parasympathetic control of heart function. In WT mice, HRV displayed a robust diurnal and circadian rhythm consistent with circadian regulation of the ANS (Fig. 2.3). Both the LF and HF domains of the HRV exhibited robust daily rhythms. In the Q175 line, the HRV was low in young mutants (Hom, Het) and this reduction was largest during the rest phase (Fig. 2.3A). The power in the LF domain was significantly reduced in the young mutants with the biggest effects during the night (Fig. 2.3B). Traditionally, the LF is viewed as a measure of regulation by the sympathetic branch of the ANS, although it is more likely a general index of ANS function [39,40]. Thus, our data clearly indicate that the autonomic outflow is disrupted in the HD mutants. Autonomic dysfunction is likely responsible for the low HRV as well as the elevated HR during the rest phase (daytime) in Q175 mice. A similar reduction in HRV was previously observed in the BACHD line [10], and evidence of disrupted ANS leading to an unstable heart beat as well as elevated levels of the sympathetic transmitter (norepinephrine) were reported in the R6/1 model [41]. It is also possible that postsynaptic receptors are altered, as suggested by a recent study showing that acetylcholine receptors (measured by α-bungarotoxin binding) are reduced in the diaphragm of BACHD mice [116]. However, earlier work examined cardiac β1-adrenergic receptor densities in R6/2 and WT mice but did not see any genotypic differences [11]. In HD patients, a similar decrease in HRV has also been reported during the presymptomatic and early stages of HD progression [18,19,21]. Reduced HRV is generally considered an indication of poor cardiovascular health and a predictor for cardiovascular disease and mortality [35,117,118].

The baroreceptor reflex is also a process dependent on autonomic function. Similar to the BACHD line [29], Q175 mice showed a dramatically blunted response in HR to the transient hypotension induced by NP suggesting that the sympathetic branch has impaired homeostatic reserve (Fig. 2.4). The primary deficit in the baroreceptor reflex in Q175 mice is unknown, as this process is mediated by various regions of the brain including the brainstem and hypothalamus, along with outputs from the ANS [18,119,120]. In HD patients, the detection of alterations in the baroreceptor circuit, such as the vagal nuclei and cerebral cortex, have established a possible structural cause for this dysfunction [19–21,119,120]. Ideally, identification of the site of dysfunction could be used to devise an appropriate therapeutic approach to manage symptoms in HD patients. Prior studies reported HRV deficits during the Valsalva maneuver, hand-grip test, and the head up tilt test in HD patients [20,22,42,43]. Furthermore, patients complain of dizziness and light-headedness upon standing, suggesting they suffer from orthostatic hypotension due to autonomic dysregulation and a deficient baroreceptor reflex [18,30]. The sympathetic nervous system appears to be most impacted during the very early stages of HD [18–20]. As the disease advances, the parasympathetic activity progressively decreases as well [20–22].

The Q175 mice displayed an age-dependent progression in heart dysfunction beginning at presymptomatic stages (3 months). Both the structure and function of the heart exhibited significant alterations due to both age and genotype (Fig 2.5D and E). The mutants' hearts were smaller and less functional by 6 months of age (Table 3 and 5) and worsen with age. Histological analysis of the hearts also found that the mutant hearts showed localized fibrotic lesions that

resembled those caused by myocardial infarction (Fig 2.6C and D) and imply that prior obstruction of the blood supply to the heart caused local cell death. These fibrotic infarcted areas are the histological signature of heart attacks. Evidence for fibrosis has also been found in another HD model, the R6/2 line [16].

The echocardiographic measurements performed on BACHD mice showed changes in heart structure and function at an early age (Fig 2.5A-C). At this time point (3 mo), motor deficits [121] and circadian rhythm dysfunction [10] are just beginning thus the cardiovascular deficits are occurring very early in the disease progression in this model. Though the slope of the changes were similar between aging WT and BACHD animals, the ejection fraction (EF) ratio of 15 mo old BACHD mice were close to or below 55, which is the threshold between normal heart function and failure. We suspect that the function would continue to weaken with age, which poses a challenge for the cardiovascular system, leaving BACHD mice more susceptible to serious cardiac events. The presence of cardiac fibrosis in 15 mo old BACHD mice (Fig 2.7) also provides evidence for cardiac stress that feeds forward to further impair heart function. WT mice show minimal fibrotic lesions at this age. The focal fibrotic lesions in the BACHD would be expected to alter wall motion synchrony and could explain the reduced EF.

The presence of fibrosis that we observed in both the Q175 and BACHD models could also increase the likelihood of arrhythmias [122] although we did not observe any in our recordings. Though the incidence of arrhythmias has not yet been examined in HD patients, other lines of evidence suggest increased susceptibility including altered ANS input to the heart [20,123]. ANS

dysfunction is consistent among a number of HD animal models including the R6/1 [41] and the R6/2 models [46]. In the BACHD model, we have found significant alterations in the baroreceptor reflex and a decline in heart-rate variability that indicate dysfunctional ANS outflow [29]. With this work, we have provided evidence that the Q175 and BACHD line recapitulates cardiovascular dysfunction seen in HD patients as well as established an age-dependent progression by which we can judge the impact of therapeutic interventions.

Cardiovascular complications are a leading cause of death in HD patients [6,7,96,97]. To date, several of the HD mouse models have been shown to exhibit cardiovascular dysfunction [9–12,17,29,41,46]. Mutant *Htt* is expressed in both the heart and brain [124], thus a critical question is whether the cardiovascular pathologies seen in HD are due to a deficit at the level of the cardiomyocytes or whether they are secondary to central nervous system dysfunction. For example, overexpression of an expanded polyQ track or *mHtt* in cardiomyocytes resulted in heart failure and a significantly reduced lifespan in both mice [17] and flies [16]. So at least some of our findings may be due to cardiomyocyte-specific deficits, e.g., the changes in the ECG waveform in young mutant mice. In addition, in HD patients, there is evidence of degeneration of brainstem nuclei, including those that control the regulation of heart function [19,20,42,67,125,126]. So it is likely that there is an HD-specific cardiomyopathology as well as cardiovascular pathology secondary to the HD-driven damage to the ANS. Overall, this body of preclinical data suggests that monitoring of the cardiovascular system in HD patients should start at an early age so therapeutic interventions can by employed to slow the progression of these pathological processes and prevent early death. Most importantly, our data suggest that this early

screening must include observations during the usual sleep hours of the day, as early anomalies may go undetected at the times of day that patients would usually interact with clinicians.

Chapter 3: Rescue of the cardiovascular symptoms in the BACHD mouse model

Introduction:

Mouse model of HD recapitulate aspects of the human disease including cardiovascular dysfunctions such as reduced contractility and cardiac output [10,29,41,46]. The animal model used in this chapter is the BACHD mouse line of mice, engineered to express the human mutation in the *Htt* gene, in a way that it can be excised by Cre recombinase (Cre) in a tissue specific manner [121]. Our previous study showed structural and functional changes in the BACHD mice as early as 3 months of age, which resemble aspects of the human HD [13,21,29]. Also, there is evidence that when soluble preamyloid oligomers similar to HD mutations are expressed exclusively in cardiomyocytes, the mice die from cardiac failure, suggesting that CV dysfunction is not solely secondary to neurodegeneration [16,17]. Therefore, we crossed the BACHD mouse line with a Myh6-Cre to reduce *mHtt* in the cardiomyocytes to obtain a better understanding of the role of cardiomyocytes in driving the CV symptoms in HD. Using this conditional BACHD mouse model, we assessed the cardiac function and structure with echocardiograms in the early disease progression. We also analyzed the gene expression of cardiac hypertrophic markers. Finally, we examined the impact of the reduction of mHtt in several behaviors that are known to be impacted by the HD mutation. Taken together, our study provides important insights into cardiovascular pathophysiology in HD.

Methods:

Generation of BMYO mice

BACHD mice on the C57BL6/J background along with littermate wild-type (WT) controls were acquired from the mouse mutant resource at The Jackson Laboratory, (JAX, Bar Harbor, Maine) in a colony maintained by the CHDI Foundation. αMHC^{Cre} (Myh6-Cre) were obtained from The Jackson Laboratory. BACHD and Myh6-Cre mice on the C57BL/6 background were bred to generate double transgenic, BACHD;Myh6-Cre (BMYO), with the mHtt floxed out in the cardiomyocytes (Fig 3.1). The following three genotypes were used in this study: WT, BACHD, and BMYO. Genotypes were confirmed by PCR of tail snips.

WT (n = 8), BACHD (n = 8), and BMYO (n = 8) male mice were group housed and kept in a 12:12 light/dark (LD) cycle with rodent chow provided *ad libitum*. Mice were examined with echocardiograms at 3 and 6 mo of age. After the last echocardiogram measurement, the heart and brain tissues of the mice were collected and morphologic and histological measurements were taken. All procedures followed guidelines of the National Institutes of Health and were approved by the UCLA Animal Research Committee.

RNA Extraction

WT, BACHD and BMYO mice (n = 3 per group) were used for gene expression analysis. Total RNA from the hearts were extracted using Trizol RNA isolation protocol (LifeTechnologies, Carlsbad, CA), then DNAse treated (TURBO DNA-free kit, Life Technologies) and column

purified (Pureline RNA Mini-kit, Life Technologies). RNA was used for Quantitative Real-Time PCR experiments described below.

Quantitative Real-Time PCR

One μg of total RNA was reverse transcribed using iScript^{TM} Reserve Transcription Supermix for RT-qPCR (Bio-Rad Laboratories). Quantitative real-time PCR (RT-qPCR) was performed using SYBR Green Mix (Applied Biosystems) on a CFX connect Real-Time System (Bio-Rad Laboratories). The gene expression was calculated using the $2^{-\Delta\Delta Ct}$ method.

To detect the human mHtt expression, primers for RT-qPCR were designed using the established protocol by Gray et al [121]. The forward primer recognized both endogenous mouse HD gene homolog and exogenous mhtt. Two reverse primers were designed to be species-specific. Forward: 5'-ATC TTG AGC CAC AGC TCC AGC CA-3'; reverse (human) 5'-GGC CTC CGA GGC TTC ATC AGG-3'; reverse (murine), 5'- TCT GAA AAC ATC TGA GAC TTC ACC AGA-3'. The primers used in this study also include the following: Myh6, Myh7, BNP, GATA4, Col1a, and Fibronectin (Qiagen).

Western blotting

Protein lysates from the heart and brain tissues were western blots were performed as previously described [13]. Immunoblots were probed with the anti-polyglutamine-expansion disease marker, 1C2 (1:1000, Chemicon), GAPDH (1:3000, GeneTex), and Fibronectin (1:500, Abcam) prepared in 5% blocking solution. To quantify, the protein levels were normalized to GAPDH.

Echocardiogram

WT, BACHD, and BMYO mice (n = 8 per genotype) were group housed and kept in a 12:12 light/dark (LD) cycle with rodent chow provided *ad libitum*. Mice were examined with echocardiograms at 3 and 6 mo of age. After the last echocardiogram measure, the heart and brain tissues of the mice were collected and morphologic and histological measurements were taken.

Echocardiograms were measured using a Siemens Acuson Sequoia C256 instrument equipped with a 15L8 15MHz probe (Siemens Medical Solutions, Mountain View, CA) as previously described. Briefly, two-dimensional, M-mode echocardiography and spectral Doppler images enabled measurement of heart dimension and function (Left Ventricle (Lv) Mass), end-diastolic dimension (EDD), end-systolic dimension (ESD), posterior wall thickness (PWT), ventricular septal thickness (VST), Lv Ejection Fraction (Lv EF). The mice were sedated with 1% isoflurane vaporized in oxygen (Summit Anesthesia Solutions, Bend, OR) and HR was monitored using electrocardiogram to maintain physiological levels (between 450 and 650).

Trichrome Histology

Heart samples were harvested, perfused, and incubated in 4% paraformaldehyde at 4° C over night, followed by incubation in 30% sucrose in PBS at 4° C. The hearts were removed from the sucrose solution and embedded in Tissue Tek O.C.T. (Sakura Finetek). Frozen whole-heart blocks were sectioned at 8-10 μm thickness with a cryostat (Leica), mounted on Superfrost slides

(Fisherbrand), and stained with Masson's Trichrome kit (Sigma-Aldrich). Masson's Trichrome-stained heart with the aid of Image J software.

Behavioral studies

Locomotor activity was recorded from single-caged mice with infrared motion sensors using our established protocols [127]. Locomotor activity was recorded in 3-min bins, and 10 days of data were averaged for analysis. The 10 days of activity data collected just before the motor performance tests was used. Analyzing the data, the period and rhythmic strength was determined as previously described [10,26,127]. The periodogram analysis used a χ^2 test with a threshold of 0.001 significance, from which the amplitude of the periodicities was determined at the circadian harmonic to obtain the rhythm power. The amount of cage activity over a 24-h period was averaged over 10 days and reported here as the hourly arbitrary units (au/h). The number of activity bouts and the average length of bouts were determined using Clocklab (Actimetrics), where each bout was counted when activity bouts were separated by a gap of 21 min (maximum gap: 21 min; threshold: 3 counts/min).

The grip strength test was used to measure neuromuscular function as maximal muscle strength of forelimbs. The grip strength ergometer (Santa Cruz Biotechnology, Santa Cruz, CA) was set up on a flat surface with a mouse grid firmly secured in place. Peak mode was utilized to enable measurement of the maximal strength exerted. Mice were tested in their active phase under dim red light (3 lux), and prior to testing, mice were acclimated to the testing room. Mice underwent five trials with an inter-trial interval of at least two minutes. For each trial, a mouse was lowered

slowly over the grid, and only its forepaws were allowed to grip the grid. While the mouse was steadily pulled back, the experimenter ensured the mouse remained horizontal until the mouse was no longer able to grip the grid. The maximal grip strength value of the mouse was recorded each trial. The grid was cleaned with 70% ethanol and allowed to dry before testing each mouse cohort. The maximum value obtained per animal is reported as maximal strength divided by bodyweight.

The challenging beam test was used to characterize the motor deficits of BACHD mutant mice in previous studies [10,127]. The beam narrows in 4 intervals from 33 mm > 24 mm > 18 mm > 6 mm, with each segment spanning 253 mm in length. The home cage of each mouse is put on the end of the beam as the motivating factor. In this study, animals were trained on the beam for 5 consecutive trials for two consecutive days. During each trial, each mouse was placed on the widest end of the beam and allowed to cross with minimal handling by the experimenter. On the testing day, a metal grid (10 Å~ 10 mm spacing, formed using 19-gauge wire) was overlaid on the beam. This overlaid grid increased the difficulty of the beam traversal task and provided a visual reference for foot slips made while crossing the grid. Each mouse was subjected to 5 consecutive trials conducted during their active (dark) phase. Trials were recorded by a camcorder under dim red-light conditions (2 lux), supplemented with infrared lighting for video recording. The videos were scored post hoc by 2 independent observers for the number of missteps (errors) made by each mouse. The observers were masked as to the treatment group of the mice that they were scoring. An error was scored when any foot dipped below the grid. The

number of errors was averaged across the 5 trials per mouse to give the final reported values. The apparatus was cleaned with 70% alcohol and allowed to dry completely between trials.

Results:

Genetic reduction of mHTT in the cardiomyocyte

To determine whether genetically reducing mHtt expression from the cardiomyocytes can rescue cardiovascular phenotypes observed in the BACHD mice, we crossed BACHD mice with Myh6-Cre mice and generated three genotypes including WT, BACHD, BACHD;Myh6-Cre (BMYO) (Fig 3.1). We used these mice to confirm the reduction of mHtt mRNA and protein levels in the cardiomyocytes (Fig 3.2). In the heart, there were significant differences in the mRNA expression (one way ANOVA: $F_{(2)} = 125.5$. $P<0.001$) with the levels of human mHtt significantly reduced in the BMYO hearts compared to the BACHD (Tukey: $q = 18.584$, $P < 0.001$) (Fig 3.2). In the striatum, there were overall significant differences in expression (one way ANOVA, $F_{(2)} = 87.706$, $P < 0.001$), but there were no differences between the expression in BACHD and BMYO groups (Tukey: $q = 0.853$, $P = 0.824$) (Fig 3.2). There were no differences between the three groups in expression of endogenous mouse Htt in the heart ($F_{(2)} = 2.045$, $P = 0.210$) or striatum ($F_{(2)} = 0.852$, $P = 0.473$).

We used western blots to measure polyglutamine-expansion in the heart and striatum of the three genotypes (Fig 3.2). In the heart, there were significant differences in the 1C2 protein (one way ANOVA: $F_{(2)} =162.549$, $P <0.001$) with the levels of the expansion significantly reduced in the

BMYO hearts compared to the BACHD (Tukey: $q = 20.801$, $P < 0.001$). In the striatum, there were overall significant differences in 1C2 expression (one way ANOVA: $F_{(2)} = 27.098$, $P < 0.001$), but there were no differences between the expression in BACHD and BMYO groups (Tukey: $q = 2.197$, $P = 0.334$).

In summary, we found a significant reduction (92%) in the mHtt expression in the BMYO hearts compared with the BACHD hearts, but not in the striatum. Consistent with the mRNA results, BMYO mice had about 89% reduction of the polyglutamine expansion marker 1C2 in the hearts compared with the BACHD mice.

The genetic reduction of the mHtt expression improves some cardiovascular functions in BMYO mice.

To assess changes in the cardiac structure and function of the three lines of mice, we utilized echocardiograms at 3 and 6-month age. Consistent with our earlier data (Chapter 2), at 3 months of age, there were few significant differences between the 3 genotypes (Table 7). At this age, the Lv of the mutants exhibited an increased mass (not significantly) and the BACHD exhibited a reduced ejection fraction ($P = 0.035$) compared to the other groups. At 6 mo of age (Fig 3.3; Table 7), both the BACHD and the BMYO exhibited enlarged left ventricle. This feature of the BACHD was not altered by the loss of the mHtt. On the other hand, the ejection fraction and heart rate was reduced compared to WT in the BACHD but not in the BMYO. For both of these parameters, the measurements from the BMYO looked more like WT. While the heart's contractility measurements (Lv fractional shortening) did not differ among all three genotypes

(Fig 3.3), there was a clear trend for a reduction in the BACHD compared to the other groups. Overall, at the age points examined, most of the echocardiogram parameters did not vary significantly. The EF refers to the percentage of blood that is pumped out of a filled ventricle with each heartbeat and this measure appeared to be most sensitive to the levels of mHtt in the cardiomyocytes.

The reduction of mHtt impacted gene expression within the BMYO hearts.

We examined the mRNA expression of disease markers in the hearts at 6-month of age using RT-qPCR (Fig 3.4; Table 8). We found that collagen 1a (Col1a) mRNA expression was significantly higher level in the BACHD hearts compared to WT although there was no significant difference between WT and BMYO.

Next, we looked at the expression of several genes important in cardiomyocyte development including Myh6, Myh7 and GATA4. These genes are known to be up-regulated in response to injury or cardiomyocyte remodeling [128–130]. We found significant increases in the expression of Myh6 and GATA4 in the hearts of the BACHD and found that this up-regulation was not seen in the BMYO line. Finally, we looked at expression of brain natriuretic peptide (BNP), which is a hormone secreted by cardiomyocytes in the heart ventricles in response to stretching. Again we found that the BACHD mutants exhibited higher expression while the BMYO line showed much lower expression. Together this data indicates that, at least transcriptionally, the BACHD hearts were under stress and that these changes were reversed in the BMYO line.

The reduction of mHtt may have reduced fibrosis within the BMYO hearts.

To assess the cardiac structure of the hearts, we sacrificed the mice at about 6 mo of age and processed their hearts and used Masson's Trichrome to visualize fibrotic tissue (Fig 3.5). We did not detect any fibrotic staining in the WT hearts, while both BACHD and BMYO hearts showed small fibrosis on the edges of the hearts. These fibrotic regions remain to be quantified. Similarly, western blots were used to measure the protein levels of fibronectin. The concentration of the anti-sera still needs to be quantified.

The reduction of mHtt in the heart improved some aspects of motor behavior.

There is compelling evidence that physical activity is an sensitive biomarker for chronic cardiovascular disease [131,132]. Therefore, in our final experiment, we sought to determine whether the genetic reduction of mHtt expression in the cardiomyocytes had beneficial impact on motor function in the BACHD mice using two measures: overall physical activity and grip strength (Fig 3.6; Table 9). We found that both BACHD and BMYO exhibited a significant reduction in activity over 24 hr compared to WT but that the BMYO line exhibit more activity than BACHD. The strength of the daily rhythms as measured by power of the periodograms was similar in both of the mutant lines so the rhythmicity of the activity data was not impacted by the reduction in mHtt in the heart. Grip strength was improved in the BMYO line compared to BACHD alone. Finally, performance on the challenge beam as measured by errors made was actually highest in the BMYO line.

Overall, the two parameters that have been suggested as biomarkers of cardiovascular function (total activity, grip strength) were improved by the reduction of mHtt in the heart.

Discussion:

As described in Chapter 1, both the clinical and preclinical research indicate that cardiovascular dysfunction should be considered a core symptom of at least a subset of HD patients. There is some evidence for cardiomyopathy, but these is even stronger evidence for dysautonomia (dysfunctional autonomic nervous system, ANS) in HD patients that can be detected early in the disease progression. Mutant huntingtin (mHTT) is ubiquitously expressed so the cardiomyopathy could be the result of deficits in the cardiomyocytes themselves and/or in the dysautonomia driven by the nervous system. In this study, we utilized the BACHD mouse model that allows specific reduction of the mHtt expression in the cardiomyocytes when crossed with the Myh6-Cre mouse line. Our data confirmed successful reduction in the mHTT mRNA and protein levels of the BMYO hearts by close to 90% (Fig 3.2). The Cre-driven recombination would have occurred early in development so that the BMYO mice that we evaluated would have had greatly reduced mHtt from the heart with high levels of mHtt in the brain. This genetic construct gives us a unique model to evaluate the contribution of the mHtt in the cardiomyocytes to the cardiovascular disease associated with HD.

One limitation of our approach is the possibility that toxicity of the prolonged Cre expression to the hearts. It has been suggested that prolonged Cre expression driven by the α-myosin heavy chain promoter can be cardiotoxic [133,134]. Unlike the BACHD mice that can live up to 18

months [10,135], we observed that most of BMYO mice did not survive longer than a year which may be due to cardiotoxicity (data not shown).

We examined the cardiovascular function and structure using echocardiograms in all three genotypes at 6-month of age. Most of the functional echo parameters did not vary between the genotypes (Table 7). There were two notable exceptions. As previously observed (Chapter 2), the Lv mass of the BACHD hearts was larger than WT. The divergence between the genotypes was already seen at 3 months but was not significant until 6 months of age. This hypertrophy was also observed in the BMYO hearts suggesting that the driver was not the mHtt in the cardiomyocytes. In addition, Lv ejection fraction (EF) was reduced in the BACHD while the EF of the BMYO heart was comparable to comparable to the WT levels (Fig 3.3). The EF refers to the percentage of blood that is pumped out of a filled ventricle with each heartbeat. It is the relation between the amount of blood expelled during each cardiac cycle relative to the size of the ventricle. It is important to note that a Lv EF of 65 – 75% is considered normal under physiologic loading conditions for mice, with an EF of below 65% being considered reduced. So even the BACHD hearts were still working at functional levels at the 6 mo time point. The findings with Lv EF were closest to our predictions for a cardiomyopathy driven by mHtt in the heart. The FS % exhibited a similar trend but the differences were not significant. Perhaps we needed to wait to an older age to see more robust differences with the echocardiogram. Prior work indicated that the EF of the BACHD hearts steadily declined with age after the 6 mo time point (Chapter 2) so we are looking at the peak of cardiac output. Taken together, these

functional data suggest that reduced mHtt expression in the cardiomyocytes help improve Lv EF in the BMYO mice.

In prior work examining the hearts of middle-aged BACHD mice (>12 mo), we found striking fibrosis as measured by trichrome staining (Chapter 2). In the present study, we visually observed some fibrotic regions in the BACHD and BMYO mouse hearts, but not in the WT (Fig 3.5). We were unable to quantify the possible differences in staining before the COVID19 research stoppage. Interestingly, the Col1a mRNA expression level in the BMYO hearts was significantly reduced compared to BACHD (Fig 3.4). Therefore, we expect to similar differences in fibrosis as measured by trichrome staining. An increase in fibrosis in the heart could explain the reduction in the ejection fraction found in the echo data. Histological studies have suggested that myocardial fibrosis can be an important driver of a reduction in EF [136,137]. We also looked at the expression of several genes important in ventricular remodeling including Myh6, Myh7 and GATA4. These genes are known to be up-regulated in response to injury or cardiomyocyte remodeling [128–130]. We found significant increases in the expression of Myh6 and GATA4 in the hearts of the BACHD and found that this up-regulation was not seen in the BMYO line. We examined expression of brain natriuretic peptide (BNP), which is a hormone secreted by cardiomyocytes in the heart ventricles in response to stretching [138,139]. Again we found that the BACHD mutants exhibited higher expression while the BMYO line showed much lower expression. Together this data indicates that, at least transcriptionally, the BACHD hearts were under stress and that these changes were reduced in the BMYO line.

Finally, we looked at impact of the cross on behavioral markers of cardiovascular health. In humans, there is strong evidence that grip strength provides a biomarker for cardiovascular function [131,132,140]. For example, a recent study from the Sattar's group examined the associations of objectively measured grip strength (GS) with incident heart failure (HF) [141]. Using the UK Biobank dataset, the authors evaluated data from 374,493 individuals. During 4 years, 631 HF events occurred in those with GS data. Higher CRF was associated with 18% lower risk for HF (hazard ratio [HR], 0.82; 95% CI, 0.76-0.88) per 1-metabolic equivalent increment increase and higher GS was associated with 19% lower incidence of HF risk (HR, 0.81; 95% CI, 0.77-0.86) per 5-kg increment increase. When GS was standardized, the HR for GS was 0.65 per 1-SD increment (95% CI, 0.58-0.72). While this data is correlational, the literature indicates that objective measurements of physical function (GS) are strongly associated with lower HF incidence. In this study, we found that grip strength was reduced in the BACHD compared to WT and that this measure was improved by the excision of the mHtt. Overall, physical activity in this case measured by total activity over 24 hr followed the same trend. Both the mutant groups exhibited the reduction in the strength of the rhythm as measured by power (Fig 3.6). Most other rhythmic parameters were not improved by the reduction of the mHtt from the heart. The central circadian clock is based in the hypothalamus so improvements in circadian output were not expected from this cross.

In summary, the clinical and preclinical research indicate that cardiovascular dysfunction should be considered a core symptom of at least a subset of HD patients. There is strong evidence for dysautonomia that can be detected early in the HD progression. There is also some evidence for cardiomyopathy and our results suggest that there is cardiac specific pathology in the BACHD pre-clinical model. Reducing mHtt specifically from cardiomyocytes did improve the Lv EF as measured by the echocardiogram, reduced the expression of several markers of heart disease, and improved a behavioral marker of cardiovascular health. We believe that this data argues that cardiomyopathy should be considered as part of the consequences of the HD mutation.

Discussion: Clinical significance and future directions

Cardiovascular (CV) disease is a leading cause of early death in the Huntington's disease (HD) patient population. Animal models are needed to understand how the mutant Htt causes pathology in the CV system in order to development new treatment strategies. In this thesis work, we first sought to determine if CV symptoms could be measured in the Q175 and BACHD mouse models of HD. In this work, we sought to test the dual hypotheses that cardiovascular dysautonomia can be detected early in disease progression in the Q175 and BACHD models and that this dysfunction varies with the daily cycle. We found overwhelming evidence for autonomic dysfunction including blunted daily rhythms in HR, reduced HRV, and almost a complete failure of the sympathetic arm of the ANS during the baroreceptor challenge. These were first demonstrations that these mouse models exhibited CV symptoms like the HD patients. Furthermore, they suggest that the disrupted circadian regulation could contribute to the pathology.

Next, we we sought to reduce mHtt expression in cardiomyocytes to ameliorate CV symptoms seen in the BACHD mice. Using this genetic reduction, we could improve some aspects of heart function and motor deficits in these mice. However, reducing mHtt in the cardiomyocytes was not sufficient to provide striking impact on the functional and structural changes in the BACHD mouse hearts. Our findings indicate that cardiovascular focused treatments may extend the health-span of the patients but the autonomic dysfunction will also need to be considered.

In HD clinical trials, antisense oligonucleotides (ASO) have shown promise to decrease the mHtt. For example, the drug candidate, RG6042 by Roche, is currently in the phase 3 trial investigating the safety and efficacy of long-term use in the HD patients. Intrathecal administration of this ASO therapy was effective at decreasing the total amount of mHtt measured in the cerebrospinal fluid by 40-60% [142]. It is yet unknown how much of reduction is required to result in the positive effect on the disease progression. The efficient way to measure the clinical outcomes is still unclear but CV measures like HRV could provide inexpensive biomarkers for treatment efficacy. These clinical studies are heavily relying on the limited studies with the mouse models. Thus, many questions of study remain to be pursued in the future preclinical studies to develop the effective therapeutic interventions and validate the effectiveness of the approach.

In investigating the impact of TRF on the gene expression rhythms in the BACHD mouse hearts (Appendix), Klf15 exhibited the largest changes among the genes of interest. Many studies have documented that Klf15 plays a key role in regulating oscillatory genes in the heart [80] and cardiac hypertrophy [143,144]. Our data show that feeding schedule induced the amplitudes of the Klf15 expression rhythms in BACHD hearts. Echocardiograms demonstrated that BACHD mice had larger left ventricular mass already at 3 mo compared with WT controls (See Chapter 2). Interesting findings from studies in this work suggest that potential therapeutic strategies that aim to modulate the expression of Klf15 to boost circadian output as well as to prevent hypertrophy in the HD. Furthermore, the cardiovascular symptoms in HD patients should be

better understood in the future studies. Underlying mechanisms of many CV symptoms including autonomic dysfunction, and cardiac hypertrophy need to be delineated to further advance the therapeutic approaches to prevent mortality and to ultimately treat this devastating disease, HD.

Appendix: Impact of time-restricted feeding on the gene expression rhythms in the BACHD mouse hearts

Introduction:

HD patients in the early stages of the disease progression exhibit low HRV [18,19,21], which is a general indication of poor cardiovascular outcomes [35,117,118]. The decreased HRV was also observed in the BACHD mouse line [10]. In our recent study, we have shown that time-restricted feeding (TRF) improves activity, motor performance, and sleep rhythms in the BACHD [74]. Additionally, TRF had the most robust effect on HRV, suggesting enhanced autonomic function in the BACHD mice [74]. Using *in vivo* imaging of BACHD and WT PER2::LUC mice, we showed that TRF elevated the amplitude and shifted the phase of the rhythm in the heart but not in the SCN. These findings demonstrated that TRF ameliorates various symptoms and boosts the circadian rhythms in the BACHD mice. In this appendix, we investigated the impact of TRF on the gene expression rhythms in the BACHD mouse hearts by collecting tissue at six time points around the 24-hr cycle. We focused on a set of the target genes including core clock, circadian output, clock-driven transcription factors, and metabolic genes.

Methods:

Time-restricted feeding (TRF)

BACHD and WT mice were first entrained to a 12:12 h Light Dark (LD) cycle for at least 2 weeks prior to any treatment. Experimental animals were then exposed to one of two feeding conditions: food available *ad libitum* (ad lib) or food available for 6 h during the middle of the active phase during zeitgeber time (ZT) 15-21. By definition, ZT 12 is the time when the lights are turned off when the mice are in an LD cycle. In this study, four groups were used with two genotypes, BACHD and WT, and two feeding conditions (ad lib or TRF). Single-housed mice were in a cage equipped with a custom-made programmable food hopper that could temporally control access to food (standard chow) and prevent food consumption during restricted times. Mice are coprophagic, and the mice were not moved to new cages between their daily feeding and fasting cycles. It is possible that the mice consumed their own feces during the fast interval. These cages were also equipped with an infrared (IR) motion detector to give us the ability to measure cage activity. The mice were held in these conditions for a total of 3 months (from 3 mo to 6 mo of age) [74].

Time course tissue collection

In order to measure the gene expression of the target genes around the clock, the heart tissues of the mice (n=4 per group) were quickly collected at ZT 2, 6, 10, 14, 18, and 22 after the last behavioral measurement. Thus, the total of 24 mice were used for each group, resulting in 96 samples harvested.

Quantitative Real-Time PCR

Total RNA was extracted from the heart tissues using our lab's established protocol consistent with previous chapters. One μg of total RNA was reverse transcribed using iScript^{TM} Reserve Transcription Supermix for RT-qPCR (Bio-Rad Laboratories). Quantitative real-time PCR (RT-qPCR) was performed using SYBR Green Mix (Applied Biosystems) on a CFX connect Real-Time System (Bio-Rad Laboratories). The gene expression was calculated using the $2^{-\Delta\Delta Ct}$ method. The expression of the target genes was normalized to GAPDH and the relative expression was analyzed. The primers used in this study are the following: Bmal1, Per2, Dbp, PPAR γ, SIRT1, Pdk4, Ucp3, Klf15, and GAPDH (Qiagen).

Statistical Analysis

We were interested in determining if TRF can alter the rhythms in gene expression measured from the heart of WT and BACHD mice. Treated BACHD mice (TRF group) were compared to age-matched untreated BACHD mice (ad lib group) in all experiments. The sample size per group was determined by both our empirical experience with the variability in the prior measures in the BACHD mice and a power analysis (SigmaPlot, SYSTAT Software, San Jose, CA) that assumed a power of 0.8 and an alpha of 0.05. To determine the impact of the treatment on temporal expression waveforms, we used a two-way analysis of variance (2-way ANOVA) with treatment and time as factors. We also used a 2-way ANOVA to assess the impact of the treatment on the amplitude and phase of the rhythms. Pairwise Multiple Comparison Procedures were made using the Holm-Sidak method. Statistical analysis was performed using SigmaPlot. Data were examined for normality (Shapiro-Wilk test) and equal variance (Brown-Forsythe test). Between-group differences were determined significant if $p < 0.05$. All values are reported as

group mean ± standard error of the mean (SEM). We report the t- or F-values as well as the degrees of freedom. Future analysis will utilize the JTK Clock software [145].

Results

Please see Figure Appendix 1.

PER2: In WT mice, we used a 2-way ANOVA to evaluate expression using time and genotype as factors. We found significant effects of time ($F_5 = 72.252$, $P < 0.001$) but not treatment ($F1 = 2.973$, $P = 0.093$). There was a significant interaction between time and treatment ($F_5 = 2.827$, $P = 0.03$). Using the Holm-Sidak multiple comparison procedure, there was a significant impact of treatment at ZT 14 ($t = 3.543$, $P = 0.001$).

In the BACHD mice, we found significant effects of time ($F_5 = 47.037$, $P < 0.001$) but not treatment ($F_1 = 0.733$, $P = 0.398$). There was a significant interaction between time and treatment ($F_5 = 3.246$, $P = 0.016$). Using the Holm-Sidak multiple comparison procedure, none of the phases showed a significant impact of treatment.

Finally, using a 2-way ANOVA to evaluate the amplitude (peak/trough) of the rhythms using genotype and treatment, we did not find any significant effect.

Therefore, our data indicate that all of the groups exhibited a robust rhythm in Per2 expression and TRF did significantly increase the expression of WT mice at ZT 14.

BMAL1: In WT mice, we used a 2-way ANOVA to evaluate expression using time and genotype as factors. We found significant effects of time ($F_5 = 76.719$, $P < 0.001$) but not treatment ($F_1 = 1.231$, $P = 0.275$). There was not a significant interaction between time and treatment ($F_5 = 1.304$, $P = 0.284$). Using the Holm-Sidak multiple comparison procedure, there was a significant impact of treatment at ZT 2 ($t = 2.599$, $P = 0.013$).

In the BACHD mice, we found significant effects of time ($F_5 = 35.830$, $P < 0.001$) but not treatment ($F_1 = 3.540$, $P = 0.068$). There was a significant interaction between time and treatment ($F_5 = 3.398$, $P = 0.013$). Using the Holm-Sidak multiple comparison procedure, there was a significant impact of treatment at ZT 2 ($t = 4.106$, $P < 0.001$).

Finally, using a 2-way ANOVA to evaluate the amplitude (peak/trough) of the rhythms using genotype and treatment as factors. We did not find a significant impact of genotype ($F_1 = 0.380$, $P = 0.549$) but there was a significant effect of treatment ($F_1 = 4.940$, $P = 0.046$).

Therefore, our data indicate that all of the groups exhibited a robust rhythm in Bmal1 expression and TRF did significantly increase the expression of WT and BACHD mice at ZT 2. The TRF treatment significantly increased the amplitude of the rhythms.

DBP: In WT mice, we used a 2-way ANOVA to evaluate expression using time and genotype as factors. We found significant effects of time ($F_5 = 19.601$, $P < 0.001$) but not treatment ($F_1 = 0.210$, $P = 0.649$). There was not a significant interaction between time and treatment ($F_5 =$

1.577, P = 0.191). Using the Holm-Sidak multiple comparison procedure, there was a significant impact of treatment at ZT 6 (t = 2.529, P = 0.016).

In the BACHD mice, we found significant effects of time (F_5 = 29.027, P < 0.001) but not treatment (F_1 = 2.022, P = 0.164). There was a significant interaction between time and treatment (F_5 = 3.743, P = 0.008). Using the Holm-Sidak multiple comparison procedure, there was a significant impact of treatment at ZT 6 (t = 3.865, P < 0.001) and ZT 10 (t = 2.136, P < 0.040).

Finally, using a 2-way ANOVA to evaluate the amplitude (peak/trough) of the rhythms using genotype and treatment as factors. We did not find a significant impact of genotype (F_1 = 2.034, P = 0.179) but there was a significant effect of treatment (F_1 = 12.107, P = 0.005).

Therefore, our data indicate that all of the groups exhibited a robust rhythm in Dbp expression and TRF did significantly increase the amplitude of the rhythms of expression in WT at ZT 6 and BACHD at ZT 6 & 10.

KLF15: In WT mice, we used a 2-way ANOVA to evaluate expression using time and genotype as factors. We found significant effects of time (F_5 = 6.068, P < 0.001) but not treatment (F_1 = 1.975, P = 0.164). There was a significant interaction between time and treatment (F_5 = 3.882, P = 0.006). Using the Holm-Sidak multiple comparison procedure, there was a significant impact of treatment at ZT 14 (t = 2.558, P = 0.015) and ZT 18 (t = 3.493, P = 0.001).

In the BACHD mice, we found significant effects of time ($F_5 = 8.130$, $P < 0.001$) but not treatment ($F_1 = 0.359$, $P = 0.553$). There was a significant interaction between time and treatment ($F_5 = 6.748$, $P < 0.001$). Using the Holm-Sidak multiple comparison procedure, there was a significant impact of treatment at ZT 10 ($t = 2.383$, $P = 0.023$) and ZT 14 ($t = 4.741$, $P < 0.001$).

Finally, using a 2-way ANOVA to evaluate the amplitude (peak/trough) of the rhythms using genotype and treatment as factors. We found a significant impact of genotype ($F_1 = 5.210$, $P = 0.041$) and treatment ($F_1 = 28.126$, $P = 0.001$).

Therefore, our data indicate that all of the groups exhibited a robust rhythm in Klf15 expression and TRF did significantly increase the amplitude of the rhythms of expression in WT at ZT 14 & 18 and BACHD at ZT 10 & 14.

PPAR γ: In WT mice, we used a 2-way ANOVA to evaluate expression using time and genotype as factors. We did not find significant effects of time ($F_5 = 0.379$, $P = 0.860$) or treatment ($F_1 = 0.669$, $P = 0.419$). There was not a significant interaction between time and treatment ($F_5 = 1.226$, $P = 0.317$). Using the Holm-Sidak multiple comparison procedure, there were no significant impact of treatment at any phase.

In the BACHD mice, we did not find significant effects of time ($F_5 = 1.378$, $P = 0.255$) or treatment ($F_1 = 1.043$, $P = 0.314$). There was not a significant interaction between time and treatment ($F_5 = 1.675$, $P = 0.166$). Using the Holm-Sidak multiple comparison procedure, there were no significant impact of treatment at any phase.

Finally, using a 2-way ANOVA to evaluate the amplitude (peak/trough) of the rhythms using genotype and treatment as factors. We did not find a significant impact of genotype ($F_1 = 0.681$, $P = 0.425$) and treatment ($F_1 = 2.842$, $P = 0.116$).

Therefore, our data indicate that none of the groups exhibited a robust rhythm in PPAR gamma expression and TRF did not alter the amplitude of the rhythms of expression.

SIRT1: In WT mice, we used a 2-way ANOVA to evaluate expression using time and genotype as factors. We did not find significant effects of time ($F_5 = 1.507$, $P = 0.212$) or treatment ($F_1 = 0.006$, $P = 0.937$). There was not a significant interaction between time and treatment ($F_5 = 0.240$, $P = 0.942$). Using the Holm-Sidak multiple comparison procedure, there were no significant impact of treatment at any phase.

In the BACHD mice, we found a significant effect of time ($F_5 = 3.546$, $P = 0.010$) but not treatment ($F_1 = 0.017$, $P = 0.898$). There was not a significant interaction between time and treatment ($F_5 = 2.338$, $P = 0.062$). Using the Holm-Sidak multiple comparison procedure, there were no significant impact of treatment at any phase.

Finally, using a 2-way ANOVA to evaluate the amplitude (peak/trough) of the rhythms using genotype and treatment as factors. We did not find a significant impact of genotype ($F_1 = 0.654$, $P = 0.434$) or treatment ($F_1 = 2.962$, $P = 0.111$).

Therefore, our data indicate that only the BACHD exhibited a rhythm in Sirt1 expression and TRF was ineffective in altering the expression of this gene.

UCP3: In WT mice, we used a 2-way ANOVA to evaluate expression using time and genotype as factors. We found significant effects of time ($F_5 = 5.986$, $P < 0.001$) but not treatment ($F_1 = 2.561$, $P = 0.118$). There was not a significant interaction between time and treatment ($F_5 = 1.234$, $P = 0.314$). Using the Holm-Sidak multiple comparison procedure, there was not a significant impact of treatment at any phase.

In the BACHD mice, we found significant effects of time ($F_5 = 8.895$, $P < 0.001$) but not treatment ($F_1 = 1.301$, $P = 0.262$). There was not a significant interaction between time and treatment ($F_5 = 2.238$, $P = 0.072$). Using the Holm-Sidak multiple comparison procedure, there was a significant impact of treatment at ZT 10 ($t = 2.032$, $P = 0.050$) and ZT 14 ($t = 2.262$, $P < 0.030$).

Finally, using a 2-way ANOVA to evaluate the amplitude (peak/trough) of the rhythms using genotype and treatment as factors. We found no significant impact of genotype ($F_1 = 0.243$, $P =$

0.631) but there was a significant impact of treatment on the amplitude of the rhythms (F_1 = 6.413, P = 0.026).

Therefore, our data indicate that all of the groups exhibited a robust rhythm in UCP3 expression and TRF did not impact the amplitude of WT rhythms. On the other hand, TRF did increase the amplitude of the rhythm of expression in the BACHD at ZT 10 & 14.

PDK4: In WT mice, we used a 2-way ANOVA to evaluate expression using time and genotype as factors. We found not significant effects of time (F_5 = 2.362, P = 0.059) but there was an impact of treatment (F_1 = 5.954, P = 0.020). There was not a significant interaction between time and treatment (F_5 = 2.234, P = 0.072). Using the Holm-Sidak multiple comparison procedure, there was a significant impact of treatment at ZT 14 (t = 3.566, P = 0.001).

In the BACHD mice, we found significant effects of time (F_5 = 8.130, P < 0.001) but not treatment (F_1 = 0.359, P = 0.553). There was a significant interaction between time and treatment (F_5 = 6.748, P < 0.001). Using the Holm-Sidak multiple comparison procedure, there was a significant impact of treatment at ZT 10 (t = 2.383, P = 0.023) and ZT 14 (t = 4.741, P < 0.001).

Finally, using a 2-way ANOVA to evaluate the amplitude (peak/trough) of the rhythms using genotype and treatment as factors. We found a significant impact of genotype (F_1 = 5.210, P = 0.041) and treatment (F_1 = 28.126, P = 0.001).

Therefore, our data indicate that all of the groups exhibited a robust rhythm in PDK4 expression and TRF did significantly increase the amplitude of the rhythms of expression in WT at ZT 14 & 18 and BACHD at ZT 10 & 14.

Summary

Overall, time restricted feeding could alter gene expression rhythms in the heart of BACHD and WT mice.

First we examined rhythms in the core clock genes, Bmal1 and Per2. With this cohort of mice (6 months of age), we did not see a significantly reduced Per2 expression rhythm as we had seen using PER2::LUC driven bioluminescence (Chapter 2). We cannot explain this difference but also noted that these mice are less impacted by the mutation (see Chapter 4) than the original cohorts. All of the groups exhibited robust daily rhythms in the expression of Per2 and Bmal1. The TRF treated mice exhibited higher amplitude rhythms with peak expression at ZT 14 for Per2 and ZT 2 for Bmal1. Together this data shows that scheduled feeding can alter the amplitude the rhythm of the molecular circadian clockwork in the heart.

Next, we looked at the expression of two of the key molecular output genes: albumin D site-binding protein (Dbp) and kruppel-like factor 15 (KLF15). The mechanisms by which the circadian clock regulates the transcription of other genes has been particularly well studied for the Dbp gene. BMAL1 and CLOCK bind to E boxes in the promoter region of Dbp to control transcription [146]. The circadian regulation of this gene has been particularly well studied in cell culture but not much is known about its expression in the heart. Here we show that both WT and BACHD hearts exhibit robust rhythms and that TRF increased the amplitude of the expression rhythms. Prior work has shown that KLF15 governs a biphasic transcriptomic oscillation in the heart with a maximum ATP production phase and a remodeling and repair phase corresponding to the active and resting phase of a rodent [80]. Depletion of KLF15 in cardiomyocytes leads to a disorganized oscillatory behavior without day/night partition despite an intact core clock. Thus, KLF15 is a nodal connection between the clock and rhythmicity in the heart. In the heart, KLF15 in the heart plays a key role in controlling the transcription of cardiac metabolism during fasting [147] and plays a protective role in preventing hypertrophy [143]. Based on this past data, it is perhaps not surprising that TRF regulates the phase and amplitude of the rhythm in KLF15 in the heart. Together this data shows that TRF treatment effectively regulates expression of key circadian output genes.

As metabolism and mitochondrial function are known to be rhythmic in the heart, we examined the expression of a couple of genes linked to metabolism. Uncoupling protein 3 (UCP3) is a key protein involved in mitochondrial metabolism and function while pyruvate dehydrogenase

kinase-4 (PDK4) is critical for pyruvate oxidation. Both of these genes have been shown to be rhythmic in the heart in prior work [76] and we found robust rhythms in both genes. TRF increased the amplitude of gene expression in both of these genes.

Our experiments did turn up some unanticipated finding. In the liver, both PPAR γ and SIRT1 are rhythmic and are regulated by feeding schedules [148]. PPAR γ is known to regulate the BMAL1 gene expression and its deletion in the vasculature leads to decrease circadian variations in BP and HR [149]. Therefore, we were surprised to not be able to find a rhythm in expression in these gene nor did we see any evidence that TRF regulated the expression of these genes. We cannot explain these unexpected findings at this time.

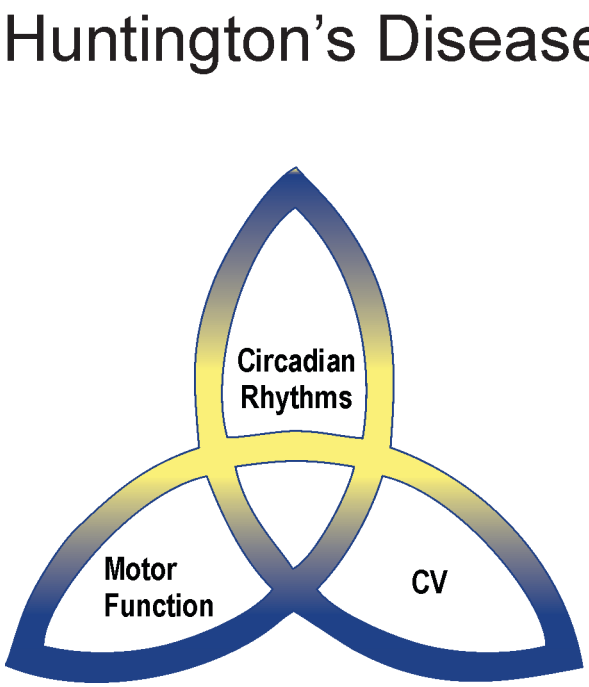

Figure 1. 1

Huntington's disease (HD) is traditionally considered a motor disease treated by neurologists. However, there is increasing evidence that HD patients and animal models exhibit cardiovascular (CV) symptoms including dysautonomia (dysfunctional autonomic nervous system, ANS). Dysautonomia has been well-characterized in PD, and we believe that it is also a core symptom of a subset of HD patients and may be usefully applied to segregate this patient population for tailored treatments. There is also a growing body of evidence that HD patients and animal models exhibit disruption in circadian timing although not in sleep homeostasis. In our work, we have been testing the hypothesis that dysfunction in the circadian system in HD contributes to the CV disease and, in this review, we will summarize our progress.

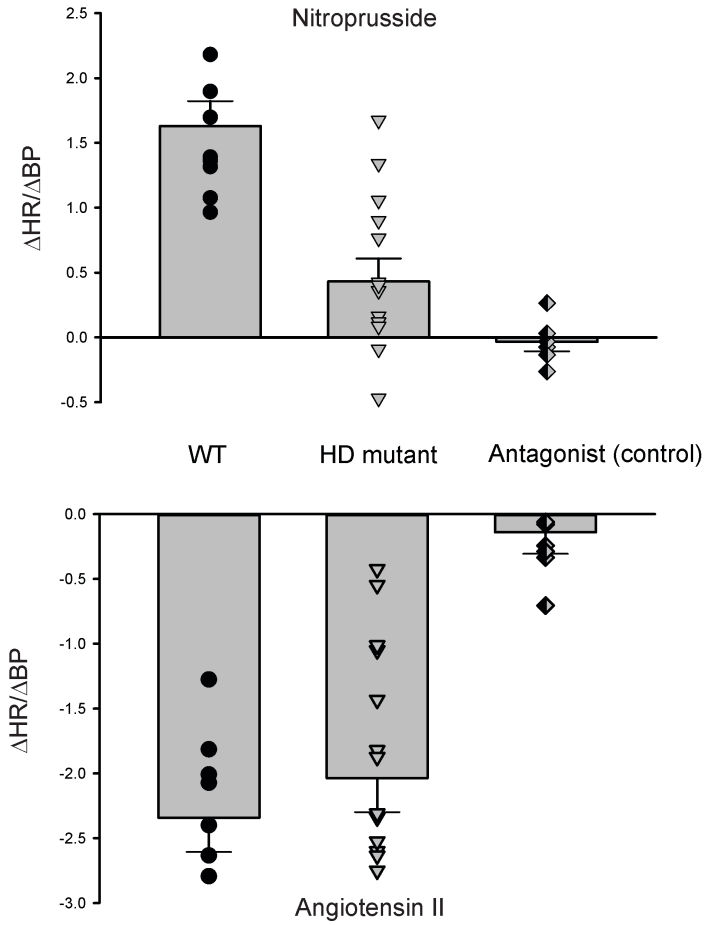

Figure 1. 2

Baroreceptor reflex is disrupted in mouse models of HD. In the baroreceptor reflex, changes in BP are detected by the baroreceptors and evoke compensatory changes in ANS. The Q175 and BACHD mutants showed a dramatically blunted response in HR to the transient hypotension induced by nitroprusside (NP) suggesting that the sympathetic branch has impaired. The effect of NP was blocked by a beta-adrenergic receptor blocker (β-blocker) propranolol. The Q175 mutants did not show a significantly altered response to transient hypertension induced by angiotensin II. HD patients complain of dizziness and light-headedness upon standing, all symptoms of baroreceptor dysregulation resulting in orthostatic hypotension. Data from [14,29].

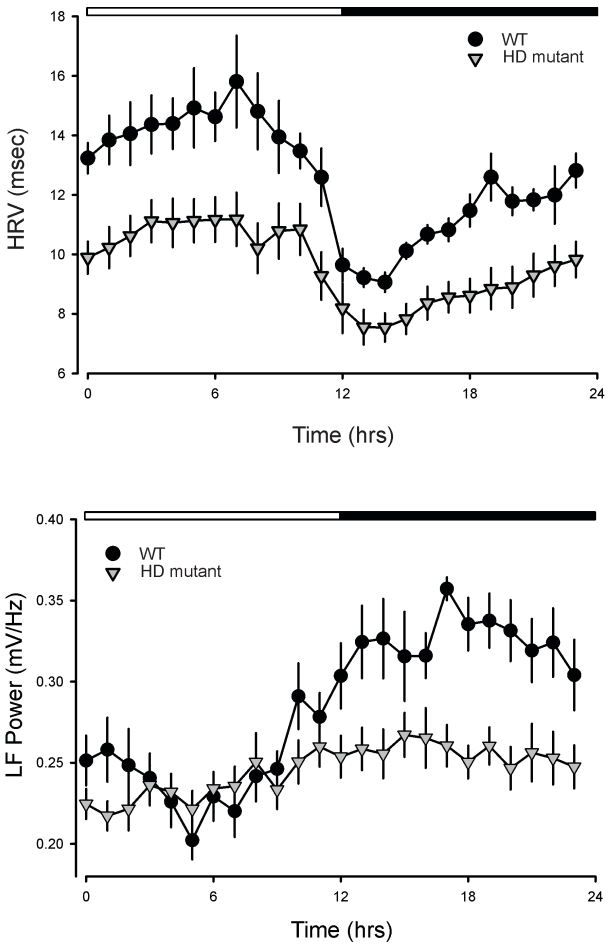

Figure 1. 3

HRV is a measure of variation in the beat-to-beat (R-R) interval that reflects the dynamic balance of sympathetic and parasympathetic control of heart function. Traditionally, HRV is an indication of CV health and low HRV proposed as a predictor for CV disease and mortality. One of the most commonly used methods for evaluation of HRV is power spectral density analysis in which high-frequency (HF) and low-frequency (LF) bands are extracted from the HRV signal, and the spectral power is calculated. Traditionally, the LF power is viewed as a measure of regulation by the sympathetic branch of the ANS, although it is more likely a general index of ANS function. We found robust daily and circadian rhythms in HRV and LP power in WT mice. As shown in the panels, HRV increased during sleep while LF power (sympathetic outflow) was higher when the mice were active. In the HD mutants (Q175), the HRV was low in young mutants and this reduction was largest during the rest phase. The power in the LF domain was significantly reduced in the young mutants with the biggest effects during the night. A similar reduction in HRV was previously observed in the BACHD line [10,13] as well as in the R6/1 model [41]. In HD patients, a similar decrease in HRV has also been reported during the presymptomatic and early stages of HD progression.

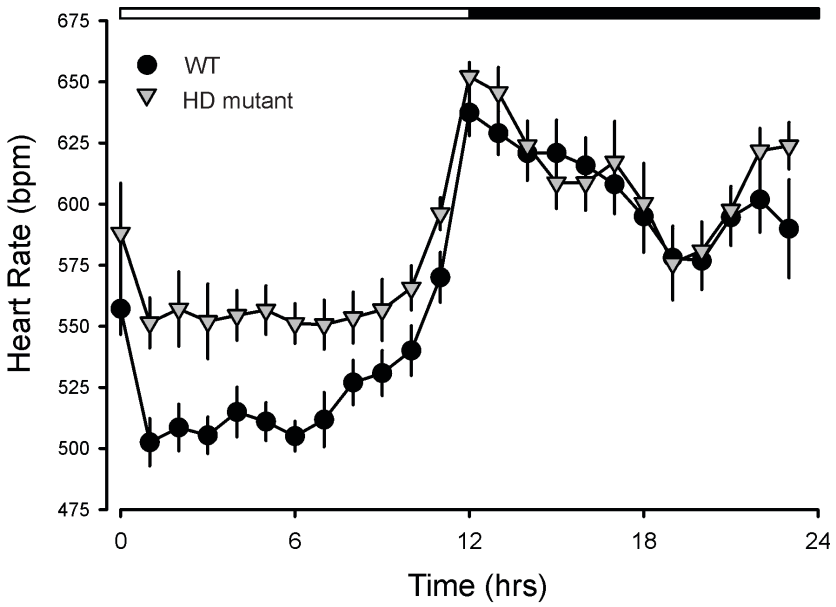

Figure 1. 4

HR varies dramatically with a daily cycle in which HR is high during the active part of the sleep/wake cycle. As measured by telemetry, HD mutants (BACHD and Q175) exhibited highly pronounced tachycardia during their normal sleep time, with high HR and reduced amplitude in the HR rhythm. These changes suggest that ANS disruption occurs early in disease progression in these mutant lines. In agreement, we also saw evidence in the BACHD of the circadian system failing to lower blood pressure (BP) during sleep [29]. The HR rhythm is also disrupted in R6/1 [41], R6/2 and HdhQ150 lines [46]. Therefore, overlapping data from several studies using different mouse models all found evidence for disrupted diurnal or circadian rhythms of HR. We have not seen evidence that this has been examined in HD patients, but the pre-clinical data supports 24-hr monitoring in patients.

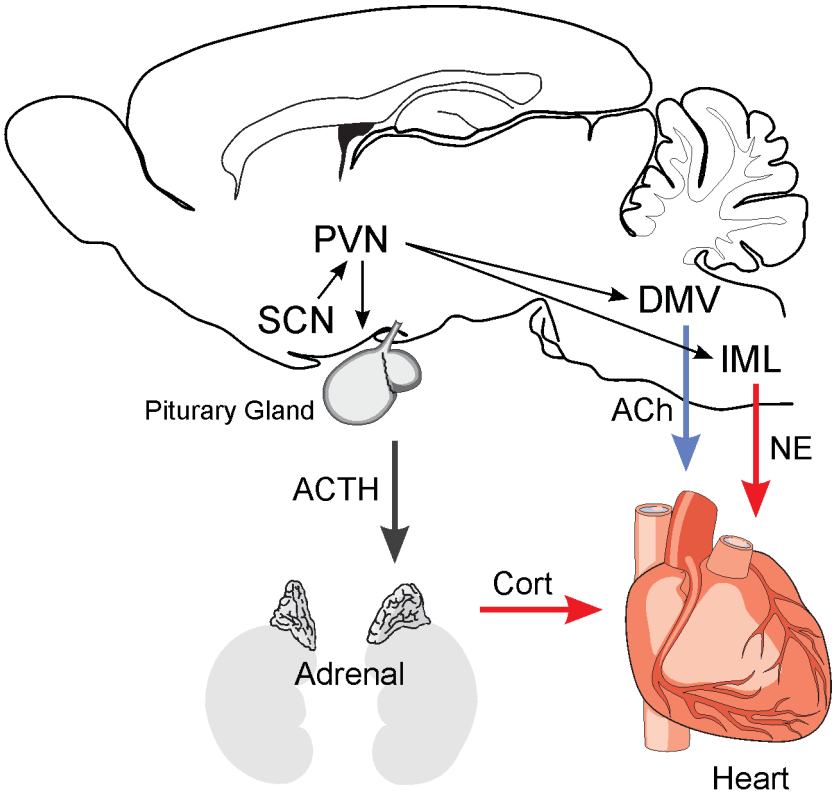

Figure 1. 5

The circuits involved in the generation of rhythms in HR and autonomic function are relatively well defined. The central circadian clock in the suprachiasmatic nucleus (SCN) orchestrates the peripheral clocks via ANS. It appears that separate populations of SCN neurons project to the paraventricular nucleus (PVN) and innervate pre-sympathetic and pre-parasympathetic cell populations. These separate pre-sympathetic and pre-parasympathetic neurons project to either the preganglionic sympathetic neurons in the intermediolateral (IML) column of the spinal cord or the preganglionic neurons of the dorsal motor nucleus of the vagus (DMV). There are axon collaterals of the pre-sympathetic PVN neurons in the nucleus tractus solitarius (NTS). Both pathways innervate the heart to regulate HR via release of acetylcholine (ACh) and norepinephrine (NE). Also, the SCN regulates the HPA axis and the secretion of cortisol. The glucocorticoid receptors are also potent regulators of CV function. In HD patients, there is evidence for the degeneration of neurons in the SCN as well the brain stem. There is also evidence for the strong expression of p62 immunopositive protein aggregates in axons of brainstem fiber tracts including the vagal nerve and the NTS [67].

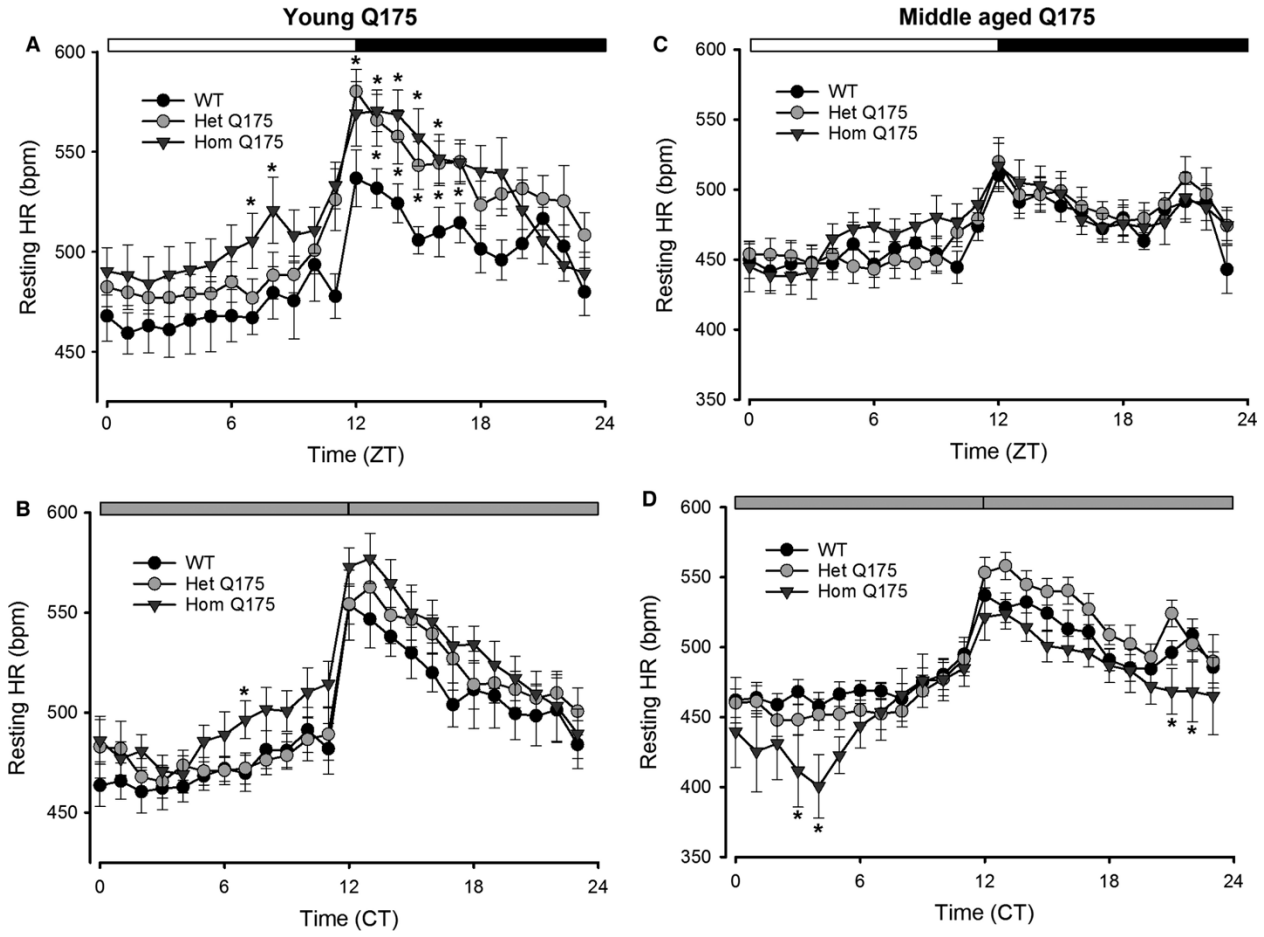

Figure 2. 1

Q175 mice exhibited altered diurnal and circadian resting HR rhythms. (A, B) The young Q175 exhibited significantly different resting HR rhythms under both LD and DD. The effects were most striking under LD conditions where the mutants showed high resting HR. (C, D) By middle age, this tachycardia reversed and we actually saw low resting HR in the Hom Q175 under DD conditions. Please see Table 1 for results of statistical tests. Asterisks indicate $P < 0.05$ between the genotypes at each of the hourly bins (ZT or CT).

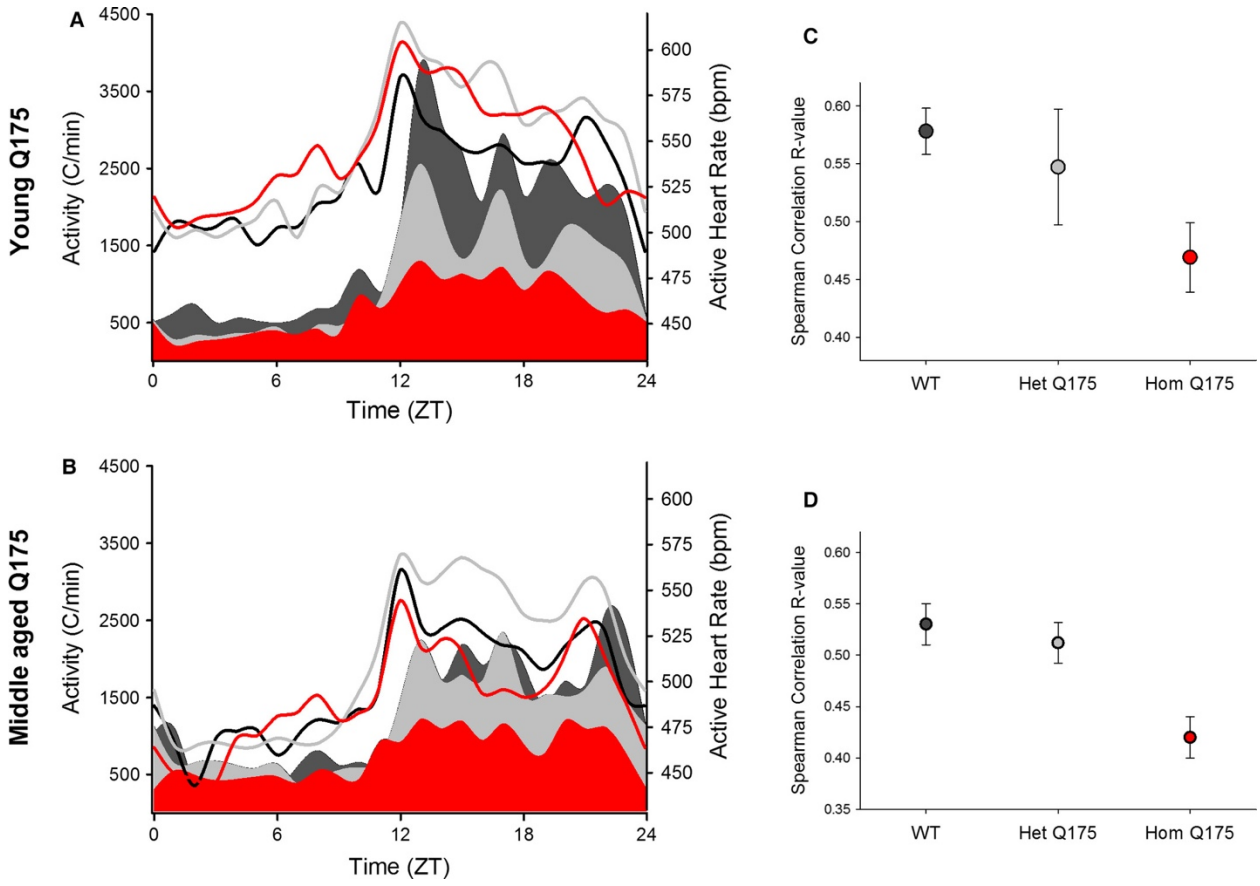

Figure 2. 2

Q175 mice exhibited an abnormal relationship between HR and activity. (A) The young adult Hom Q175 exhibited high HR even while they exhibited low levels of activity. (B) By middle age, the Hom Q175 exhibited lower HR and lower activity in the night. WT data shown with black lines (HR) and fill (activity); the Het Q175 data are shown with gray lines (HR) and fill (activity); the Hom Q175 data are shown with red lines (HR) and fill (activity). (C) Q175 homozygotes exhibited significant loss of correlation of HR with activity levels ($P < 0.001$) in young mice. (D) By middle age, differences are diminished by the effects of aging and the progression of autonomic pathology in the mutants. WT data shown with black lines (HR) and fill (activity); Het Q175 data shown with gray lines (HR) and fill (activity); Hom Q175 data shown with red lines (HR) and fill (activity). WT, wild-type.

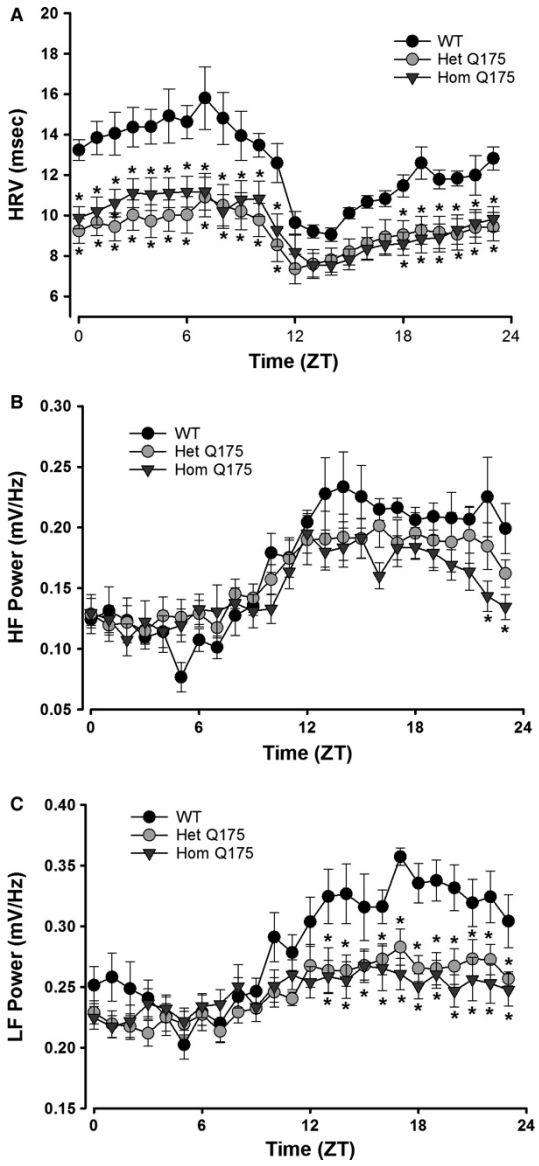

Figure 2. 3

Q175 mice exhibited low HRV as measured at 3 months. (A) The young Q175 (Hom, Het) exhibited significantly reduced HRV. Most phases of the daily cycle were impacted. (B) The HF domain (1.5–5.0 Hz) was largely unaltered except at 2 phases late in the night. (C) The LF domain (0.2–1.5 Hz) was reduced in the mutants (Hom, Het) throughout the night. Please see Table 1 for results of statistical tests. Asterisks indicate $P < 0.05$ between the genotypes at each of the hourly bins (ZT or CT).

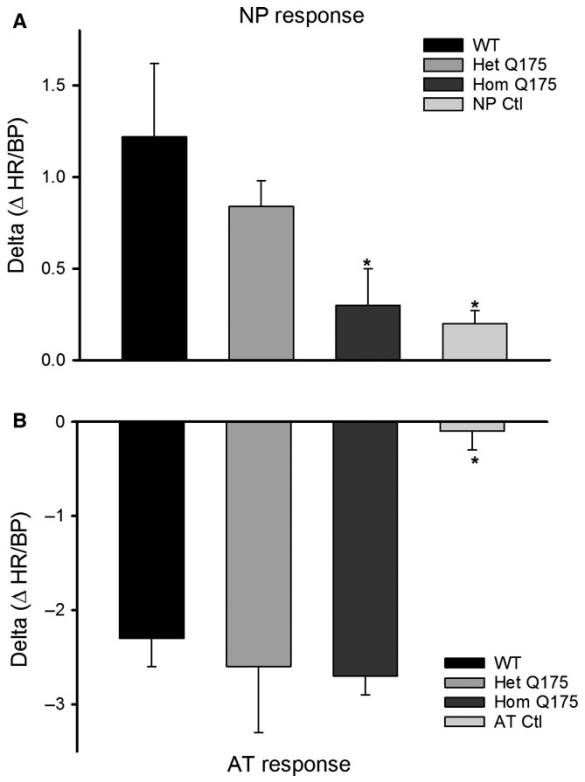

Figure 2. 4

Baroreceptor evaluations were used to determine the autonomic responsivity to blood pressure perturbations (WT, n = 7; Het, n = 6; Hom, n = 9). As expected, the WT mice had normal reflex responses. (A) When the blood pressure was transiently lowered with nitroprusside (NP, 40 lg/kg), the heart rate was elevated. (B) When the blood pressure was transiently increased with angiotensin II (AT, 4 lg/kg), the heart rate dropped in compensation. The impact of ATII and NP were blocked by pretreatment with sympathetic and parasympathetic receptor antagonists (750 lg/kg propranolol, 75 lg/kg glycopyrrolate). The Hom Q175 mice had very blunted HR responses to NP (n = 9). While some of the Het Q175 (2 out of 6 animals) showed a greatly reduced response to the NP injection, the overall NP-response was not significantly different from WT. WT, wild-type, ATII, administration of angiotensin II.

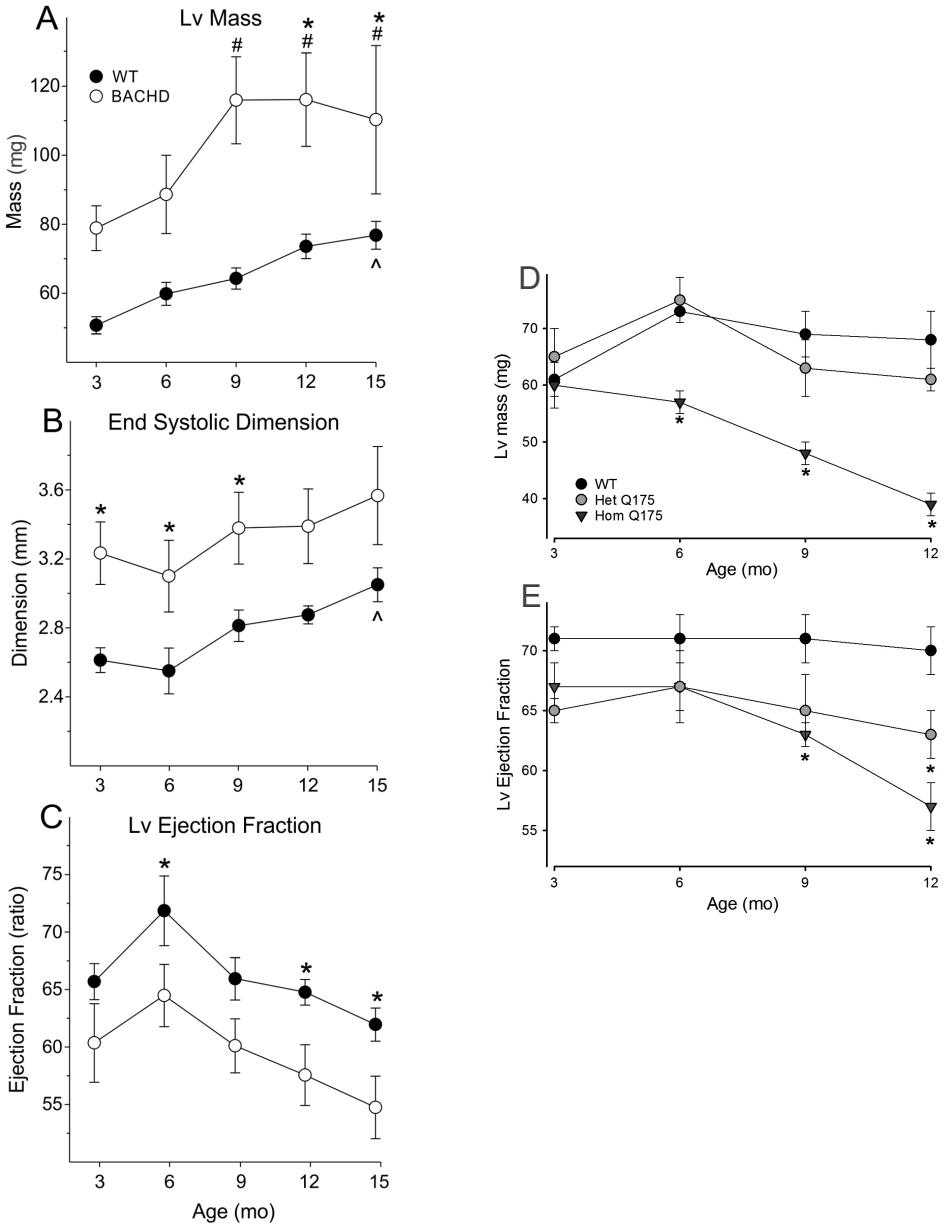

Figure 2. 5

Echocardiogram indicates structural and functional differences early in the disease progression. Structural (A) and functional (B, C) parameters of the heart from WT (n = 8) and BACHD (n = 9) mice were measured from 3 to 15 mo of age. The age-dependent progression in heart dysfunction of Q175 mice was evaluated in a separate cohort of mice using echocardiograms starting at 3 months of age and progressing to 12 months (WT, n = 12; Het, n = 10; Hom, n = 10). Both cardiac structural (Lv mass (D), EDD, ESD) and functional (Lv % FS, E/A ratio, and Lv EF (E)) deficits were observed and exhibited significant effects of age and genotype (Table 3). ^ $P<0.05$ within WT vs. 3 mo. # $P<0.05$ within BACHD vs. 3 mo. * $P<0.05$ for genotypic differences.

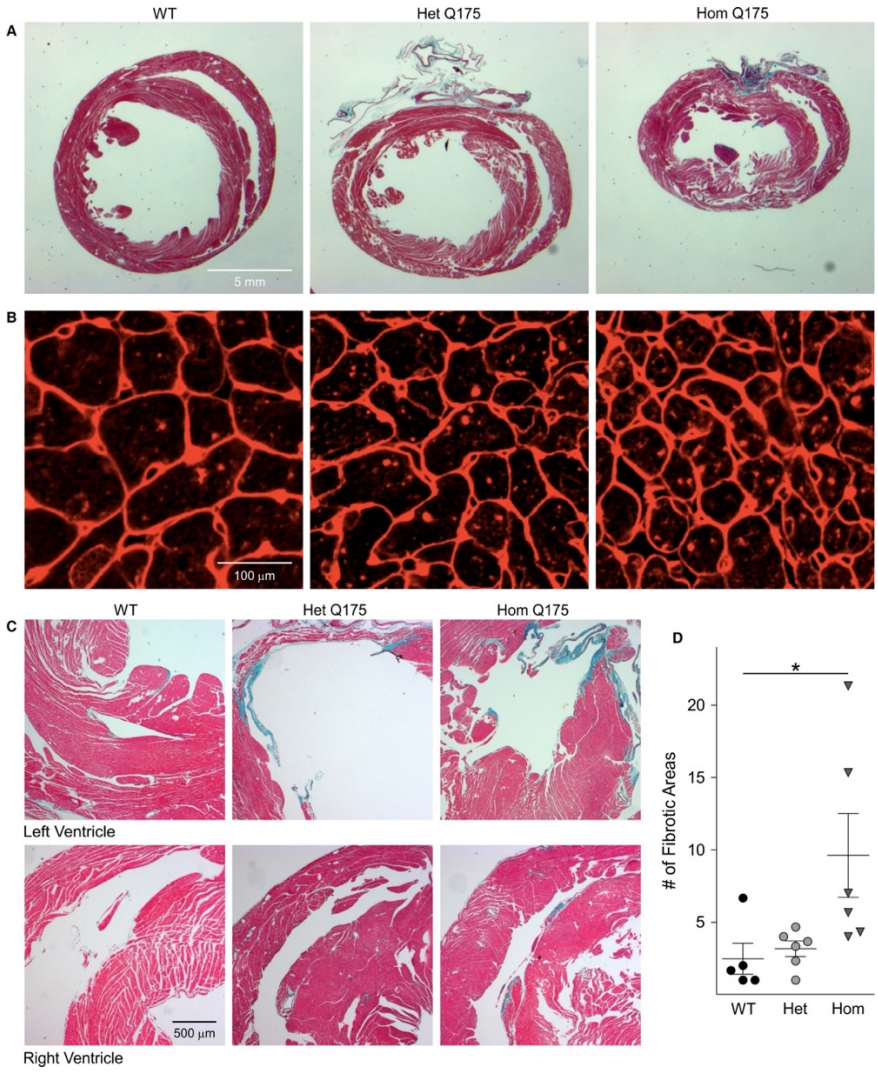

Figure 2. 6

Histological analyses indicated heart pathology in the Q175 mouse. (A) Representative images of Masson's trichrome stained hearts of each genotype showing that the gross dimensions of the Hom Q175 heart were strikingly smaller. (B) Mutants had reduced cardiomyocyte size as well as altered cytoarchitecture as shown by WGA staining. (C) Masson's trichrome stain revealed greatly increased incidence of fibrotic lesions in Q175 Hom hearts. (D) These infarcts were present in each genotype, but were more common (about 3–4 folds) in both ventricles and anteriorly in the interventricular septum of the Hom Q175. Please see Table 5 and 6 for the results of statistical tests. Data are shown as the Mean ± SEM (n = 5–6 animals/genotype). *P < 0.05. The comparison between the number of infarcts was made with Kruskal–Wallis ANOVA followed by Dunn's Multiple Comparison Test.

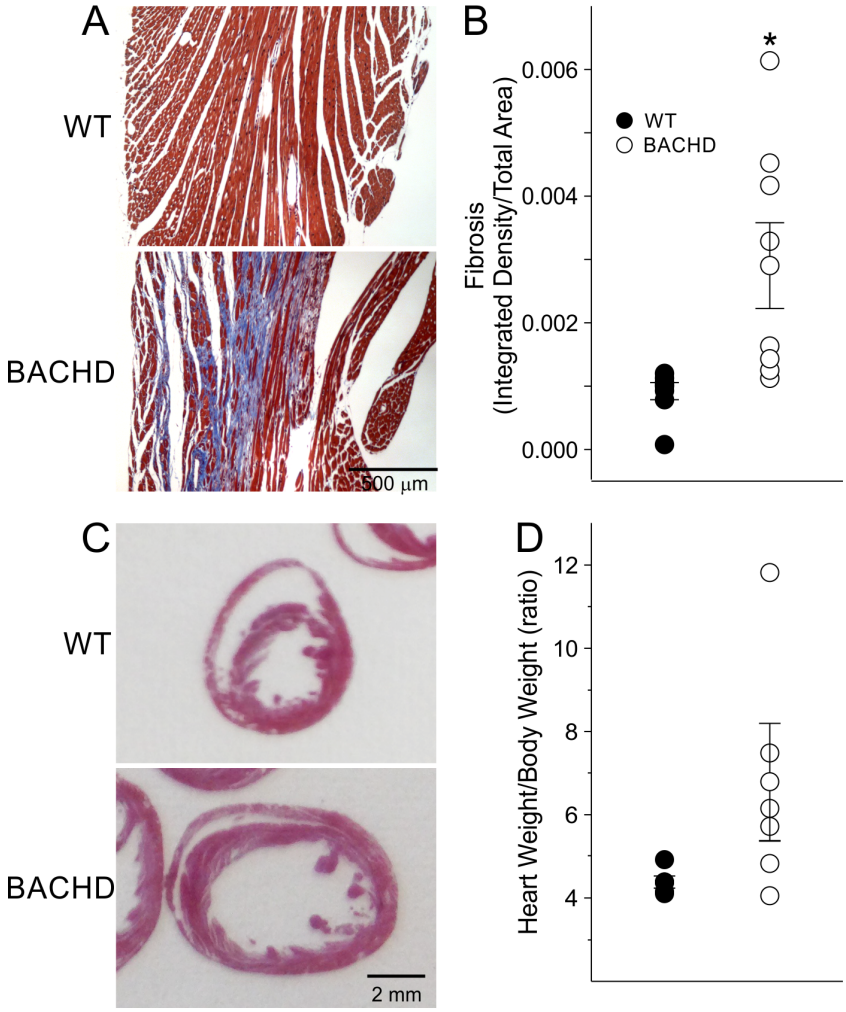

Figure 2. 7

Histological analysis finds evidence of fibrosis and hypertrophy in the BACHD hearts. Examples of Masson's Trichrome stained heart sections from 15 mo old WT and BACHD mice (A). Quantification of fibrosis by measuring the integrated density of fibrotic tissue and divided by tissue area detected significantly increased areas of fibrosis in BACHD mice (B). Examples of hematoxylin and eosin (H&E) stained heart sections from 15 mo old WT and BACHD mice (C). Morphometry measurements comparing heart weight relative to body weight between 15 mo old WT and BACHD mice (D). * $P<0.05$ for genotypic differences.

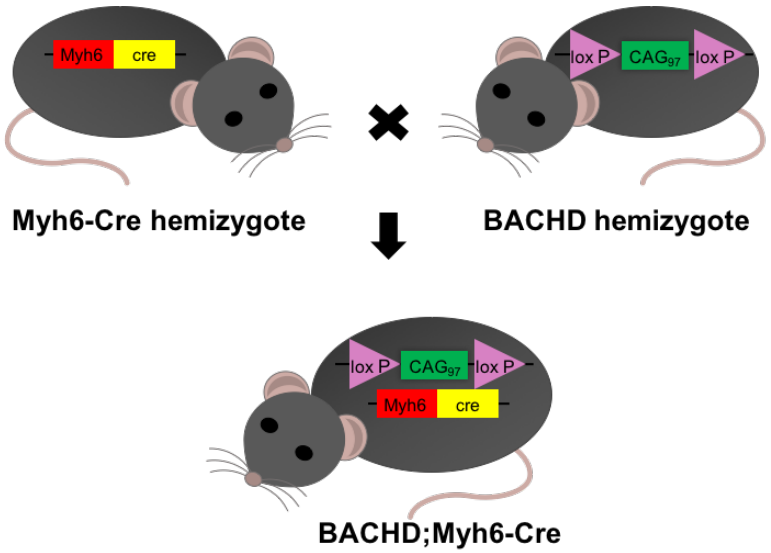

Figure 3. 1

Genetic reduction of mHTT expression in the heart of BACHD mice. The full-length mHTT with two *loxP* sites enables cell specific reduction of mHTT using Cre-crecombinase (Cre). Mice hemizygous for the BACHD transgene will be crossed to mice hemizygous for the cardiomyocyte-specific Myh6-Cre transgene. Approximately 25% of the offspring will be double transgenic (BACHD;Myh6-Cre), BMYO, with the *mHtt* floxed out in the cardiomyocytes.

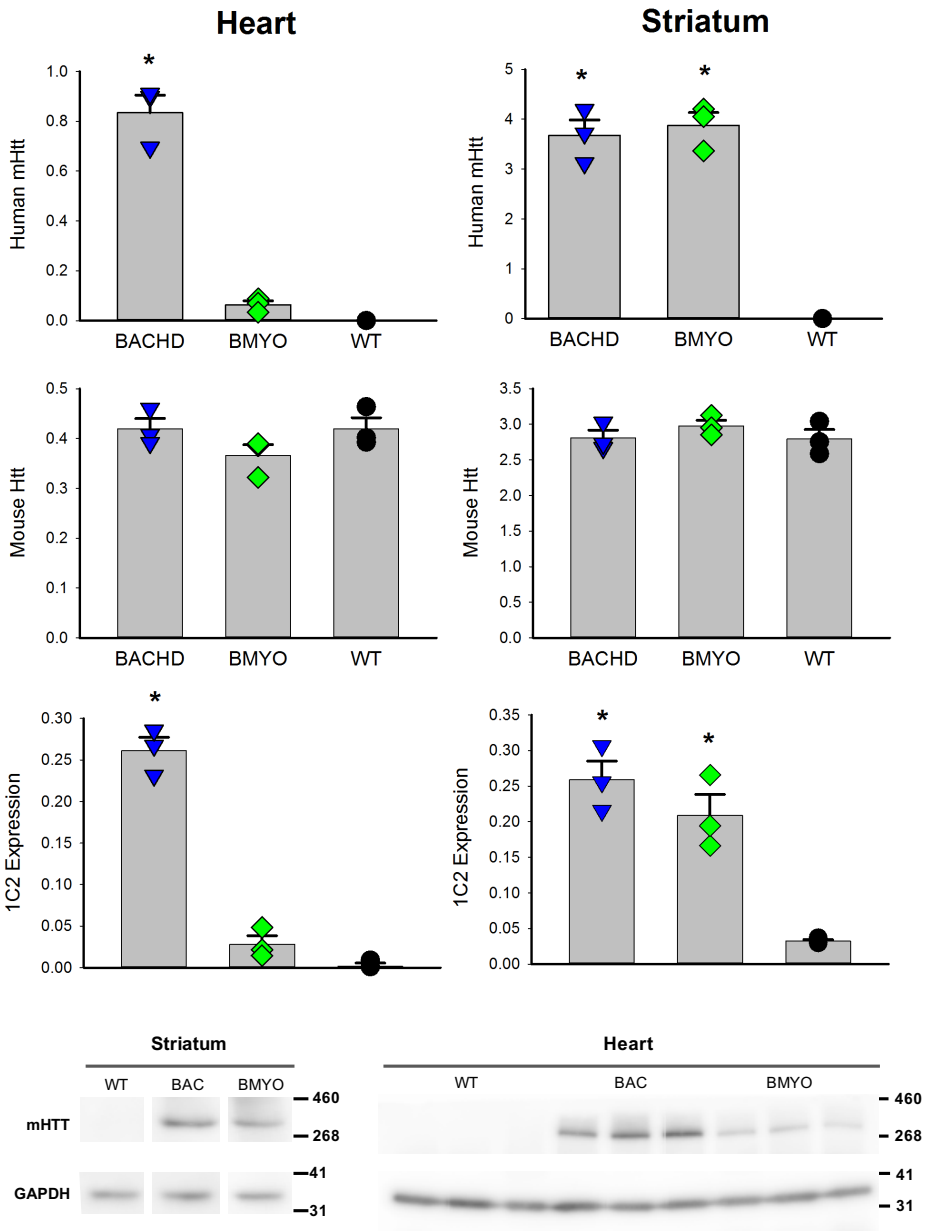

Figure 3. 2

Confirmation of the genetic reduction of human mHTT mRNA and protein expression in the heart in BMYO mice. (A) Quantification of mHtt expression levels normalized to GAPDH in the striatum and heart in WT, BACHD, and BMYO mice (n=3 per genotype; *P<0.05, **P<0.01, ***P<0.001, ****P<0.0001, one-way ANOVA). (B) Western blot with the expanded polyQ specific antibody, 1C2, to detect mHTT protein levels in WT, BACHD, and BMYO mice. GAPDH was used as control. The following quantification shows the mHTT protein levels normalized to GAPDH in the striatum and heart of WT, BACHD, and BMYO mice. n=3 per genotype; *P<0.05, one-way ANOVA.

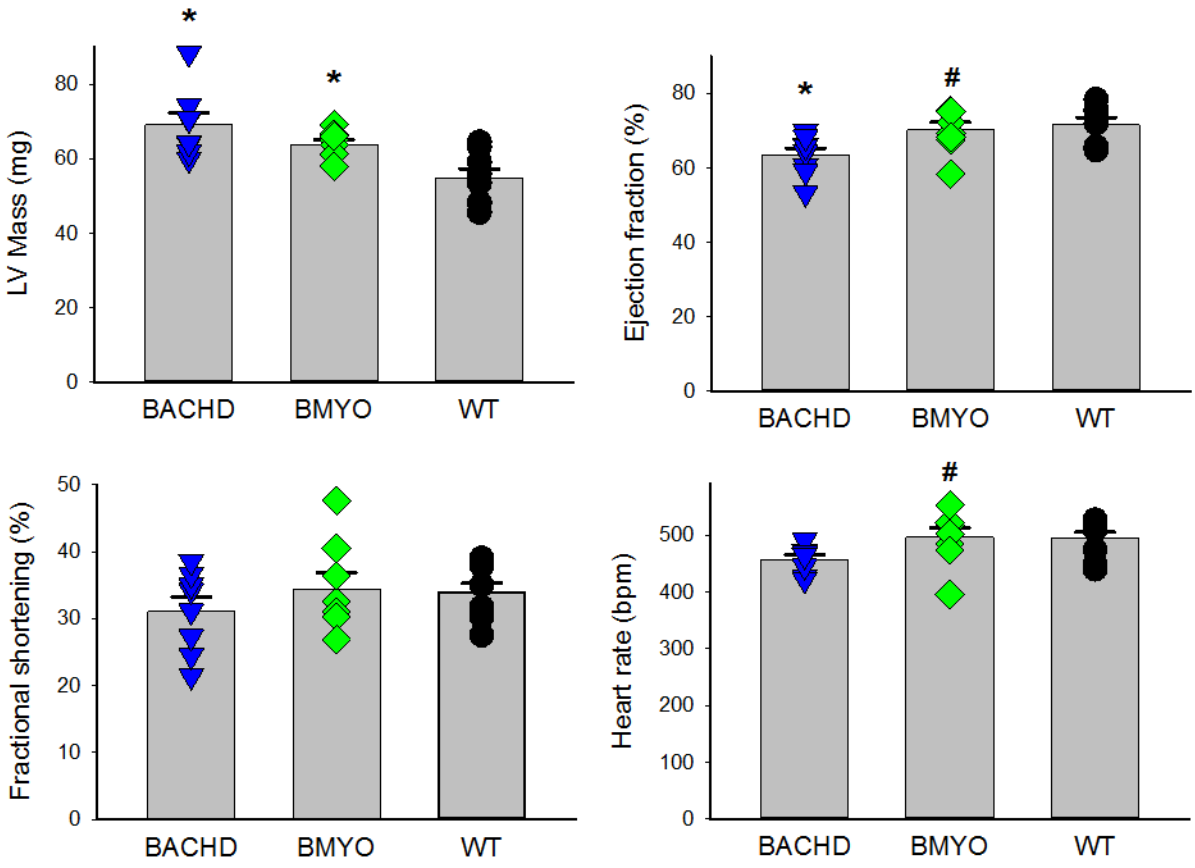

Figure 3. 3

Left ventricular (LV) ejection fraction and diastolic function were improved in BMYO mice. The ratio of early to late diastolic filling (E/A ratio). n=8 per genotype; *P<0.05 vs WT.

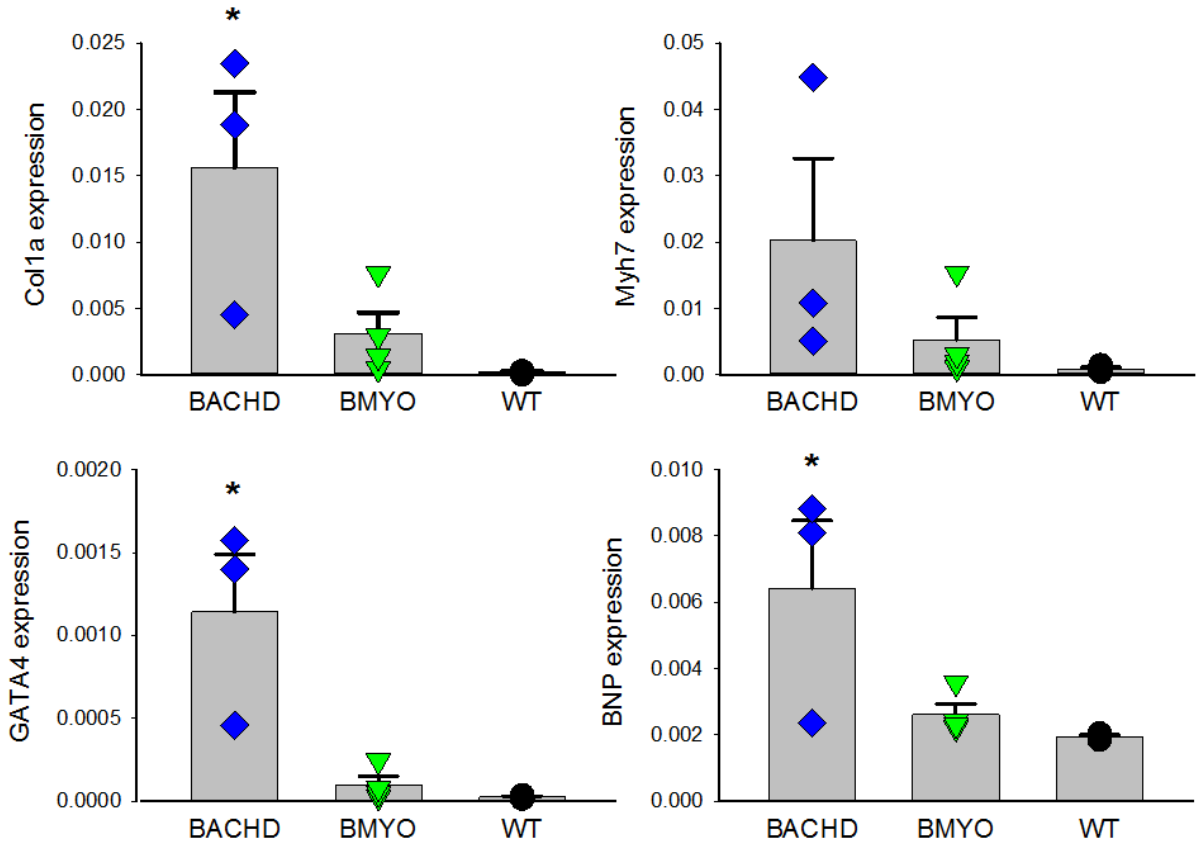

Figure 3. 4

Hypertrophy and fibrosis markers were lower in BMYO hearts compared with BACHD hearts. The gene expression is normalized to GAPDH. n=3-4 per genotype; Age=6mo. *P<0.05.

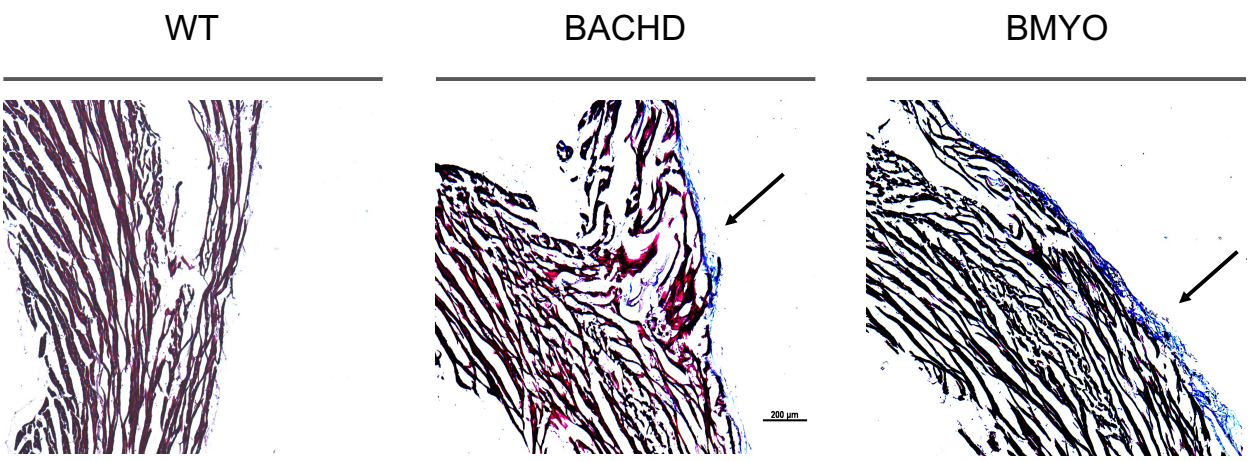

Figure 3. 5

Masson's Trichrome staining showing fibrosis in the hearts of the BACHD and BMYO mice. n=3 per genotype. Age=6mo. Scale bar = 200 µm.

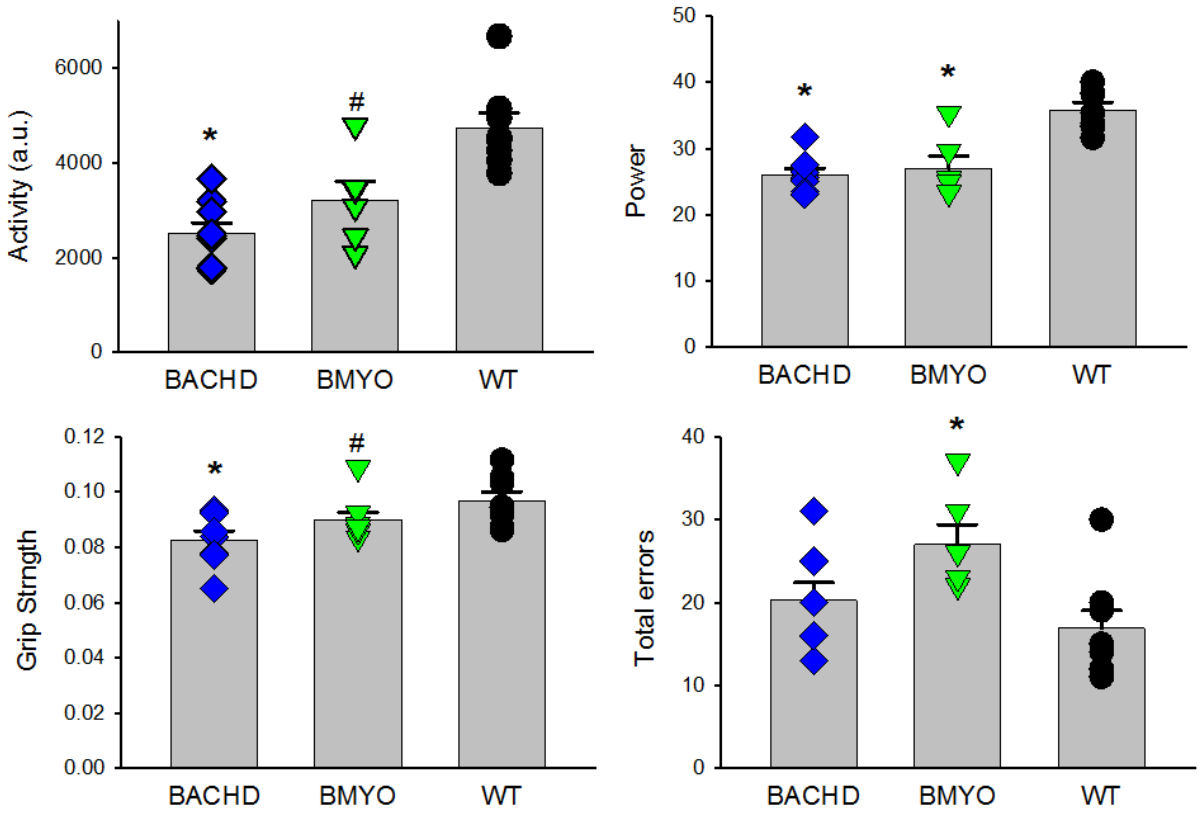

Figure 3. 6

Activity, rhythmic power, and grip strength are improved in BMYO mice. The averaged level of hourly cage activity (au/hr). The strength of the activity rhythm is indicated by the power (% variance) of the χ^2 periodogram analysis. Grip strength (N/g) is maximal strength divided by the animal's body weight. Total errors indicate the total number of errors made by an animal on the challenging beam test. Age = 6mo, n=5-8 per genotype; *P<0.05 vs WT.

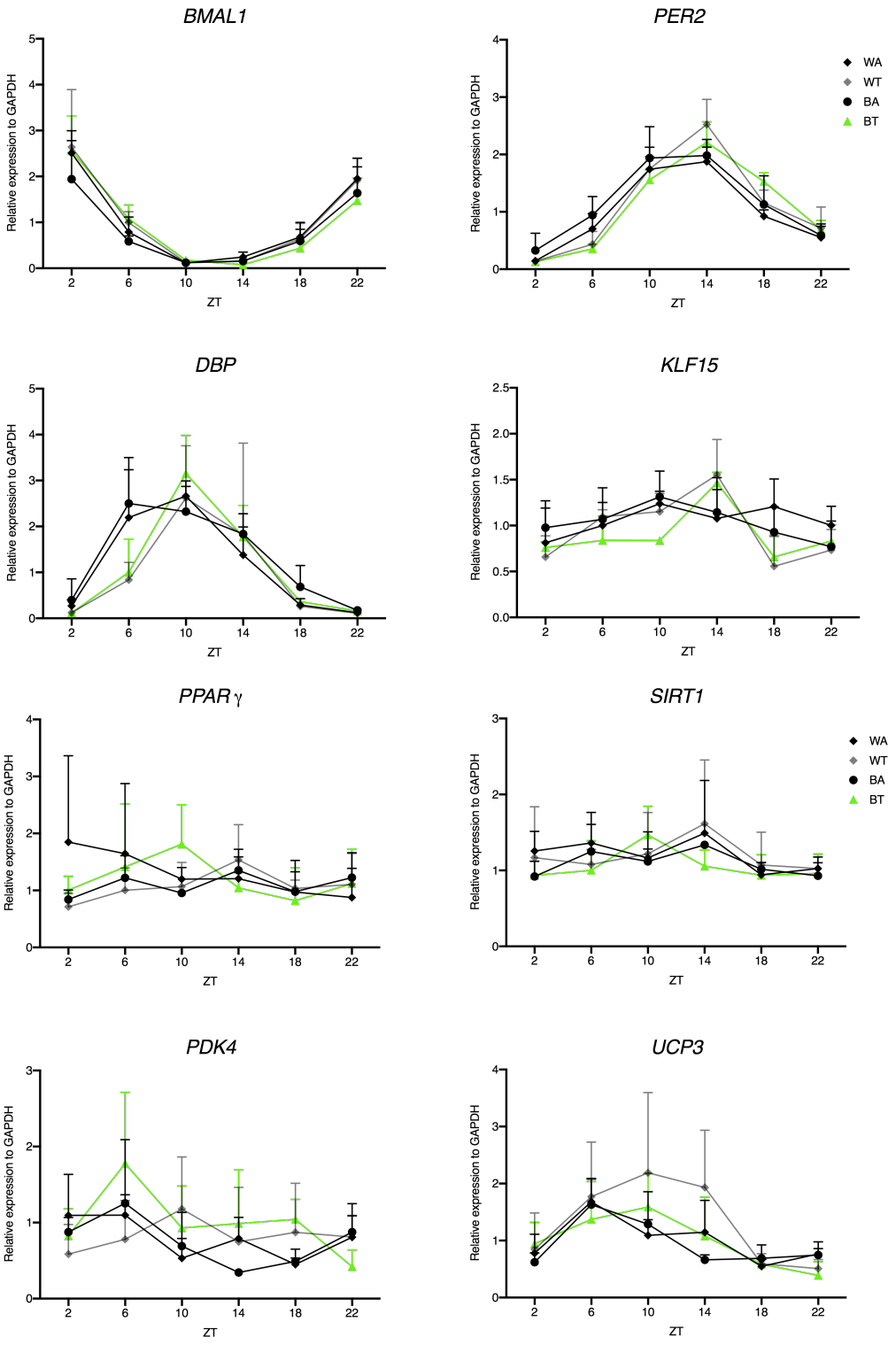
BMAL1
PER2
DBP
KLF15
PPARγ
SIRT1
PDK4
UCP3
Relative expression to GAPDH
ZT
WA
WT
BA
BT

Figure Appendix 1

Relative gene expression of core clock, clock driven transcription factors, and metabolism genes in the hearts of the four groups of mice at ZT 2, 6, 10, 14, 18, and 22. The relative expression is normalized to GAPDH (n=4 per group for each time point). The four groups are WT *ad lib* (WA), WT TRF (WT), BACHD *ad lib* (BA), and BACHD TRF (BT). Age = 6 mo.

Table 1

Electrocardiographic parameters in young Q175 and WT animals held in a LD cycle. ECG values were continuously measured and placed into hourly bins

One-way ANOVA was used to assess differences between the genotypes in the day or night. A paired *t*-test was used to access day/night differences within a genotype.

ECG parameters		WT	Het Q175	Hom Q175	ANOVA genotype
RR (msec)	Day	124 ± 2	121 ± 2	115 ± 2[2]	$F = 4.8$, $P = 0.019$
	Night	107 ± 1[1]	106 ± 2[1]	108 ± 2[1]	$F = 0.6$, $P = 0.533$
PR (msec)	Day	36 ± 1	34 ± 1	35 ± 1	$F = 0.4$, $P = 0.698$
	Night	33 ± 1[1]	32 ± 1[1]	33 ± 1[1]	$H = 0.3$, $P = 0.858$
QRS (msec)	Day	13.2 ± 0.1	13.5 ± 0.2	13.2 ± 0.2	$H = 3.8$, $P = 0.147$
	Night	12.8 ± 0.1[1]	13.1 ± 0.2[1]	12.6 ± 0.1[1]	$H = 5.0$, $P = 0.080$
QR (msec)	Day	6.5 ± 0.1	6.6 ± 0.1	6.6 ± 0.1	$F = 0.3$, $P = 0.724$
	Night	6.3 ± 0.1[1]	6.4 ± 0.1[1]	6.3 ± 0.1[1]	$F = 0.4$, $P = 0.662$
QAT (msec)	Day	31 ± 6	31 ± 5	20 ± 1[2]	$H = 8.6$, $P = 0.013$
	Night	34 ± 6[1]	30 ± 4	21 ± 1[2]	$F = 3.9$, $P = 0.036$
ST (msec)	Day	51 ± 3	56 ± 3	55 ± 3	$H = 2.9$, $P = 0.236$
	Night	52 ± 4	52 ± 3[1]	52 ± 3[1]	$H = 0.2$, P = 0.871
MxdV (mV/msec)	Day	274 ± 22	348 ± 27	329 ± 41	$F = 1.4$, $P = 0.251$
	Night	348 ± 28[1]	411 ± 36[1]	394 ± 43[1]	$F = 0.8$, $P = 0.468$

One-way ANOVA was used to assess differences between the genotypes in the day or night. A paired *t*-test was used to access day/night differences within a genotype.

[1] $P < 0.05$ day versus night within a genotype.

[2] $P < 0.05$ significant difference compared to WT.

Table 2

Echocardiographic parameters in Q175 and WT animals beginning at 3 mo of age.

Two-dimensional, M-mode echocardiography and spectral Doppler images enabled measurement of heart dimension and function including Left ventricle mass (Lv mass), end-diastolic dimension (EDD), end-systolic dimension (ESD), posterior wall thickness (PWT), ventricular septal thickness (VST), aorta ejection time (Ao-ET), ratio of the early (E) to late (A) ventricular filling velocities (E/A ratio), fractional shortening (FS%), Lv Ejection Fraction (Lv EF).

[1] $P < 0.05$ significant difference compared to WT.

	WT	Het Q175	Hom Q175
Age (months)	3	3	3
Lv mass (mg)	61 ± 3	65 ± 5	60 ± 4
EDD (mm)	4.1 ± 0.1	3.9 ± 0.1	3.8 ± 0.1
ESD (mm)	2.7 ± 0.1	2.7 ± 0.1	2.6 ± 0.1
Ao-ET (msec)	50 ± 1	52 ± 2	54 ± 2
FS (%)	35 ± 1	33 ± 1	32 ± 1
E/A	1.7 ± 0.1	1.7 ± 0.1	1.8 ± 0.1
Lv EF	71 ± 1	65 ± 1	67 ± 2
Age (months)	6	6	6
Lv mass (mg)	72 ± 3	74 ± 4	57 ± 2
EDD (mm)	4.2 ± 0.1	4.2 ± 0.1	3.8 ± 0.1
ESD (mm)	2.7 ± 0.1	2.8 ± 0.1	2.5 ± 0.1
Ao-ET (msec)	52 ± 1	52 ± 1	58 ± 2[1]
FS (%)	35 ± 2	33 ± 2	34 ± 1
E/A	1.8 ± 0.1	1.8 ± 0.1	1.7 ± 0.1
Lv EF	71 ± 2	67 ± 2.3	67 ± 3
Age (months)	9	9	9
Lv mass (mg)	69 ± 4	63 ± 5	48 ± 2[1]
EDD (mm)	4.2 ± 0.1	4.0 ± 0.1	3.4 ± 0.1
ESD (mm)	2.7 ± 0.1	2.8 ± 0.1	2.5 ± 0.1
Ao-ET (msec)	48 ± 1	53 ± 1	54 ± 2[1]
FS (%)	36 ± 2	28 ± 2[1]	27 ± 1[1]
E/A	1.7 ± 0.1	1.6 ± 0.1	1.5 ± 0.1[1]
Lv EF	71 ± 2	65 ± 3	63 ± 1[1]
Age (months)	12	12	12
Lv mass (mg)	68 ± 5	61 ± 2[1]	39 ± 2[1]
EDD (mm)	4.1 ± 0.1	3.8 ± 0.1	3.2 ± 0.1
ESD (mm)	2.7 ± 0.1	2.8 ± 0.1	2.4 ± 0.1
Ao-ET (msec)	50 ± 1	52 ± 2	57 ± 1[1]
FS (%)	34 ± 2	26 ± 2[1]	25 ± 1[1]
E/A	1.9 ± 0.1	1.5 ± 0.1[1]	1.5 ± 0.1[1]
Lv EF	70 ± 2	64 ± 3[1]	58 ± 2[1]

Table 3

Two-way ANOVA was used to determine whether each of the echocardiographic parameters measured in Q175 and WT mice were significantly different.

Genotype and age were the two factors. Measurements were made when the mice were 3, 6, 9, and 12 months of age.

	Lv mass (mg)	EDD (mm)	ESD (mm)	Ao-ET (ms)	FS (%)	Lv EF
Genotype	$F = 23.1$, $P < 0.001$	$F = 34.1$, $P < 0.001$	$F = 6.1$, $P = 0.003$	$F = 21.6$, $P < 0.001$	$F = 8.6$, $P < 0.001$	$F = 10.6$, $P < 0.001$
Age	$F = 6.4$, $P < 0.001$	$F = 6.6$, $P < 0.001$	$F = 0.2$, $P = 0.887$	$F = 3.1$, $P = 0.031$	$F = 4.5$, $P = 0.005$	$F = 5.0$, $P = 0.003$
Interaction	$F = 3.2$, $P = 0.006$	$F = 2.9$, $P = 0.01$	$F = 0.5$, $P = 0.780$	$F = 0.5$, $P = 0.787$	$F = 1.6$, $P = 0.156$	$F = 1.5$, $P = 0.197$

Table 4

Echocardiographic parameters in BACHD and WT animals beginning at 3 mo of age.

	WT (*n* = 8)					BACHD (*n* = 9)					2-way ANOVA		
Age (mo)	**3**	**6**	**9**	**12**	**15**	**3**	**6**	**9**	**12**	**15**	***Genotype***	***Age***	***Interaction***
Lv Mass (g)	51±2	60±3	64±3	74±4	77±4*	79±6	89±11	116 ±13†‡	116 ±13†‡	110 ±21†‡	F_1 = 7.5, P = 0.02	F_4 = 11.5,P< 0.001	F_4 = 1.64, P = 0.18
ESD (mm)	2.6 ±0.1	2.5 ±0.1	2.8 ±0.1	2.9±0.1	3.0 ±0.1*	3.2 ±0.2‡	3.1 ±0.2‡	3.4±0.2‡	3.4±0.2	3.6±0.3	F_1 = 6.2, P = 0.03	F_4 = 7.8, P< 0.001	F_4 = 0.11, P = 0.98
EDD (mm)	3.8 ±0.1	3.9 ±0.1	4.1 ±0.1	4.2 ±01*	4.4 ±0.1*	4.5 ±0.1‡	4.4±0.2	4.6±0.2‡	4.6±0.2	4.7±0.3	F_1 = 4.7, P = 0.046	F_4 = 6.2, P< 0.001	F_4 = 1.21, P = 0.32
PWT (mm)	0.44 ±0.02	0.48 ±0.01	0.48 ±0.01	0.52 ±0.01*	0.50 ±0.02	0.50 ±0.01‡	0.55 ±0.02‡	0.64 ±0.02†‡	0.66 ±0.02†‡	0.58 ±0.03†‡	F_1 = 36.5, P< 0.001	F_4 = 15.0, P< 0.001	F_4 = 3.08, P = 0.02
LvEF (ratio)	66±2	72±3	66±2	65±1	62±1	60±3	64±3‡	60±2	57±2‡	54±3‡	F_1 = 6.1, P = 0.030	F_4 = 8.2, P< 0.001	F_4 = 0.14, P = 0.97

* P<0.05 within WT, significant difference vs 3 mo;

† P<0.05 within HD, significant difference vs 3 mo;

‡ P<0.05 significant difference between genotypes in the same age group.

doi:10.1371/journal.pone.0147269.t001

Table 5

Morphological measurements in WT and Q175 mutants. were performed in heart coronal sections at the mid-ventricular level chosen based on the visual presence of papillary muscles in the left ventricle (Lv).

Since the Lv were not perfectly round, we refer to the lumen measurements as circumference/perimeter. Values are presented as the Mean ± SEM. WT, $n = 5$; Het Q175, $n = 6$; Hom Q175, $n = 6$).

- [a] $P < 0.001$ versus WT.
- [b] $P < 0.05$.
- [c] $P < 0.005$.
- [d] $P < 0.0005$ versus WT.
- [e] $P < 0.05$.
- [f] $P < 0.005$ versus Het one-way ANOVA followed by Bonferroni's multiple comparison test.

	WT	Het Q175	Hom Q175	One-way ANOVA
Body Weight (g)	28 ± 0.7	26 ± 0.4	21 ± 0.4[a]	$F = 64.5$, $P < 0.001$
Heart Weight (mg)	153 ± 4	151 ± 1	125 ± 2[a]	$H = 19.4$, $P < 0.001$
Total heart cross sectional area (mm^2)	31.2 ± 1.3	27.1 ± 1.7	20.7 ± 0.7[d,f]	$F = 16$; $P = 0.0002$
Circumference/perimeter (mm)	20.0 ± 0.3	18.8 ± 0.6	17.2 ± 0.5[c]	$F = 7.9$; $P = 0.0049$
Interventricular septum thickness (mm)	1.1 ± 0.1	1.1 ± 0.1	1.0 ± 0.06	$F = 0.6$, $P = 0.561$
Lv thickness (mm)	1.09 ± 0.06	1.09 ± 0.07	1.12 ± 0.05	$F = 0.08$, $P = 0.917$
Lv lumen cross sectional area (mm^2)	8.9 ± 1.0	6.8 ± 0. 6	4.0 ± 0.3[d,e]	$F = 13.7$, $P = 0.0005$
Lv lumen circumference/perimeter (mm)	10.7 ± 0.6	10.0 ± 0.6	8.2 ± 0.5[b]	$F = 5.26$; $P = 0.0198$

Table 6

Histological measurements of hearts of 15 mo WT and BACHD mice.

Histological Measurements	WT (*n* = 8)	BACHD (*n* = 9)	*t*-test
Heart Weight/Body Weight	4.4 ± 0.1	6.6 ± 2.8	$T = 1.72$, $P = 0.119$
Heart Weight/Tibia Length	10.0 ± 0.1	12.8 ± 2.1	$T = 21.0$, $P = 0.126$
Heart Weight (mg)	180 ± 2	220 ± 33	$T = 21.5$, $P = 0.126$
Body Weight (g)	41 ± 2	35 ± 4	$T = 1.43$, $P = 0.187$
Tibia Length (mm)	18.0 ± 0.1	18.0 ± 0.1	$T = 0.31$, $P = 0.761$
Fibrosis (integrated density/total area)	9.2 ± 1.4	29.0 ± 6.8*	$T = 45.0$, $P = 0.015$

* $P<0.05$ significant difference between genotypes.

doi:10.1371/journal.pone.0147269.t002

Table 7

Echocardiographic parameters in BACHD, BMYO and WT animals at 3 mo and 6 mo of age. Two-dimensional, M-mode echocardiography and spectral Doppler images enabled measurement of heart dimension and function including Left ventricle mass (Lv mass), end-diastolic dimension (EDD), end-systolic dimension (ESD), posterior wall thickness (PWT), ventricular septal thickness (VST), ratio of the early (E) to late (A) ventricular filling velocities (E/A ratio), fractional shortening (FS%), Lv Ejection Fraction (Lv EF), heart rate (HR). One-way ANOVA was used to evaluate the possible significance of the findings. If normality or equal variance tests failed, then a Kruskal-Wallis one way ANVOA on ranks was used instead.

	BACHD	**BMYO**	**WT**	**Stats**
Age (mo)	3	3	3	
Lv mass (mg)	62 ± 6	64 ± 4	54 ± 4	$F_{(2)} = 1.784$; P = 0.193
EDD (mm)	4.0 ± 0.1	4.0 ± 0.1	4.0 ± 0.1	$F_{(2)} = 0.023$; P = 0.977
ESD (mm)	2.6 ± 0.1	2.8 ± 0.2	2.5 ± 0.2	$F_{(2)} = 1.111$; P = 0.348
Ao-ET (ms)	58 ± 1	59 ± 1	55 ± 2	$F_{(2)} = 3.668$; P = 0.043
FS (%)	30 ± 2	35 ± 1	37 ± 2	$F_{(2)} = 3.186$; P = 0.062
E/A	1.9 ± 0.1	2.0 ± 0.1	2.0 ± 0.1	$F_{(2)} = 0.027$; P = 0.973
Lv EF	63 ± 2	68 ± 1	71 ± 3	$F_{(2)} = 3.952$; P = 0.035
HR (bpm)	459 ± 10	481 ± 10	514 ± 23	$H_{(2)} = 3.126$; P = 0.209
Age (mo)	6	6	6	
Lv mass (mg)	66 ± 4	68 ± 2	55 ± 2	$F_{(2)} = 5.210$; P = 0.015
EDD (mm)	4.2 ± 0.1	4.2 ± 0.1	4.1 ± 0.1	$F_{(2)} = 2.149$; P = 0.142
ESD (mm)	2.6 ± 0.1	2.8 ± 0.2	2.5 ± 0.2	$F_{(2)} = 1.111$; P = 0.348
Ao-ET (ms)	53 ± 2	51 ± 2	54 ± 2	$F_{(2)} = 0.647$; P = 0.534
FS (%)	30 ± 2	35 ± 1	37 ± 2	$F_{(2)} = 3.186$; P = 0.062
E/A	1.9 ± 0.1	2.0 ± 0.1	2.0 ± 0.1	$F_{(2)} = 0.027$; P = 0.973
Lv EF	63 ± 2	69 ± 2	71 ± 2	$F_{(2)} = 6.689$; P = 0.006
HR (bpm)	457 ± 8	512 ± 10	494 ± 12	$H_{(2)} = 6.743$; P = 0.034

Table 8

Quantitative real-time PCR (RT-qPCR) measurements of gene expression in the hearts of BACHD, BMYO and WT animals at 6 mo of age. Primers targeted collagen 1a (*Col1a*), myosin heavy chain, α isoform (*Myh6*), ventricular/slow myosin heavy chain isoform (*Myh7*), MYH7 genecardiac sarcomeric genes, Myh6 and Myh7, the GATA4 transcription factor (GATA4), and brain natriuretic peptide (BNP). In each case, expression was normalized to the expression of GAPDH. One-way ANOVA was used to evaluate the possible significance of the findings. If normality or equal variance tests failed, then a Kruskal-Wallis one way ANVOA on ranks was used instead.

	BACHD	**BMYO**	**WT**	**Stats**
Col1a	0.0156 ± 0.005	0.0031 ± 0.003	0.0002 ± 0.0001	$F_{(2)} = 6.410$; P = 0.026
Myh6	1.179 ± 0.254	0.185 ± 0.118	0.027 ± 0.0.010	$F_{(2)} = 15.245$; P = 0.003
Myh7	0.020 ± 0.012	0.005 ± 0.003	0.001 ± 0.0003	$F_{(2)} = 2.095$; P = 0.194
GATA4	0.0011 ± 0.0003	0.00001 ± 0.00004	0.00002 ± 0.000006	$H_{(2)} = 7.318$; P = 0.004
BNP	0.006 ± 0.002	0.003 ± 0.0003	0.002 ± 0.0003	$H_{(2)} = 6.745$; P = 0.010

Table 9

Behavioral measurements of motor function from BACHD, BMYO and WT animals at 6 mo of age. Infrared monitors were used to measure total cage activity over a 10-day duration. The average activity levels during a 24 hr cycle are reported below. In addition, the strength of diurnal rhythms in cage activity were assessed using periodogram and the results reported as power (% variation). Maximal forelimb grip strength was measured by a meter during the night and normalize to body weight. Finally, performance on a challenging beam was measured and the number of errors (mis-steps) are shown below. One-way ANOVA was used to evaluate the possible significance of the findings. If normality or equal variance tests failed, then a Kruskal-Wallis one way ANVOA on ranks was used instead. Age = 6 mo.

	BACHD	**BMYO**	**WT**	**Stats**
Activity (a.u) per 24 hrs	2504 ± 224	2884 ± 227	4741 ± 317	$F_{(2)} = 21.440$; $P < 0.001$
Power (% variation)	26.0 ± 0.9	27.0 ± 1.9	35.8 ± 1.1	$F_{(2)} = 17.053$; $P < 0.001$
Grip strength (N/g)	0.083 ± 0.003	0.090 ± 0.002	0.097 ± 0.003	$F_{(2)} = 5.323$; $P = 0.013$
Challenging beam (errors)	20.2 ± 2.1	27.0 ± 2.4	16.9 ± 2.1	$H_{(2)} = 7.802$; $P = 0.020$

References:

1. Kuljis D, Schroeder AM, Kudo T, Loh DH, Willison DL, Colwell CS. Sleep and circadian dysfunction in neurodegenerative disorders: insights from a mouse model of Huntington's disease. Minerva Pneumol. 2012;51: 93–106.

2. Bates GP, Dorsey R, Gusella JF, Hayden MR, Kay C, Leavitt BR, et al. Huntington disease. Nat Rev Dis Primers. 2015;1: 15005. doi:10.1038/nrdp.2015.5

3. Ciammola A, Sassone J, Alberti L, Meola G, Mancinelli E, Russo MA, et al. Increased apoptosis, huntingtin inclusions and altered differentiation in muscle cell cultures from Huntington's disease subjects. Cell Death and Differentiation. 2006;13: 2068–2078. doi:10.1038/sj.cdd.4401967

4. Saft C, Zange J, Andrich J, Müller K, Lindenberg K, Landwehrmeyer B, et al. Mitochondrial impairment in patients and asymptomatic mutation carriers of Huntington's disease. Mov Disord. 2005;20: 674–679. doi:10.1002/mds.20373

5. Pouladi MA, Morton AJ, Hayden MR. Choosing an animal model for the study of Huntington's disease. Nature Reviews Neuroscience. 2013;14: 708–721. doi:10.1038/nrn3570

6. Sørensen SA, Fenger K. Causes of death in patients with Huntington's disease and in unaffected first degree relatives. J Med Genet. 1992;29: 911–914.

7. Abildtrup M, Shattock M. Cardiac Dysautonomia in Huntington's Disease. J Huntingtons Dis. 2013;2: 251–261. doi:10.3233/JHD-130054

8. Stephen CD, Hung J, Schifitto G, Hersch SM, Rosas HD. Electrocardiogram Abnormalities Suggest Aberrant Cardiac Conduction in Huntington's Disease. Mov Disord Clin Pract. 2018;5: 306–311. doi:10.1002/mdc3.12596

9. Buonincontri G, Wood NI, Puttick SG, Ward AO, Carpenter TA, Sawiak SJ, et al. Right ventricular dysfunction in the R6/2 transgenic mouse model of Huntington's disease is unmasked by dobutamine. J Huntingtons Dis. 2014;3: 25–32. doi:10.3233/JHD-130083

10. Kudo T, Schroeder A, Loh DH, Kuljis D, Jordan MC, Roos KP, et al. Dysfunctions in circadian behavior and physiology in mouse models of Huntington's disease. Experimental Neurology. 2011;228: 80–90. doi:10.1016/j.expneurol.2010.12.011

11. Mihm MJ, Amann DM, Schanbacher BL, Altschuld RA, Bauer JA, Hoyt KR. Cardiac dysfunction in the R6/2 mouse model of Huntington's disease. Neurobiology of Disease. 2007;25: 297–308. doi:10.1016/j.nbd.2006.09.016

12. Wood NI, Sawiak SJ, Buonincontri G, Niu Y, Kane AD, Carpenter TA, et al. Direct evidence of progressive cardiac dysfunction in a transgenic mouse model of Huntington's disease. J Huntingtons Dis. 2012;1: 57–64. doi:10.3233/JHD-2012-120004

13. Schroeder AM, Wang HB, Park S, Jordan MC, Gao F, Coppola G, et al. Cardiac Dysfunction in the BACHD Mouse Model of Huntington's Disease. Sadoshima J, editor. PLOS ONE. 2016;11: e0147269. doi:10.1371/journal.pone.0147269

14. Cutler TS, Park S, Loh DH, Jordan MC, Yokota T, Roos KP, et al. Neurocardiovascular deficits in the Q175 mouse model of Huntington's disease. Physiol Rep. 2017;5. doi:10.14814/phy2.13289

15. Joviano-Santos JV, Santos-Miranda A, Botelho AFM, de Jesus ICG, Andrade JN, de Oliveira Barreto T, et al. Increased oxidative stress and CaMKII activity contribute to electro-mechanical defects in cardiomyocytes from a murine model of Huntington's disease. FEBS J. 2019;286: 110–123. doi:10.1111/febs.14706

16. Melkani GC, Trujillo AS, Ramos R, Bodmer R, Bernstein SI, Ocorr K. Huntington's disease induced cardiac amyloidosis is reversed by modulating protein folding and oxidative stress pathways in the Drosophila heart. PLoS Genet. 2013;9: e1004024. doi:10.1371/journal.pgen.1004024

17. Pattison JS, Sanbe A, Maloyan A, Osinska H, Klevitsky R, Robbins J. Cardiomyocyte Expression of a Polyglutamine Preamyloid Oligomer Causes Heart Failure. Circulation. 2008;117: 2743–2751. doi:10.1161/CIRCULATIONAHA.107.750232

18. Kobal J, Meglic B, Mesec A, Peterlin B. Early sympathetic hyperactivity in Huntington's disease. European Journal of Neurology. 2004;11: 842–848. doi:10.1111/j.1468-1331.2004.00894.x

19. Kobal J, Melik Z, Cankar K, Bajrovic FF, Meglic B, Peterlin B, et al. Autonomic dysfunction in presymptomatic and early symptomatic Huntington's disease. Acta Neurol Scand. 2010;121: 392–399. doi:10.1111/j.1600-0404.2009.01251.x

20. Bär KJ, Boettger MK, Andrich J, Epplen JT, Fischer F, Cordes J, et al. Cardiovagal modulation upon postural change is altered in Huntington's disease. Eur J Neurol. 2008;15: 869–871. doi:10.1111/j.1468-1331.2008.02173.x

21. Andrich J, Schmitz T, Saft C, Postert T, Kraus P, Epplen JT, et al. Autonomic nervous system function in Huntington's disease. J Neurol Neurosurg Psychiatr. 2002;72: 726–731.

22. Sharma KR, Romano JG, Ayyar DR, Rotta FT, Facca A, Sanchez-Ramos J. Sympathetic skin response and heart rate variability in patients with Huntington disease. Arch Neurol. 1999;56: 1248–1252.

23. Goodman AOG, Rogers L, Pilsworth S, McAllister CJ, Shneerson JM, Morton AJ, et al. Asymptomatic sleep abnormalities are a common early feature in patients with Huntington's disease. Curr Neurol Neurosci Rep. 2011;11: 211–217. doi:10.1007/s11910-010-0163-x

24. Morton AJ. Circadian and sleep disorder in Huntington's disease. Exp Neurol. 2013;243: 34–44. doi:10.1016/j.expneurol.2012.10.014

25. Morton AJ, Wood NI, Hastings MH, Hurelbrink C, Barker RA, Maywood ES. Disintegration of the sleep-wake cycle and circadian timing in Huntington's disease. J Neurosci. 2005;25: 157–163. doi:10.1523/JNEUROSCI.3842-04.2005

26. Loh DH, Kudo T, Truong D, Wu Y, Colwell CS. The Q175 mouse model of Huntington's disease shows gene dosage- and age-related decline in circadian rhythms of activity and sleep. PLoS ONE. 2013;8: e69993. doi:10.1371/journal.pone.0069993

27. Kuljis DA, Gad L, Loh DH, MacDowell Kaswan Z, Hitchcock ON, Ghiani CA, et al. Sex Differences in Circadian Dysfunction in the BACHD Mouse Model of Huntington's Disease. PLoS ONE. 2016;11: e0147583. doi:10.1371/journal.pone.0147583

28. Colwell CS, Matveyenko AV. Timing Is Everything: Implications for Metabolic Consequences of Sleep Restriction. Diabetes. 2014;63: 1826–1828. doi:10.2337/db14-0283

29. Schroeder AM, Loh DH, Jordan MC, Roos KP, Colwell CS. Baroreceptor reflex dysfunction in the BACHD mouse model of Huntington's disease. PLoS Currents. 2011;3: RRN1266. doi:10.1371/currents.RRN1266

30. Aziz NA, Anguelova GV, Marinus J, Van Dijk JG, Roos RAC. Autonomic symptoms in patients and pre-manifest mutation carriers of Huntington's disease: Autonomic symptoms in Huntington's disease. European Journal of Neurology. 2010;17: 1068–1074. doi:10.1111/j.1468-1331.2010.02973.x

31. Goldstein DS. Dysautonomia in Parkinson disease. Compr Physiol. 2014;4: 805–826. doi:10.1002/cphy.c130026

32. Romagnolo A, Zibetti M, Merola A, Canova D, Sarchioto M, Montanaro E, et al. Cardiovascular autonomic neuropathy and falls in Parkinson disease: a prospective cohort study. J Neurol. 2018. doi:10.1007/s00415-018-9104-4

33. Claassen DO, Adler CH, Hewitt LA, Gibbons C. Characterization of the symptoms of neurogenic orthostatic hypotension and their impact from a survey of patients and caregivers. BMC Neurol. 2018;18: 125. doi:10.1186/s12883-018-1129-x

34. Norcliffe-Kaufmann L, Kaufmann H, Palma J-A, Shibao CA, Biaggioni I, Peltier AC, et al. Orthostatic heart rate changes in patients with autonomic failure caused by

neurodegenerative synucleinopathies. Ann Neurol. 2018;83: 522–531. doi:10.1002/ana.25170

35. Thayer JF, Yamamoto SS, Brosschot JF. The relationship of autonomic imbalance, heart rate variability and cardiovascular disease risk factors. International Journal of Cardiology. 2010;141: 122–131. doi:10.1016/j.ijcard.2009.09.543

36. Wulsin LR, Horn PS, Perry JL, Massaro JM, D'Agostino RB. Autonomic Imbalance as a Predictor of Metabolic Risks, Cardiovascular Disease, Diabetes, and Mortality. J Clin Endocrinol Metab. 2015;100: 2443–2448. doi:10.1210/jc.2015-1748

37. Kemp AH, Koenig J, Thayer JF. From psychological moments to mortality: A multidisciplinary synthesis on heart rate variability spanning the continuum of time. Neurosci Biobehav Rev. 2017;83: 547–567. doi:10.1016/j.neubiorev.2017.09.006

38. Shaffer F, McCraty R, Zerr CL. A healthy heart is not a metronome: an integrative review of the heart's anatomy and heart rate variability. Front Psychol. 2014;5: 1040. doi:10.3389/fpsyg.2014.01040

39. Burr RL. Interpretation of normalized spectral heart rate variability indices in sleep research: a critical review. Sleep. 2007;30: 913–919.

40. Heathers JAJ. Everything Hertz: methodological issues in short-term frequency-domain HRV. Front Physiol. 2014;5: 177. doi:10.3389/fphys.2014.00177

41. Kiriazis H, Jennings NL, Davern P, Lambert G, Su Y, Pang T, et al. Neurocardiac dysregulation and neurogenic arrhythmias in a transgenic mouse model of Huntington's disease: Neurocardiac phenotype in Huntington's disease mice. The Journal of Physiology. 2012;590: 5845–5860. doi:10.1113/jphysiol.2012.238113

42. Aminoff MJ, Gross M. Vasoregulatory activity in patients with Huntington's chorea. J Neurol Sci. 1974;21: 33–38.

43. Den Heijer JC, Bollen WL, Reulen JP, van Dijk JG, Kramer CG, Roos RA, et al. Autonomic nervous function in Huntington's disease. Arch Neurol. 1988;45: 309–312.

44. Boudreau P, Yeh W-H, Dumont GA, Boivin DB. Circadian variation of heart rate variability across sleep stages. Sleep. 2013;36: 1919–1928. doi:10.5665/sleep.3230

45. Morris CJ, Yang JN, Scheer FAJL. The impact of the circadian timing system on cardiovascular and metabolic function. Prog Brain Res. 2012;199: 337–358. doi:10.1016/B978-0-444-59427-3.00019-8

46. Mielcarek M, Inuabasi L, Bondulich MK, Muller T, Osborne GF, Franklin SA, et al. Dysfunction of the CNS-heart axis in mouse models of Huntington's disease. PLoS Genet. 2014;10: e1004550. doi:10.1371/journal.pgen.1004550

47. Franklin SS, O'Brien E, Staessen JA. Masked hypertension: understanding its complexity. Eur Heart J. 2017;38: 1112–1118. doi:10.1093/eurheartj/ehw502

48. Bowles NP, Thosar SS, Herzig MX, Shea SA. Chronotherapy for Hypertension. Curr Hypertens Rep. 2018;20: 97. doi:10.1007/s11906-018-0897-4

49. Nader N, Chrousos GP, Kino T. Interactions of the Circadian CLOCK System and the HPA Axis. Trends Endocrinol Metab. 2010;21: 277–286. doi:10.1016/j.tem.2009.12.011

50. Nicolaides NC, Charmandari E, Chrousos GP, Kino T. Circadian endocrine rhythms: the hypothalamic–pituitary–adrenal axis and its actions. Ann N Y Acad Sci. 2014;1318: 71–80. doi:10.1111/nyas.12464

51. Takahashi JS, Hong H-K, Ko CH, McDearmon EL. The genetics of mammalian circadian order and disorder: implications for physiology and disease. Nat Rev Genet. 2008;9: 764–775. doi:10.1038/nrg2430

52. Buijs RM. Chapter 1 - The autonomic nervous system: a balancing act. In: Buijs RM, Swaab DF, editors. Handbook of Clinical Neurology. Elsevier; 2013. pp. 1–11. doi:10.1016/B978-0-444-53491-0.00001-8

53. Buijs RM, la Fleur SE, Wortel J, Van Heyningen C, Zuiddam L, Mettenleiter TC, et al. The suprachiasmatic nucleus balances sympathetic and parasympathetic output to peripheral organs through separate preautonomic neurons. J Comp Neurol. 2003;464: 36–48. doi:10.1002/cne.10765

54. Buijs RM, Escobar C, Swaab DF. Chapter 15 - The circadian system and the balance of the autonomic nervous system. In: Buijs RM, Swaab DF, editors. Handbook of Clinical Neurology. Elsevier; 2013. pp. 173–191. doi:10.1016/B978-0-444-53491-0.00015-8

55. Fahrenkrug J, Popovic N, Georg B, Brundin P, Hannibal J. Decreased VIP and VPAC2 receptor expression in the biological clock of the R6/2 Huntington's disease mouse. J Mol Neurosci. 2007;31: 139–148.

56. Kotliarova S, Jana NR, Sakamoto N, Kurosawa M, Miyazaki H, Nekooki M, et al. Decreased expression of hypothalamic neuropeptides in Huntington disease transgenic mice with expanded polyglutamine-EGFP fluorescent aggregates. J Neurochem. 2005;93: 641–653. doi:10.1111/j.1471-4159.2005.03035.x

57. Williams RH, Morton AJ, Burdakov D. Paradoxical function of orexin/hypocretin circuits in a mouse model of Huntington's disease. Neurobiol Dis. 2011;42: 438–445. doi:10.1016/j.nbd.2011.02.006

58. Clark CG, Hasser EM, Kunze DL, Katz DM, Kline DD. Endogenous Brain Derived Neurotrophic Factor in the Nucleus Tractus Solitarius Tonically Regulates Synaptic and Autonomic Function. J Neurosci. 2011;31: 12318–12329. doi:10.1523/JNEUROSCI.0746-11.2011

59. Wan R, Weigand LA, Bateman R, Griffioen K, Mendelowitz D, Mattson MP. Evidence that BDNF regulates heart rate by a mechanism involving increased brainstem parasympathetic neuron excitability. J Neurochem. 2014;129: 573–580. doi:10.1111/jnc.12656

60. Wang H, Zhou X-F. Injection of brain-derived neurotrophic factor in the rostral ventrolateral medulla increases arterial blood pressure in anaesthetized rats. Neuroscience. 2002;112: 967–975. doi:10.1016/S0306-4522(02)00085-4

61. Duan W, Guo Z, Jiang H, Ware M, Mattson MP. Reversal of behavioral and metabolic abnormalities, and insulin resistance syndrome, by dietary restriction in mice deficient in brain-derived neurotrophic factor. Endocrinology. 2003;144: 2446–2453. doi:10.1210/en.2002-0113

62. Griffioen KJ, Wan R, Brown TR, Okun E, Camandola S, Mughal MR, et al. Aberrant heart rate and brainstem brain-derived neurotrophic factor (BDNF) signaling in a mouse model of Huntington's disease. Neurobiol Aging. 2012;33: 1481.e1-5. doi:10.1016/j.neurobiolaging.2011.11.030

63. Gabery S, Murphy K, Schultz K, Loy CT, McCusker E, Kirik D, et al. Changes in key hypothalamic neuropeptide populations in Huntington disease revealed by neuropathological analyses. Acta Neuropathol. 2010;120: 777–788. doi:10.1007/s00401-010-0742-6

64. van Wamelen DJ, Aziz NA, Roos R a. C, Swaab DF. Hypothalamic alterations in Huntington's disease patients: comparison with genetic rodent models. J Neuroendocrinol. 2014;26: 761–775. doi:10.1111/jne.12190

65. Zuccato C, Marullo M, Conforti P, MacDonald ME, Tartari M, Cattaneo E. Systematic assessment of BDNF and its receptor levels in human cortices affected by Huntington's disease. Brain Pathol. 2008;18: 225–238. doi:10.1111/j.1750-3639.2007.00111.x

66. Zuccato C, Ciammola A, Rigamonti D, Leavitt BR, Goffredo D, Conti L, et al. Loss of huntingtin-mediated BDNF gene transcription in Huntington's disease. Science. 2001;293: 493–498. doi:10.1126/science.1059581

67. Rüb U, Hentschel M, Stratmann K, Brunt E, Heinsen H, Seidel K, et al. Huntington's disease (HD): Degeneration of select nuclei and widespread occurrence of neuronal nuclear and axonal inclusions in the brainstem. Brain Pathol. 2014;24: 247–260. doi:10.1111/bpa.12115

68. Mohawk JA, Green CB, Takahashi JS. Central and Peripheral Circadian Clocks in Mammals. Annual Review of Neuroscience. 2012;35: 445–462. doi:10.1146/annurev-neuro-060909-153128

69. Webb AB, Angelo N, Huettner JE, Herzog ED. Intrinsic, nondeterministic circadian rhythm generation in identified mammalian neurons. Proc Natl Acad Sci USA. 2009;106: 16493–16498. doi:10.1073/pnas.0902768106

70. Colwell CS. Linking neural activity and molecular oscillations in the SCN. Nature Reviews Neuroscience. 2011;12: 553–569. doi:10.1038/nrn3086

71. Kuljis D, Kudo T, Tahara Y, Ghiani CA, Colwell CS. Pathophysiology in the suprachiasmatic nucleus in mouse models of Huntington's disease. Journal of Neuroscience Research. 2018;96: 1862–1875. doi:10.1002/jnr.24320

72. Pallier PN, Maywood ES, Zheng Z, Chesham JE, Inyushkin AN, Dyball R, et al. Pharmacological imposition of sleep slows cognitive decline and reverses dysregulation of circadian gene expression in a transgenic mouse model of Huntington's disease. J Neurosci. 2007;27: 7869–7878. doi:10.1523/JNEUROSCI.0649-07.2007

73. Schroeder AM, Colwell CS. How to fix a broken clock. Trends Pharmacol Sci. 2013;34: 605–619. doi:10.1016/j.tips.2013.09.002

74. Whittaker DS, Loh DH, Wang H-B, Tahara Y, Kuljis D, Cutler T, et al. Circadian-based Treatment Strategy Effective in the BACHD Mouse Model of Huntington's Disease. J Biol Rhythms. 2018;33: 535–554. doi:10.1177/0748730418790401

75. Maywood ES, Fraenkel E, McAllister CJ, Wood N, Reddy AB, Hastings MH, et al. Disruption of peripheral circadian timekeeping in a mouse model of Huntington's disease and its restoration by temporally scheduled feeding. J Neurosci. 2010;30: 10199–10204. doi:10.1523/JNEUROSCI.1694-10.2010

76. Young ME, Razeghi P, Taegtmeyer H. Clock genes in the heart: characterization and attenuation with hypertrophy. Circ Res. 2001;88: 1142–1150.

77. Durgan DJ, Hotze MA, Tomlin TM, Egbejimi O, Graveleau C, Abel ED, et al. The intrinsic circadian clock within the cardiomyocyte. Am J Physiol Heart Circ Physiol. 2005;289: H1530-1541. doi:10.1152/ajpheart.00406.2005

78. Canaple L, Rambaud J, Dkhissi-Benyahya O, Rayet B, Tan NS, Michalik L, et al. Reciprocal regulation of brain and muscle Arnt-like protein 1 and peroxisome proliferator-activated

receptor alpha defines a novel positive feedback loop in the rodent liver circadian clock. Mol Endocrinol. 2006;20: 1715–1727. doi:10.1210/me.2006-0052

79. Martino TA, Young ME. Influence of the cardiomyocyte circadian clock on cardiac physiology and pathophysiology. J Biol Rhythms. 2015;30: 183–205. doi:10.1177/0748730415575246

80. Zhang L, Prosdocimo DA, Bai X, Fu C, Zhang R, Campbell F, et al. KLF15 Establishes the Landscape of Diurnal Expression in the Heart. Cell Rep. 2015;13: 2368–2375. doi:10.1016/j.celrep.2015.11.038

81. Jeyaraj D, Haldar SM, Wan X, McCauley MD, Ripperger JA, Hu K, et al. Circadian rhythms govern cardiac repolarization and arrhythmogenesis. Nature. 2012;483: 96–99. doi:10.1038/nature10852

82. Martino TA, Tata N, Belsham DD, Chalmers J, Straume M, Lee P, et al. Disturbed diurnal rhythm alters gene expression and exacerbates cardiovascular disease with rescue by resynchronization. Hypertension. 2007;49: 1104–1113. doi:10.1161/HYPERTENSIONAHA.106.083568

83. Martino TA, Oudit GY, Herzenberg AM, Tata N, Koletar MM, Kabir GM, et al. Circadian rhythm disorganization produces profound cardiovascular and renal disease in hamsters. Am J Physiol Regul Integr Comp Physiol. 2008;294: R1675-1683. doi:10.1152/ajpregu.00829.2007

84. Bunger MK, Walisser JA, Sullivan R, Manley PA, Moran SM, Kalscheur VL, et al. Progressive arthropathy in mice with a targeted disruption of the Mop3/Bmal-1 locus. Genesis. 2005;41: 122–132. doi:10.1002/gene.20102

85. Laposky A, Easton A, Dugovic C, Walisser J, Bradfield C, Turek F. Deletion of the mammalian circadian clock gene BMAL1/Mop3 alters baseline sleep architecture and the response to sleep deprivation. Sleep. 2005;28: 395–409.

86. Kondratov RV, Kondratova AA, Gorbacheva VY, Vykhovanets OV, Antoch MP. Early aging and age-related pathologies in mice deficient in BMAL1, the core componentof the circadian clock. Genes Dev. 2006;20: 1868–1873. doi:10.1101/gad.1432206

87. Lefta M, Campbell KS, Feng H-Z, Jin J-P, Esser KA. Development of dilated cardiomyopathy in Bmal1-deficient mice. Am J Physiol Heart Circ Physiol. 2012;303: H475-485. doi:10.1152/ajpheart.00238.2012

88. Young ME, Brewer RA, Peliciari-Garcia RA, Collins HE, He L, Birky TL, et al. Cardiomyocyte-specific BMAL1 plays critical roles in metabolism, signaling, and maintenance of contractile function of the heart. J Biol Rhythms. 2014;29: 257–276. doi:10.1177/0748730414543141

89. Bray MS, Shaw CA, Moore MWS, Garcia RAP, Zanquetta MM, Durgan DJ, et al. Disruption of the circadian clock within the cardiomyocyte influences myocardial contractile function, metabolism, and gene expression. Am J Physiol Heart Circ Physiol. 2008;294: H1036-1047. doi:10.1152/ajpheart.01291.2007

90. Durgan DJ, Tsai J-Y, Grenett MH, Pat BM, Ratcliffe WF, Villegas-Montoya C, et al. Evidence Suggesting that the Cardiomyocyte Circadian Clock Modulates Responsiveness of the Heart to Hypertrophic Stimuli in Mice. Chronobiol Int. 2011;28: 187–203. doi:10.3109/07420528.2010.550406

91. Ayas NT, White DP, Manson JE, Stampfer MJ, Speizer FE, Malhotra A, et al. A Prospective Study of Sleep Duration and Coronary Heart Disease in Women. Arch Intern Med. 2003;163: 205–209. doi:10.1001/archinte.163.2.205

92. Morris CJ, Purvis TE, Hu K, Scheer FAJL. Circadian misalignment increases cardiovascular disease risk factors in humans. Proc Natl Acad Sci USA. 2016;113: E1402-1411. doi:10.1073/pnas.1516953113

93. Rutters F, Lemmens SG, Adam TC, Bremmer MA, Elders PJ, Nijpels G, et al. Is social jetlag associated with an adverse endocrine, behavioral, and cardiovascular risk profile? J Biol Rhythms. 2014;29: 377–383. doi:10.1177/0748730414550199

94. Furlan Raffaello, Barbic Franca, Piazza Simona, Tinelli Mauro, Seghizzi Paolo, Malliani Alberto. Modifications of Cardiac Autonomic Profile Associated With a Shift Schedule of Work. Circulation. 2000;102: 1912–1916. doi:10.1161/01.CIR.102.16.1912

95. Margolis RL, Ross CA. Diagnosis of Huntington disease. Clin Chem. 2003;49: 1726–1732.

96. Chiu E, Alexander L. Causes of death in Huntington's disease. Med J Aust. 1982;1: 153.

97. Lanska DJ, Lanska MJ, Lavine L, Schoenberg BS. Conditions associated with Huntington's disease at death. A case-control study. Arch Neurol. 1988;45: 878–880.

98. Bode FJ, Stephan M, Wiehager S, Nguyen HP, Björkqvist M, von Hörsten S, et al. Increased numbers of motor activity peaks during light cycle are associated with reductions in adrenergic alpha(2)-receptor levels in a transgenic Huntington's disease rat model. Behav Brain Res. 2009;205: 175–182. doi:10.1016/j.bbr.2009.06.031

99. Oakeshott S, Balci F, Filippov I, Murphy C, Port R, Connor D, et al. Circadian Abnormalities in Motor Activity in a BAC Transgenic Mouse Model of Huntington's Disease. PLoS Curr. 2011;3: RRN1225. doi:10.1371/currents.RRN1225

100. Campen MJ, Tagaito Y, Jenkins TP, Balbir A, O'Donnell CP. Heart rate variability responses to hypoxic and hypercapnic exposures in different mouse strains. J Appl Physiol. 2005;99: 807–813. doi:10.1152/japplphysiol.00039.2005

101. Thireau J, Zhang BL, Poisson D, Babuty D. Heart rate variability in mice: a theoretical and practical guide. Exp Physiol. 2008;93: 83–94. doi:10.1113/expphysiol.2007.040733

102. Badilini F, Maison-Blanche P, Champomier P, Provost JC, Coumel P, Milon H. Frequency-domain heart rate variability in 24-hour Holter recordings: role of spectral method to assess circadian patterns and pharmacological autonomic modulation. J Electrocardiol. 2000;33: 147–157.

103. Rozen S, Skaletsky H. Primer3 on the WWW for general users and for biologist programmers. Methods Mol Biol. 2000;132: 365–386.

104. Ghiani CA, Starcevic M, Rodriguez-Fernandez IA, Nazarian R, Cheli VT, Chan LN, et al. The dysbindin-containing complex (BLOC-1) in brain: developmental regulation, interaction with SNARE proteins and role in neurite outgrowth. Molecular Psychiatry. 2010;15: 204–215. doi:10.1038/mp.2009.58

105. Coppola G. Designing, performing, and interpreting a microarray-based gene expression study. Methods Mol Biol. 2011;793: 417–439. doi:10.1007/978-1-61779-328-8_28

106. Smyth GK. Linear models and empirical bayes methods for assessing differential expression in microarray experiments. Stat Appl Genet Mol Biol. 2004;3: Article3. doi:10.2202/1544-6115.1027

107. Ruby NF, Dark J, Burns DE, Heller HC, Zucker I. The suprachiasmatic nucleus is essential for circadian body temperature rhythms in hibernating ground squirrels. J Neurosci. 2002;22: 357–364.

108. Saleh MA, Winget CM. Effect of suprachiasmatic lesions on diurnal heart rate rhythm in the rat. Physiol Behav. 1977;19: 561–564.

109. Scheer F a. JL, Pirovano C, Van Someren EJW, Buijs RM. Environmental light and suprachiasmatic nucleus interact in the regulation of body temperature. Neuroscience. 2005;132: 465–477. doi:10.1016/j.neuroscience.2004.12.012

110. Stephan FK, Nunez AA. Elimination of circadian rhythms in drinking, activity, sleep, and temperature by isolation of the suprachiasmatic nuclei. Behav Biol. 1977;20: 1–61.

111. Warren WS, Champney TH, Cassone VM. The suprachiasmatic nucleus controls the circadian rhythm of heart rate via the sympathetic nervous system. Physiol Behav. 1994;55: 1091–1099.

112. Witte K, Schnecko A, Buijs RM, van der Vliet J, Scalbert E, Delagrange P, et al. Effects of SCN lesions on circadian blood pressure rhythm in normotensive and transgenic hypertensive rats. Chronobiol Int. 1998;15: 135–145.

113. Leak RK, Moore RY. Topographic organization of suprachiasmatic nucleus projection neurons. J Comp Neurol. 2001;433: 312–334.

114. Deurveilher S, Semba K. Indirect projections from the suprachiasmatic nucleus to the median preoptic nucleus in rat. Brain Res. 2003;987: 100–106.

115. Lu J, Zhang YH, Chou TC, Gaus SE, Elmquist JK, Shiromani P, et al. Contrasting effects of ibotenate lesions of the paraventricular nucleus and subparaventricular zone on sleep-wake cycle and temperature regulation. J Neurosci. 2001;21: 4864–4874.

116. de Aragão BC, Rodrigues HA, Valadão PAC, Camargo W, Naves LA, Ribeiro FM, et al. Changes in structure and function of diaphragm neuromuscular junctions from BACHD mouse model for Huntington's disease. Neurochem Int. 2016;93: 64–72. doi:10.1016/j.neuint.2015.12.013

117. Bigger JT, Fleiss JL, Steinman RC, Rolnitzky LM, Kleiger RE, Rottman JN. Frequency domain measures of heart period variability and mortality after myocardial infarction. Circulation. 1992;85: 164–171.

118. Buccelletti E, Gilardi E, Scaini E, Galiuto L, Persiani R, Biondi A, et al. Heart rate variability and myocardial infarction: systematic literature review and metanalysis. Eur Rev Med Pharmacol Sci. 2009;13: 299–307.

119. Benarroch EE. The central autonomic network: functional organization, dysfunction, and perspective. Mayo Clin Proc. 1993;68: 988–1001.

120. Ma X, Abboud FM, Chapleau MW. Analysis of afferent, central, and efferent components of the baroreceptor reflex in mice. Am J Physiol Regul Integr Comp Physiol. 2002;283: R1033-1040. doi:10.1152/ajpregu.00768.2001

121. Gray M, Shirasaki DI, Cepeda C, André VM, Wilburn B, Lu X-H, et al. Full-length human mutant huntingtin with a stable polyglutamine repeat can elicit progressive and selective neuropathogenesis in BACHD mice. J Neurosci. 2008;28: 6182–6195. doi:10.1523/JNEUROSCI.0857-08.2008

122. Nguyen TP, Qu Z, Weiss JN. Cardiac fibrosis and arrhythmogenesis: the road to repair is paved with perils. J Mol Cell Cardiol. 2014;70: 83–91. doi:10.1016/j.yjmcc.2013.10.018

123. Sassone J, Colciago C, Cislaghi G, Silani V, Ciammola A. Huntington's disease: the current state of research with peripheral tissues. Exp Neurol. 2009;219: 385–397. doi:10.1016/j.expneurol.2009.05.012

124. Strong TV, Tagle DA, Valdes JM, Elmer LW, Boehm K, Swaroop M, et al. Widespread expression of the human and rat Huntington's disease gene in brain and nonneural tissues. Nature Genetics. 1993;5: 259–265. doi:10.1038/ng1193-259

125. Izzo JL, Taylor AA. The sympathetic nervous system and baroreflexes in hypertension and hypotension. Curr Hypertens Rep. 1999;1: 254–263.

126. Squitieri F, Cannella M, Giallonardo P, Maglione V, Mariotti C, Hayden MR. Onset and pre-onset studies to define the Huntington's disease natural history. Brain Res Bull. 2001;56: 233–238.

127. Wang H-B, Whittaker DS, Truong D, Mulji AK, Ghiani CA, Loh DH, et al. Blue light therapy improves circadian dysfunction as well as motor symptoms in two mouse models of Huntington's disease. Neurobiology of Sleep and Circadian Rhythms. 2017;2: 39–52. doi:10.1016/j.nbscr.2016.12.002

128. Tomita-Mitchell A, Stamm KD, Mahnke DK, Kim M-S, Hidestrand PM, Liang HL, et al. Impact of MYH6 variants in hypoplastic left heart syndrome. Physiol Genomics. 2016;48: 912–921. doi:10.1152/physiolgenomics.00091.2016

129. Hayashi K, Teramoto R, Nomura A, Asano Y, Beerens M, Kurata Y, et al. Impact of functional studies on exome sequence variant interpretation in early-onset cardiac conduction system diseases. Cardiovasc Res. 2020. doi:10.1093/cvr/cvaa010

130. Whitcomb J, Gharibeh L, Nemer M. From embryogenesis to adulthood: Critical role for GATA factors in heart development and function. IUBMB Life. 2020;72: 53–67. doi:10.1002/iub.2163

131. Celis-Morales CA, Welsh P, Lyall DM, Steell L, Petermann F, Anderson J, et al. Associations of grip strength with cardiovascular, respiratory, and cancer outcomes and all cause mortality: prospective cohort study of half a million UK Biobank participants. BMJ. 2018;361: k1651. doi:10.1136/bmj.k1651

132. Bohannon RW. Grip Strength: An Indispensable Biomarker For Older Adults. Clin Interv Aging. 2019;14: 1681–1691. doi:10.2147/CIA.S194543

133. Pugach EK, Richmond PA, Azofeifa JG, Dowell RD, Leinwand LA. Prolonged Cre expression driven by the α-myosin heavy chain promoter can be cardiotoxic. J Mol Cell Cardiol. 2015;86: 54–61. doi:10.1016/j.yjmcc.2015.06.019

134. Rehmani T, Salih M, Tuana BS. Cardiac-Specific Cre Induces Age-Dependent Dilated Cardiomyopathy (DCM) in Mice. Molecules. 2019;24. doi:10.3390/molecules24061189

135. Massin MM. Circadian rhythm of heart rate and heart rate variability. Archives of Disease in Childhood. 2000;83: 179–182. doi:10.1136/adc.83.2.179

136. Krayenbuehl HP, Hess OM, Monrad ES, Schneider J, Mall G, Turina M. Left ventricular myocardial structure in aortic valve disease before, intermediate, and late after aortic valve replacement. Circulation. 1989;79: 744–755. doi:10.1161/01.cir.79.4.744

137. Hein S, Arnon E, Kostin S, Schönburg M, Elsässer A, Polyakova V, et al. Progression from compensated hypertrophy to failure in the pressure-overloaded human heart: structural deterioration and compensatory mechanisms. Circulation. 2003;107: 984–991. doi:10.1161/01.cir.0000051865.66123.b7

138. Cao Z, Jia Y, Zhu B. BNP and NT-proBNP as Diagnostic Biomarkers for Cardiac Dysfunction in Both Clinical and Forensic Medicine. Int J Mol Sci. 2019;20. doi:10.3390/ijms20081820

139. Matsuo A, Nagai-Okatani C, Nishigori M, Kangawa K, Minamino N. Natriuretic peptides in human heart: Novel insight into their molecular forms, functions, and diagnostic use. Peptides. 2019;111: 3–17. doi:10.1016/j.peptides.2018.08.006

140. Gubelmann C, Vollenweider P, Marques-Vidal P. Association of grip strength with cardiovascular risk markers. Eur J Prev Cardiol. 2017;24: 514–521. doi:10.1177/2047487316680695

141. Sillars A, Celis-Morales CA, Ho FK, Petermann F, Welsh P, Iliodromiti S, et al. Association of Fitness and Grip Strength With Heart Failure: Findings From the UK Biobank Population-Based Study. Mayo Clin Proc. 2019;94: 2230–2240. doi:10.1016/j.mayocp.2019.04.041

142. Tabrizi SJ, Leavitt BR, Landwehrmeyer GB, Wild EJ, Saft C, Barker RA, et al. Targeting Huntingtin Expression in Patients with Huntington's Disease. N Engl J Med. 2019;380: 2307–2316. doi:10.1056/NEJMoa1900907

143. Fisch S, Gray S, Heymans S, Haldar SM, Wang B, Pfister O, et al. Kruppel-like factor 15 is a regulator of cardiomyocyte hypertrophy. Proc Natl Acad Sci USA. 2007;104: 7074–7079. doi:10.1073/pnas.0701981104

144. Patel SK, Ramchand J, Crocitti V, Burrell LM. Kruppel-Like Factor 15 Is Critical for the Development of Left Ventricular Hypertrophy. Int J Mol Sci. 2018;19. doi:10.3390/ijms19051303

145. Hughes ME, Hogenesch JB, Kornacker K. JTK_CYCLE: an efficient nonparametric algorithm for detecting rhythmic components in genome-scale data sets. J Biol Rhythms. 2010;25: 372–380. doi:10.1177/0748730410379711

146. Stratmann M, Suter DM, Molina N, Naef F, Schibler U. Circadian Dbp Transcription Relies on Highly Dynamic BMAL1-CLOCK Interaction with E Boxes and Requires the Proteasome. Molecular Cell. 2012;48: 277–287. doi:10.1016/j.molcel.2012.08.012

147. Sugi K, Hsieh PN, Ilkayeva O, Shelkay S, Moroney B, Baadh P, et al. Kruppel-like factor 15 is required for the cardiac adaptive response to fasting. PLOS ONE. 2018;13: e0192376. doi:10.1371/journal.pone.0192376

148. Masri S, Orozco-Solis R, Aguilar-Arnal L, Cervantes M, Sassone-Corsi P. Coupling circadian rhythms of metabolism and chromatin remodelling. Diabetes Obes Metab. 2015;17 Suppl 1: 17–22. doi:10.1111/dom.12509

149. Wang N, Yang G, Jia Z, Zhang H, Aoyagi T, Soodvilai S, et al. Vascular PPARγ Controls Circadian Variation in Blood Pressure and Heart Rate through Bmal1. Cell Metabolism. 2008;8: 482–491. doi:10.1016/j.cmet.2008.10.009